CARDIOLOGY

Cardiac ryanodine receptor calcium release deficiency syndrome

Bo Sun[1,2]*, Jinjing Yao[1]*, Mingke Ni[1]*, Jinhong Wei[1], Xiaowei Zhong[1], Wenting Guo[1], Lin Zhang[1], Ruiwu Wang[1], Darrell Belke[1], Yong-Xiang Chen[1], Krystien V.V. Lieve[3,4], Anders K. Broendberg[5], Thomas M. Roston[6], Ivan Blankoff[7], Janneke A. Kammeraad[8], Johannes C. von Alvensleben[9], Julieta Lazarte[10], Alexander Vallmitjana[11], Loryn J. Bohne[12], Robert A. Rose[12], Raul Benitez[11], Leif Hove-Madsen[13], Carlo Napolitano[4,14,15], Robert A. Hegele[10], Michael Fill[16], Shubhayan Sanatani[17†], Arthur A.M. Wilde[3,4†], Jason D. Roberts[18†], Silvia G. Priori[4,14,15,19†], Henrik K. Jensen[5†], S. R. Wayne Chen[1,16†]

Cardiac ryanodine receptor (RyR2) gain-of-function mutations cause catecholaminergic polymorphic ventricular tachycardia, a condition characterized by prominent ventricular ectopy in response to catecholamine stress, which can be reproduced on exercise stress testing (EST). However, reports of sudden cardiac death (SCD) have emerged in EST-negative individuals who have loss-of-function (LOF) RyR2 mutations. The clinical relevance of RyR2 LOF mutations including their pathogenic mechanism, diagnosis, and treatment are all unknowns. Here, we performed clinical and genetic evaluations of individuals who suffered from SCD and harbored an LOF RyR2 mutation. We carried out electrophysiological studies using a programed electrical stimulation protocol consisting of a long-burst, long-pause, and short-coupled (LBLPS) ventricular extra-stimulus. Linkage analysis of RyR2 LOF mutations in six families revealed a combined logarithm of the odds ratio for linkage score of 11.479 for a condition associated with SCD with negative EST. A RyR2 LOF mouse model exhibited no catecholamine-provoked ventricular arrhythmias as in humans but did have substantial cardiac electrophysiological remodeling and an increased propensity for early afterdepolarizations. The LBLPS pacing protocol reliably induced ventricular arrhythmias in mice and humans having RyR2 LOF mutations, whose phenotype is otherwise concealed before SCD. Furthermore, treatment with quinidine and flecainide abolished LBLPS-induced ventricular arrhythmias in model mice. Thus, RyR2 LOF mutations underlie a previously unknown disease entity characterized by SCD with normal EST that we have termed RyR2 Ca^{2+} release deficiency syndrome (CRDS). Our study provides insights into the mechanism of CRDS, reports a specific CRDS diagnostic test, and identifies potentially efficacious anti-CRDS therapies.

INTRODUCTION

The cardiac ryanodine receptor (RyR2) governs the release of Ca^{2+} from the sarcoplasmic reticulum (SR), which is essential for excitation-contraction coupling in the heart and has a major role in the pathogenesis of cardiac arrhythmias (*1*–*4*). Mutations in *RYR2* cause catecholaminergic polymorphic ventricular tachycardia (CPVT), a cardiac channelopathy associated with malignant ventricular arrhythmias (VAs) and sudden cardiac death (SCD) (*4*–*8*). CPVT develops due to RyR2 gain-of-function (GOF) mutations and the resultant diastolic spontaneous Ca^{2+} release and delayed afterdepolarizations (DADs) that can trigger malignant polymorphic ventricular tachycardia (VT). The hallmark of CPVT is increasing ventricular ectopy that progresses to more complex arrhythmias, most typically bidirectional VT, in response to catecholamine stress (*4*). CPVT can be reliably reproduced on exercise stress testing (EST), making EST a useful CPVT diagnostic tool (*4*–*11*).

In contrast to CPVT-causing RyR2 GOF mutations, recent work has begun to identify mutations among survivors of cardiac arrest that exhibit a RyR2 loss of function (LOF) or suppression of function on in vitro functional testing (*12*–*16*). However, the clinical

[1]Libin Cardiovascular Institute of Alberta, Department of Physiology and Pharmacology, University of Calgary, Calgary, AB T2N 4Z6, Canada. [2]Medical School, Kunming University of Science and Technology, Kunming 650504, China. [3]Amsterdam University Medical Centre, location AMC, Heart Center, Department of Clinical and Experimental Cardiology, Amsterdam 1105AZ, Netherlands. [4]European Reference Network 'ERN GUARD-Heart', Amsterdam, Netherlands. [5]Department of Cardiology, Aarhus University Hospital, and Department of Clinical Medicine, Health, Aarhus University, Palle Juul-Jensens Blv 99, DK-8200 Aarhus N, Denmark. [6]Division of Cardiology, Department of Medicine, University of British Columbia, Vancouver, BC V5Z 1M9, Canada. [7]C.H.U. Charleroi, Hôpital Civil Marie Curie Chaussée de Bruxelles 140 6042 Charleroi, Belgium. [8]Department of Pediatric Cardiology, Sophia Children's Hospital, Erasmus University Medical Centre, Doctor Molewaterplein 40, 3015 GD Rotterdam, Netherlands. [9]Division of Cardiology, Heart Institute, Children's Hospital Colorado, University of Colorado, Aurora, CO 80045, USA. [10]Department of Medicine and Robarts Research Institute, Schulich School of Medicine and Dentistry, Western University, London, ON N6A 5B7, Canada. [11]Department of Automatic Control, Universitat Politècnica de Catalunya, 08034 Barcelona, Spain. [12]Departments of Cardiac Sciences and Physiology and Pharmacology, Libin Cardiovascular Institute of Alberta, Cumming School of Medicine, University of Calgary, Calgary, AB T2N 4Z6, Canada. [13]Biomedical Research Institute Barcelona (IIBB-CSIC) and IIB Sant Pau, Hospital de Sant Pau, Barcelona 08025, Spain. [14]Division of Cardiology and Molecular Cardiology, IRCCS Maugeri Foundation-University of Pavia, 27100 Pavia, Italy. [15]Department of Molecular Medicine, University of Pavia, 27100 Pavia, Italy. [16]Department of Physiology and Biophysics, Rush University Medical Center, Chicago, IL 60612, USA. [17]Child and Family Research Institute, Department of Pediatrics, University of British Columbia, Vancouver, BC V6H 3V4, Canada. [18]Section of Cardiac Electrophysiology, Division of Cardiology, Department of Medicine, Western University, London, ON N6A 5A5, Canada. [19]Molecular Cardiology Laboratory, Centro de Investigaciones Cardiovasculares Carlos III, 28029 Madrid, Spain.

*These authors contributed equally to this work.

†Corresponding author. Email: swchen@ucalgary.ca (S.R.W.C.); hkjensen@clin.au.dk (H.K.J.); silvia.priori@icsmaugeri.it (S.G.P.); jason.roberts@lhsc.on.ca (J.D.R.); a.a.wilde@amsterdamumc.nl (A.A.M.W.); ssanatani@cw.bc.ca (S.S.)

ramifications of RyR2 LOF mutations are unclear. Patients having RyR2 LOF mutations do not exhibit the CPVT phenotype. The phenotype of carriers of RyR2 LOF mutations, aside from their fatal or near-fatal cardiac events, has been otherwise within normal limits on cardiac testing (*12*, *15*–*17*). As a result, these patients are often assigned a cryptic diagnosis of idiopathic ventricular fibrillation.

Clarification of the clinical relevance of RyR2 LOF mutations has become imperative. It is currently unknown whether these genetic variants are truly causal for a potentially life-threatening disorder or merely incidental and noncausal genomic background noise, which is notably high in the *RYR2* gene (~3%) (*18*, *19*). Should these genetic variants be drivers of malignant arrhythmias, this would be critical knowledge for SCD risk management of the patients and their family members. Here, we provide clinical, genetic, and functional evidence that definitively establishes RyR2 LOF mutations as being causative for a previously unknown disease entity that we call RyR2 Ca^{2+} release deficiency syndrome (CRDS). We also introduce a diagnostic testing maneuver for this otherwise concealed condition and provide evidence for medical therapies that may effectively prevent life-threatening events in patients having RyR2 LOF mutations.

RESULTS

A previously unknown cardiac arrhythmia linked to RyR2 LOF

We identified six families in whom the probands had suffered SCD or aborted SCD (aSCD) and had rare RyR2 mutations (Q3774L, I3995V, D4112N, T4196I, D4646A, or Q4879H) that were subsequently identified to result in LOF or suppression of function on in vitro functional evaluation (Fig. 1, fig. S1, and Table 1). None of the probands or genotype-positive family members exhibited a typical CPVT phenotype. Combining these six families (with 20 SCD/aSCD) and four previously reported families (with 11 SCD/aSCD) having RyR2 LOF mutations (I4855M, A4860G, S4938F, and K4594R/I2075T) (*12*, *15*–*17*) showed that 31 of 46 (67%) RyR2 mutant carriers experienced SCD/aSCD, but none of the 46 (0%) RyR2 mutation-negative individuals suffered from life-threatening VAs (fig. S1 and Table 1).

To statistically evaluate the link between RyR2 LOF mutations and this arrhythmic disease entity, we used the two-point linkage analysis using LIPED (*20*). This analysis revealed a combined maximal logarithm of the odds ratio for linkage (LOD) score from six families (I3995V, D4112N, T4196I, D4646A, I4855M, and R4594K/I2075T) of 11.479 at 0% recombination, which is equivalent to odds of 301,300,000,000:1 in favor of complete linkage between phenotype and genotype (table S1). There were too few informative meioses in three families (Q3774L, A4860G, and S4938F) to calculate linkage. Q4879H is a de novo aSCD-associated RyR2 mutation found in the proband, whereas neither parent was clinically or genetically affected (see the "Linkage analysis in *RYR2* mutation families" section in the Supplementary Materials).

The RyR2 mutations identified are located in the RyR2's central domain, U-motif, S2-S3 loop, pore domain (S5-S6), or C-terminal domain—all of which are critical for channel gating (Fig. 2A). To assess the functional impact of these RyR2 mutations, we measured caffeine-induced Ca^{2+} release and store overload–induced Ca^{2+} release (SOICR) in human embryonic kidney (HEK) 293 cells expressing either RyR2 wild type (WT) or mutants. RyR2 mutations Q3774L, I3995V, D4112N, T4196I, D4646A, Q4879H, I4855M, A4860G, and S4938F markedly suppressed caffeine-induced Ca^{2+} release and SOICR without altering the store capacity. Specifically, higher caffeine concentrations and higher intra-ER (endoplasmic reticulum) Ca^{2+} concentrations were required to activate the mutant RyR2s, compared to RyR2-WT (Fig. 2, B to D, and figs. S2 and S3). The expression of these RyR2 mutants was comparable to that of the RyR2-WT (fig. S3, A and B). Some mutants had additional actions on SOICR termination threshold and/or RyR2-mediated fractional Ca^{2+} release (fig. S3, C to F). Furthermore, all six newly identified RyR2 mutations impaired the cytosolic Ca^{2+} activation and diminished the luminal Ca^{2+} activation of single RyR2 channels (Fig. 2, E and F, and fig. S4). As for the RyR2 K4594R/I2075T double mutation, it also markedly suppressed caffeine-induced Ca^{2+} release largely due to the impact of the K4594R mutation, because the impact of the double RyR2 K4594R/I2075 mutation and the single K4594R mutation is similar (fig. S2D). Note that, although all of these RyR2 LOF mutants exhibited reduced channel activities, they were still functional (i.e., not dead). Collectively, our clinical, genetic, functional, and statistical analyses definitively establish the link between RyR2 LOF and a previously unknown disease entity characterized by SCD/aSCD with negative EST. We call this previously unknown disease entity RyR2-CRDS.

RyR2-D4646A$^{+/-}$ diminishes spontaneous SR Ca^{2+} release and stress-induced VAs

To explore the mechanism by which CRDS RyR2 mutations cause SCD, we generated a knock-in mouse model expressing one of the RyR2 LOF mutations, D4646A (fig. S5). As in humans, only heterozygous RyR2-D4646A mutant mice (RyR2-D4646A$^{+/-}$), but no homozygous mutant mice, were produced, suggesting that homozygous RyR2-D4646A$^{+/+}$ mutation is embryonically lethal. We first determined the impact of the heterozygous RyR2-D4646A$^{+/-}$ mutation on intracellular Ca^{2+} handling. Specifically, we assessed the propensity for store overload–induced spontaneous SR Ca^{2+} release, a well-known consequence of typical CPVT RyR2 mutations (*4*, *21*, *22*), in WT and D4646A$^{+/-}$ mutant intact hearts. Elevating extracellular Ca^{2+} concentration to 4 to 8 mM (to promote SR Ca^{2+} overload) triggered spontaneous Ca^{2+} waves in WT hearts. The same maneuver induced little or no Ca^{2+} waves in the D4646A$^{+/-}$ mutant hearts (Fig. 3, A to C). The D4646A$^{+/-}$ mutant hearts were also resilient to caffeine- and epinephrine-promoted spontaneous Ca^{2+} waves (fig. S6, A to C). Thus, this CRDS RyR2 LOF mutation markedly suppresses spontaneous Ca^{2+} waves in intact hearts, unlike the well-studied CPVT-linked RyR2 GOF mutations (*4*, *21*–*24*).

We also tested the susceptibility of the RyR2-D4646A$^{+/-}$ mutant mice to stress-induced VAs. High doses of caffeine and epinephrine are commonly used as pharmacological promoters in CPVT model mouse studies (*23*). However, the same pharmacological mixture did not promote VAs in the D4646A$^{+/-}$ mice (Fig. 3, D to G). Again, unlike typical CPVT RyR2 GOF mutations, this CRDS RyR2 LOF mutation protected the heart against stress-induced VAs. This action is consistent with the negative EST and the absence of typical CPVT phenotypes in human RyR2 D4646A$^{+/-}$ mutant carriers (see the "Genetic analyses and clinical evaluation of RyR2 mutant carriers presenting with life-threatening VAs distinct from CPVT" section in the Supplementary Materials).

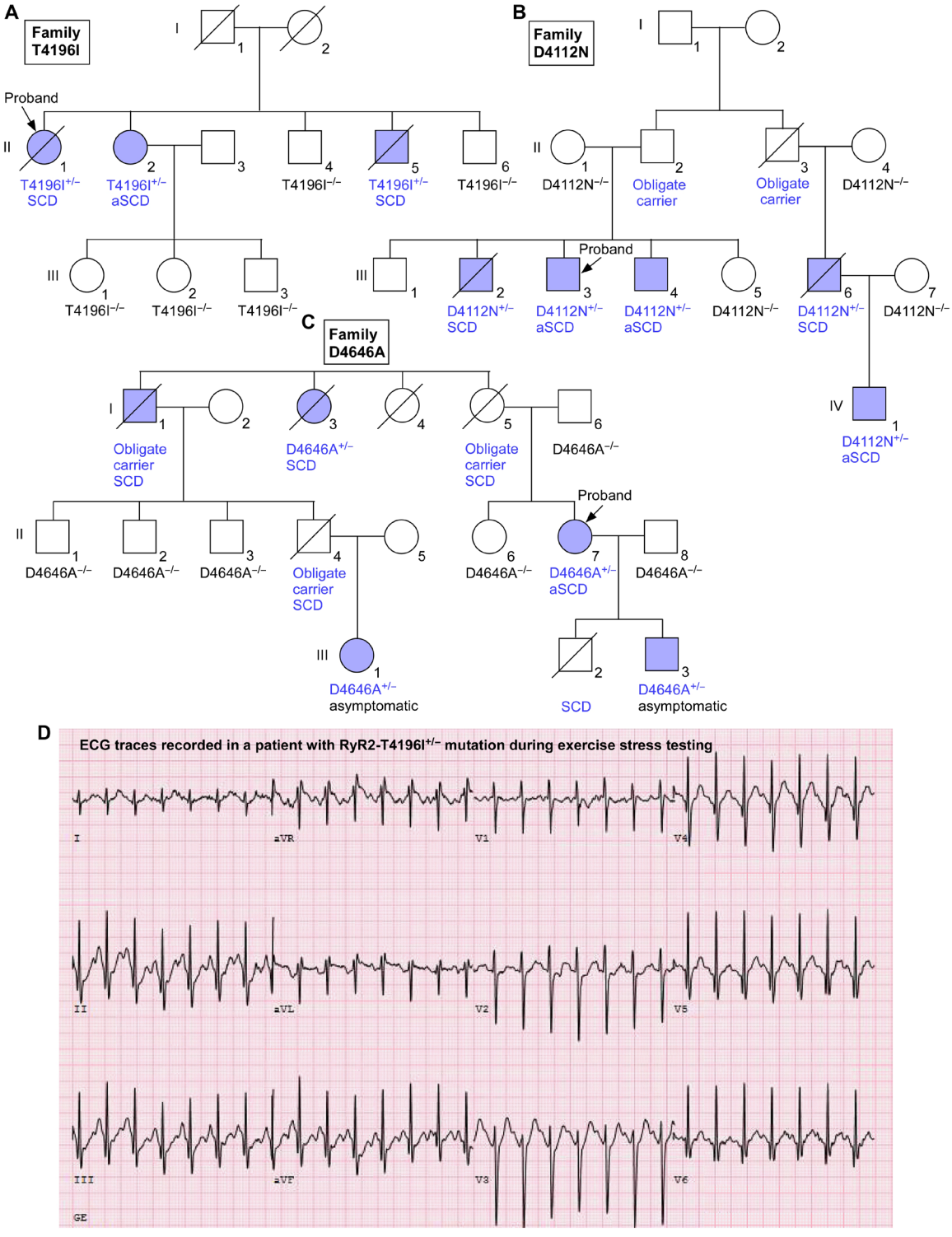

Fig. 1. Pedigrees of families with non-CPVT–associated RyR2 mutations. Families with RyR2 mutations T4196I$^{+/-}$ (**A**), D4112N$^{+/-}$ (**B**), and D4646A$^{+/-}$ (**C**). (**D**) ECG traces recorded during exercise stress testing. The letters on the ECG traces annotate the leads. There were no PVCs observed during the entire testing, and QT intervals under all conditions tested were within the normal limit. Squares and circles indicate males and females, respectively; blue symbols represent mutation carriers/obligate carriers; open symbols represent mutation-negative/unaffected persons; symbols with a slash represent deceased persons. Probands are indicated by an arrow. SCD, sudden cardiac death; aSCD, aborted SCD.

Table 1. Primary symptoms and exercise stress test outcome of RyR2 mutant carriers presenting with ventricular arrhythmias distinct from CPVT. SCD, sudden cardiac death; aSCD, aborted SCD; SUD, sudden unexplained death; LVNC, left ventricular non-compaction cardiomyopathy; IVF, idiopathic ventricular fibrillation; scTdP, short-coupled variant of Torsade de Pointes; LOF, loss of function. RyR2 mutations I4855M, A4860G, S4938F, and K4594R/I2075T have been previously reported (*12*, *15*–*17*). The functional impact of RyR2-I4855M, RyR2-A4860G, and RyR2-S4938F has been previously reported (*13*–*16*), but that of the K4594R/I2075T was characterized in this study.

RyR2 mutation	Primary symptoms	Exercise stress test (EST)	Symptomatic mutant carriers (total)	Symptomatic mutant-negative carriers (total)	Mutation impact
Q3774L$^{+/-}$	aSCD	Negative	1 (4)	0 (1)	LOF
I3995V$^{+/-}$	SCD/aSCD/SUD	Negative	5 (8)	0 (16)	LOF
D4112N$^{+/-}$	SCD/aSCD	Negative	5 (7)	0 (4)	LOF
T4196I$^{+/-}$	SCD/aSCD	Negative	3 (3)	0 (5)	LOF
D4646A$^{+/-}$	SCD/aSCD	Negative	5 (7)	0 (6)	LOF
Q4879H$^{+/-}$	aSCD	Negative	1 (1) (de novo)	0 (2)	LOF
I4855M$^{+/-}$	SCD/LVNC	Negative	2 (3)	0 (3)	LOF
A4860G$^{+/-}$	SCD/IVF	Negative	2 (3)	0 (1)	LOF
S4938F$^{+/-}$	scTdP	Negative	1 (3)	0 (4)	LOF
K4594R$^{+/-}$/I2075T$^{+/-}$	SCD/aSCD	Negative	6 (7)	0 (4)	LOF
			31 (46) (67%)	**0 (46) (0%)**	

RyR2-D4646A$^{+/-}$ promotes Ca^{2+} alternans, prolongs Ca^{2+} release refractoriness, alters action potential waveform, and enhances EAD propensity

To determine whether the RyR2 D4646A$^{+/-}$ mutation affects depolarization-induced SR Ca^{2+} release, we measured Ca^{2+} transients evoked by electrical stimulation at different frequencies in intact hearts. Although the D4646A$^{+/-}$ mutation suppresses spontaneous SR Ca^{2+} release, the amplitude, time to peak, and decay time of depolarization-induced Ca^{2+} transients at low stimulation frequencies in CRDS D4646A$^{+/-}$ mutant hearts or isolated cardiomyocytes were similar to those in WT (Fig. 3, H to M, and fig. S6, D to I). At high stimulation frequencies, however, mutant hearts were more prone to Ca^{2+} alternans (fig. S7, A to D). When stimulated at 10 Hz, WT hearts showed little or no Ca^{2+} alternans, whereas mutant hearts displayed substantial Ca^{2+} alternans. The effect of the CRDS D4646A$^{+/-}$ mutation on SR Ca^{2+} release refractoriness was also measured, and the D4646A$^{+/-}$ mutation prolonged the refractoriness (fig. S7, E to G).

To determine whether this CRDS RyR2 mutation alters action potential (AP) properties, the whole-cell patch-clamp technique was used to record APs in isolated WT and D4646A$^{+/-}$ mutant ventricular myocytes. The AP waveform in the D4646A$^{+/-}$ cells was markedly different from that in WT cells. The AP duration at 50% (APD_{50}) was shorter, and APD_{90} was prolonged in CRDS D4646A$^{+/-}$ mutant ventricular myocytes, whereas the AP amplitude and resting membrane potential were unchanged (Fig. 3, N to R). Intriguingly, D4646A$^{+/-}$ mutant cells were highly susceptible to early afterdepolarizations (EADs) compared to WT cells (Fig. 3, S and T). Thus, this CRDS RyR2 LOF mutation D4646A$^{+/-}$ produces systolic arrhythmogenic abnormalities, in stark contrast to the diastolic arrhythmogenic Ca^{2+} dysregulation associated with CPVT-causing RyR2 GOF mutations.

RyR2-D4646A$^{+/-}$ causes cardiac electrophysiological and structural remodeling

Although the RyR2-D4646A$^{+/-}$ mutation suppresses RyR2 function, the amplitude of Ca^{2+} transients in mutant ventricular myocytes was unchanged. This implies that the suppression of RyR2 function may have been compensated for by an increase in surface Ca^{2+} influx. To test this possibility, we measured the L-type Ca^{2+} channel current (I_{CaL}) using whole-cell patch-clamp. The I_{CaL} current density in D4646A$^{+/-}$ mutant ventricular myocytes was markedly enhanced compared to WT (Fig. 4, A to C). If more Ca^{2+} enters the cell per AP, then one would expect more to exit as well. Consistent with this prediction, the Na/Ca exchange current (I_{NCX}) was substantially augmented in D4646A$^{+/-}$ mutant ventricular myocytes (Fig. 4, D to G). This increased I_{CaL} and I_{NCX} current explains the prolonged APD_{90} and the higher EAD propensity in the mutant cells.

To explore why the D4646A$^{+/-}$ mutation shortens APD_{50}, we measured the transient outward K^+ current (I_{to}) and the Na current (I_{Na}). These are currents that govern early repolarization. The I_{to} current density and voltage-dependent activation were markedly enhanced in RyR2-D4646A$^{+/-}$ mutant ventricular myocytes compared to WT (Fig. 4, H to K, and fig. S8, A to D). As for I_{Na}, RyR2-D4646A$^{+/-}$ ventricular myocytes have a leftward (hyperpolarization) shift in voltage-dependent activation and inactivation compared to WT (Fig. 4, L to P). Together, these data indicate that the CRDS RyR2 D4646A$^{+/-}$ mutation results in a substantial electrophysiological remodeling of surface membrane currents.

We next performed histological and echocardiographic analyses to assess whether the D4646A$^{+/-}$ mutation affects cardiac structure and mechanical function. There were no marked differences in cardiac morphology and fibrosis between the WT and D4646A$^{+/-}$ mutant hearts as revealed by hematoxylin/eosin and picrosirius red staining (fig. S8, E and F). The D4646A$^{+/-}$ hearts displayed slightly reduced heart rate (~10%) and moderately increased (~20%) left ventricular wall thickness, whereas other echocardiographic parameters (such as ejection fraction, fractional shortening, stroke volume, and cardiac output) were unchanged (table S2).

To gain insights into the molecular basis of this electrophysiological and structural remodeling, we performed immunoblotting and MitoSOX staining analyses. The surface expression of Cav1.2

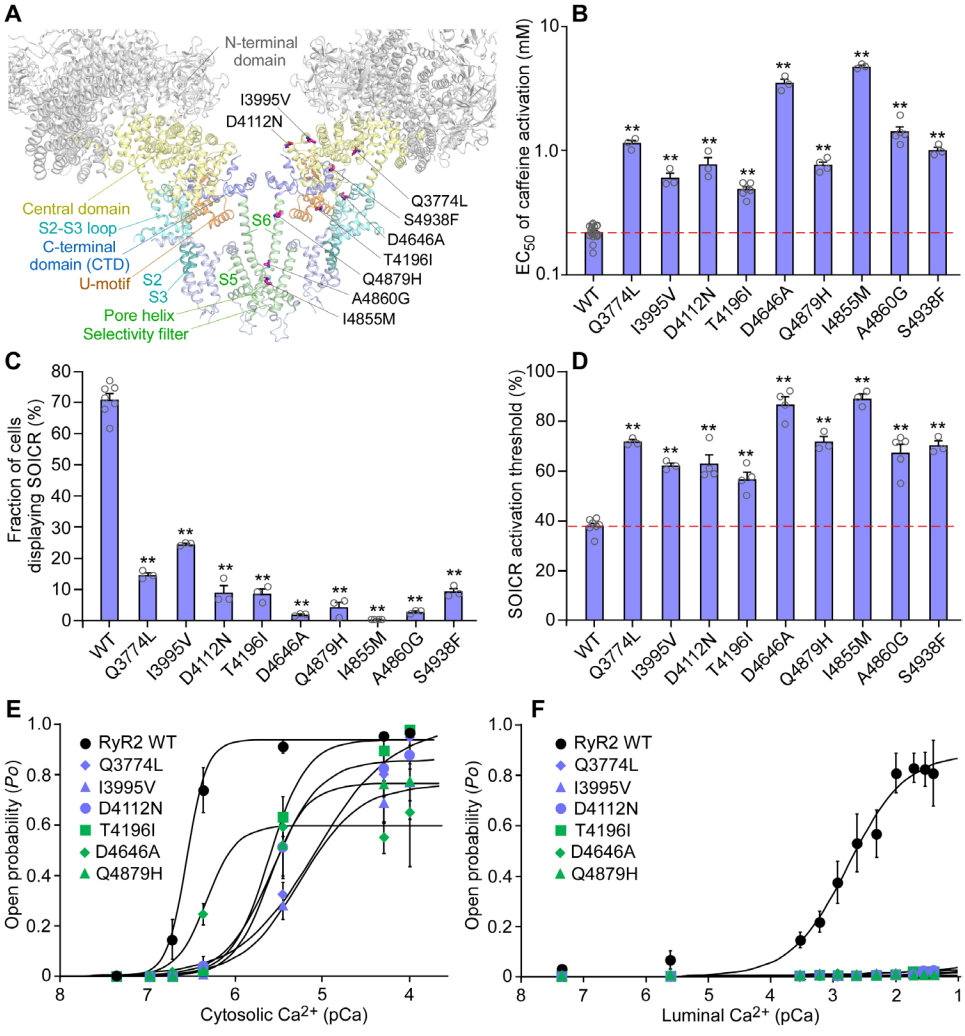

Fig. 2. Functional characterization of non-CPVT–associated RyR2 mutations. (**A**) Three-dimensional localization of RyR2 mutations. (**B**) EC_{50} (median effective concentration) values of caffeine-induced Ca^{2+} releases in HEK293 cells. Data are means ± SEM from RyR2-WT ($n = 18$), Q3774L ($n = 3$), I3995V ($n = 3$), D4112N ($n = 3$), T4196I ($n = 6$), D4646A ($n = 3$), Q4879H ($n = 4$), I4855M ($n = 3$), A4860G ($n = 5$), and S4938F ($n = 3$) (one-way ANOVA with Dunnett's post hoc test, $^{**}P < 0.01$ versus WT). Red dashed line represents the WT level. (**C**) Percentages of HEK293 cells displaying Ca^{2+} oscillations at 2 mM extracellular Ca^{2+} ($[Ca^{2+}]_o$). Data are means ± SEM from RyR2-WT ($n = 7$), Q3776L ($n = 3$), I3995V ($n = 3$), D4112N ($n = 3$), T4196I ($n = 3$), D4646A ($n = 3$), Q4879H ($n = 3$), I4855M ($n = 3$), A4860G ($n = 3$), and S4938F ($n = 3$) (one-way ANOVA with Dunnett's post hoc test, $^{**}P < 0.01$ versus WT). (**D**) Activation thresholds for store overload–induced Ca^{2+} release (SOICR) in HEK293 cells. Data are means ± SEM from RyR2-WT ($n = 7$), Q3774L ($n = 3$), I3995V ($n = 3$), D4112N ($n = 4$), T4196I ($n = 4$), D4646A ($n = 4$), Q4879H ($n = 3$), I4855M ($n = 3$), A4860G ($n = 5$), and S4938F ($n = 3$) (one-way ANOVA with Dunnett's post hoc test, $^{**}P < 0.01$ versus WT) (n refers to the number of separate experiments). Red dashed line represents the WT level. (**E**) Open probability (Po) of single RyR2-WT or mutant channels activated by cytosolic Ca^{2+}. Data are means ± SEM from RyR2-WT ($n = 6$ channels), Q3774L ($n = 5$), I3995V ($n = 5$), D4112N ($n = 5$), T4196I ($n = 5$), D4646A ($n = 6$), and Q4879H ($n = 5$). (**F**) Po of single RyR2-WT or mutant channels activated by luminal Ca^{2+}. Data are means ± SEM from RyR2-WT ($n = 8$ channels), Q3774L ($n = 5$), I3995V ($n = 5$), D4112N ($n = 5$), T4196I ($n = 5$), D4646A ($n = 5$), and Q4879H ($n = 5$).

was unchanged (fig. S8, G to J). MitoSOX staining revealed no evidence for altered oxidative stress in D4646A$^{+/-}$ ventricular myocytes (fig. S8, K and L). There were no significant differences in the total protein expression of Cav1.2, Cavβ2, NCX1.1, Nav1.5, Kv4.2, Kv4.3, KChIP2, KChIP4, RyR2, SERCA2a, CASQ2, triadin, or junctin between WT and D4646A$^{+/-}$ hearts (figs. S9 and S10). There was an increase in the expression of the phosphatase PP2 (protein phosphatase 2) in the D4646A$^{+/-}$ heart compared to WT, whereas phosphorylation of RyR2 (at S2808 and S2814) and calcium/calmodulin-dependent protein kinase II (CaMKII) and the total protein expression of CaM, PP1, protein kinase A (PKA), and CaMKII were unchanged (fig. S10). Thus, alterations in the expression of channel modulators (e.g., PP2) may in part contribute to the remodeling.

A diagnostic test for RyR2-CRDS

There are currently no clinical tests to distinguish potentially lethal RyR2 LOF mutations from presumably benign RyR2 rare variants, observed in ~3% of the general population (*18*, *19*). To address this unmet need, we leveraged our RyR2-D4646A$^{+/-}$ mouse model to develop a RyR2-CRDS–specific diagnostic procedure. We performed in vivo intracardiac electrogram recordings to assess the VA inducibility of three common stimulation protocols: a burst pacing, a long pause, and a short-coupled premature ventricular complex (S1S2 stimulation). None of the common stimulation protocols reliably induced VAs in CRDS RyR2-D4646A$^{+/-}$ mice (Fig. 5, A to F). We then identified an effective three-component protocol. This protocol consists of a long-burst, long-pause, and short-coupled (LBLPS) extra-stimulus. This LBLPS protocol robustly and consistently triggered VAs in CRDS RyR2-D4646A$^{+/-}$ mutant mice (Fig. 5, G to L). To assess CRDS specificity of this LBLPS stimulation protocol, we applied it to both WT and CPVT RyR2-R4496C$^{+/-}$ GOF mutant mice. The LBLPS stimulation protocol induced little or no VAs in WT or CPVT mice (Fig. 5, G to L), indicating that the LBLPS protocol is RyR2-CRDS specific.

An electrical pattern reminiscent of the LBLPS protocol was captured just before VA onset by an implantable cardioverter defibrillator (ICD) in a patient harboring the CRDS RyR2-D4112N$^{+/-}$ mutation (Fig. 5M). This observation and the robust effectiveness of LBLPS in mice prompted us to study the LBLPS protocol in humans harboring CRDS RyR2 mutations. We successfully recruited and tested two patients with RyR2-CRDS harboring the I3995V$^{+/-}$ and T4196I$^{+/-}$ mutation, respectively. The LBLPS stimulation sequence induced an episode of polymorphic VA in these patients with CRDS RyR2 (Fig. 5, N and O). Although still in the proof-of-concept stage in humans, LBLPS appears to be a viable CRDS-specific diagnostic tool. This is critical given that the phenotype of

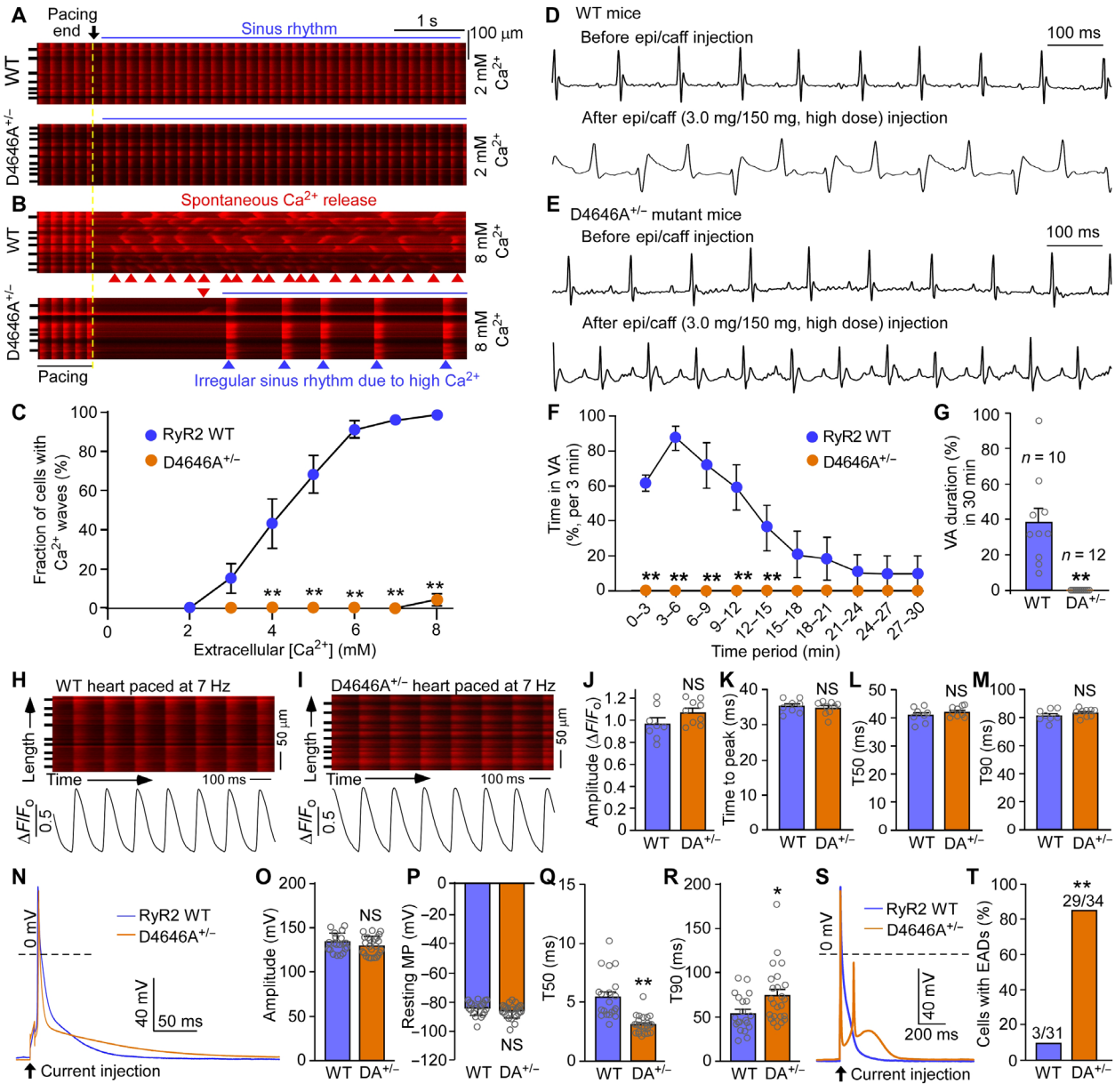

Fig. 3. Effects of RyR2-D4646A$^{+/-}$ on spontaneous Ca^{2+} release, stress-induced VAs, Ca^{2+} transients, and action potential. In situ confocal line-scanning imaging of Ca^{2+} transients in intact RyR2-WT and D4646A$^{+/-}$ mutant mouse hearts perfused with 2 mM (**A**) or 8 mM (**B**) extracellular Ca^{2+} and paced at 6 Hz followed by an abrupt cessation. Red arrowheads indicate spontaneous Ca^{2+} release events. Blue arrowheads indicate irregular sinus rhythm due to high Ca^{2+}. (**C**) Percentages of cells in intact WT or D4646A$^{+/-}$ hearts that displayed spontaneous Ca^{2+} waves. Data are means ± SEM from RyR2-WT ($n = 7$ hearts) and D4646A$^{+/-}$ ($n = 7$ hearts) (two-way ANOVA repeated measurement with Bonferroni's post hoc test, $^{**}P < 0.01$versus WT). ECG traces of RyR2-WT (**D**) and D4646A$^{+/-}$ (**E**) mice before and after injection of epinephrine (epi; 3.0 mg/kg) and caffeine (caff; 150 mg/kg). VA duration (%) within each 3-min (**F**) or 30-min (**G**) ECG recordings. Data are means ± SEM from RyR2-WT ($n = 10$ mice) and D4646A$^{+/-}$ ($n = 12$ mice) (Student's t test, $^{**}P < 0.01$ versus WT). Depolarization-evoked Ca^{2+} transients in intact RyR2-WT (**H**) and D4646A$^{+/-}$ mutant hearts (**I**). Cell boundaries are indicated by short bars to the left. The $\Delta F/F_o$ traces depict the average fluorescence signal of the scan area. (**J**) Amplitude, (**K**) time to peak, (**L**) time to 50% decay of Ca^{2+} transients, and (**M**) time to 90% decay of Ca^{2+} transients at 7 Hz. Data are means ± SEM from RyR2-WT ($n = 8$ hearts) and D4646A$^{+/-}$ ($n = 9$ hearts). (Student's t test; NS, not significant) (**N**) Whole-cell current-clamp recordings of action potential (AP). (**O**) AP amplitude and (**P**) resting membrane potential (MP) from RyR2-WT ($n = 20$ cells, four mice) and D4646A$^{+/-}$ ($n = 24$ cells, five mice) (Mann-Whitney U test and Student's t test). AP duration (APD) at (**Q**) 50% and (**R**) 90% repolarization (APD_{50} and APD_{90}), respectively. Data are means ± SEM from RyR2-WT ($n = 20$ cells, four mice) and D4646A$^{+/-}$ ($n = 24$ cells, five mice) (Mann-Whitney U test; $^{*}P < 0.05$ and $^{**}P < 0.01$ versus WT). (**S**) Membrane potential recordings at 1 Hz. (**T**) Percentages of cells showing early afterdepolarizations (EADs). Data are means ± SEM from RyR2-WT ($n = 31$ cells, six mice) (chi-square test; $^{**}P < 0.01$ versus WT) and D4646A$^{+/-}$ ($n = 34$ cells, six mice).

RyR2-CRDS would otherwise be concealed before the onset of life-threatening VAs. Hence, this diagnostic tool may distinguish dangerous RyR2 LOF mutations from the benign background genomic noise.

Quinidine and flecainide suppress VA in CRDS model mice

We used the LBLPS protocol and the D4646A$^{+/-}$ mouse model to explore potential medical therapies for CRDS. Our electrophysiological studies revealed that the RyR2 D4646A$^{+/-}$ mutation results in

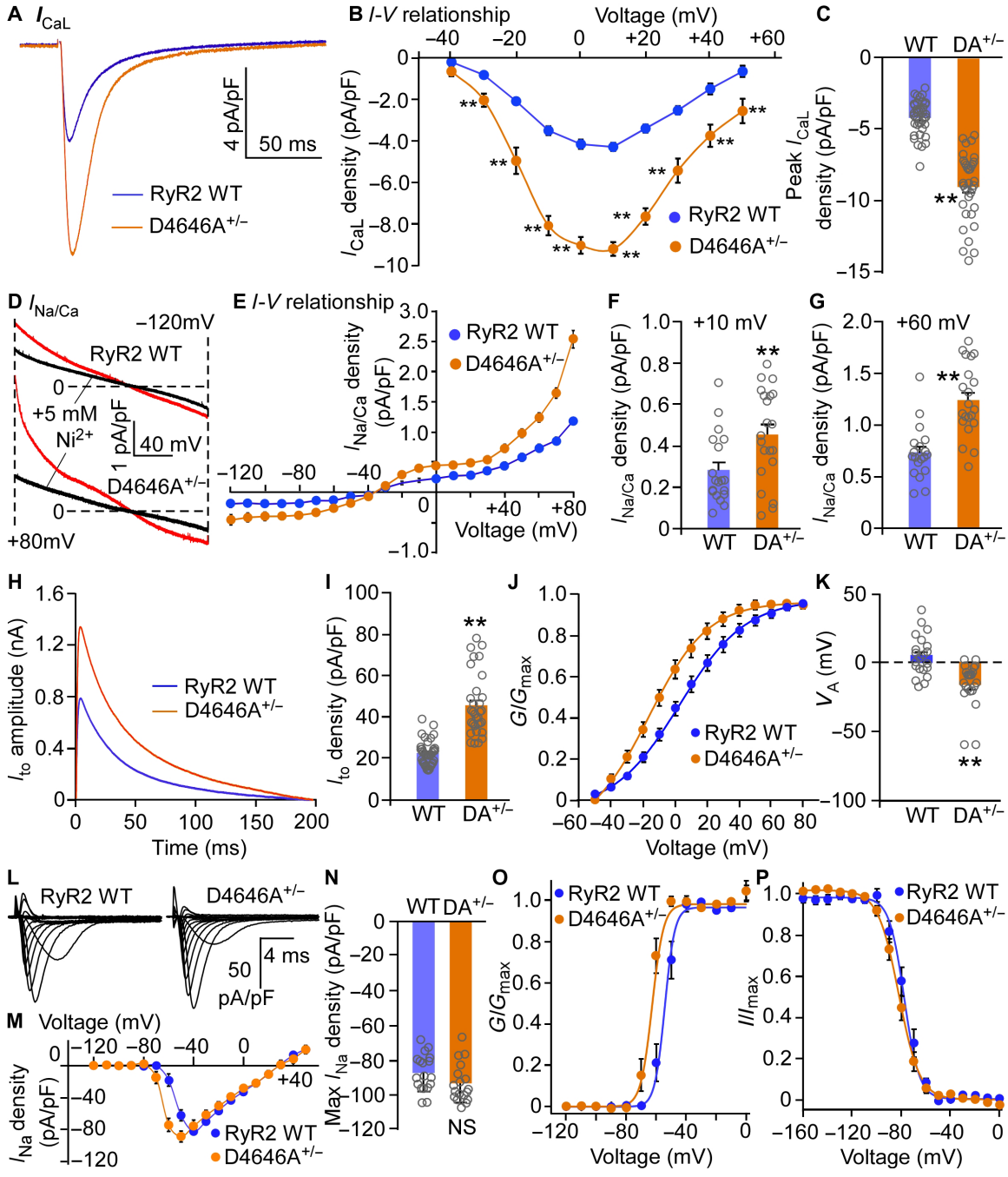

Fig. 4. Effects of RyR2-D4646A$^{+/-}$ on Ca^{2+}, K^+, and Na^+ currents in murine ventricular myocytes. (**A**) Whole-cell voltage-clamp recording of the L-type Ca^{2+} current (I_{CaL}). (**B**) Current-voltage relationship (*I-V* curve) of I_{CaL}. (**C**) Peak I_{CaL} densities at +10 mV. Data are means ± SEM from RyR2-WT ($n = 39$ cells, five mice) and D4646A$^{+/-}$ ($n = 35$ cells, six mice). (**D**) The Na/Ca exchange current (I_{NCX}) before and after addition of 5 mM Ni^{2+}. (**E**) *I-V* relationship of I_{NCX}. I_{NCX} densities at +10 mV (**F**) and at +60 mV (**G**). Data are means ± SEM from RyR2-WT ($n = 19$ cells, four mice) and D4646A$^{+/-}$ ($n = 21$ cells, four mice). (**H**) Whole-cell voltage-clamp recording of the transient outward K^+ current (I_{to}). (**I**) Peak I_{to} densities. Data are means ± SEM from RyR2-WT ($n = 38$ cells, four mice) and D4646A$^{+/-}$ ($n = 33$ cells, five mice). (**J**) Voltage dependence of steady-state activation of I_{to} (G for K^+ conductance). (**K**) Half-activated voltage (V_A) of I_{to}. Data are means ± SEM from RyR2-WT ($n = 21$ cells, four mice) and D4646A$^{+/-}$ ($n = 20$ cells, five mice). (**L**) Whole-cell voltage-clamp recording of the sodium current (I_{Na}). (**M**) *I-V* relationships of I_{Na}. (**N**) Maximum I_{Na} density from RyR2-WT ($n = 18$ cells, four mice) and D4646A$^{+/-}$ ($n = 18$ cells, four mice). Voltage dependence of steady-state activation (**O**) and inactivation (**P**) of I_{Na}. Data are means ± SEM from RyR2-WT ($n = 18$ cells, four mice) and D4646A$^{+/-}$ ($n = 18$ cells, four mice) (Mann-Whitney *U* test and Student's *t* test; $^{**}P < 0.01$ versus WT).

substantial electrophysiological remodeling, including increased L-type Ca^{2+} channel (I_{CaL}) and transient outward K^+ (I_{to}) currents, and a hyperpolarization shift in the voltage-dependent activation of the Na^+ channel (Fig. 4). Thus, suppressing these channels in RyR2-D4646A$^{+/-}$ mouse hearts may limit the VA risk associated with CRDS. Quinidine sulfate and flecainide have multiple inhibitory actions on both outward and inward currents (I_{Na}, I_{CaL}, and I_{to}) (*25*–*29*). Pretreatment of the D4646A$^{+/-}$ mutant mice with

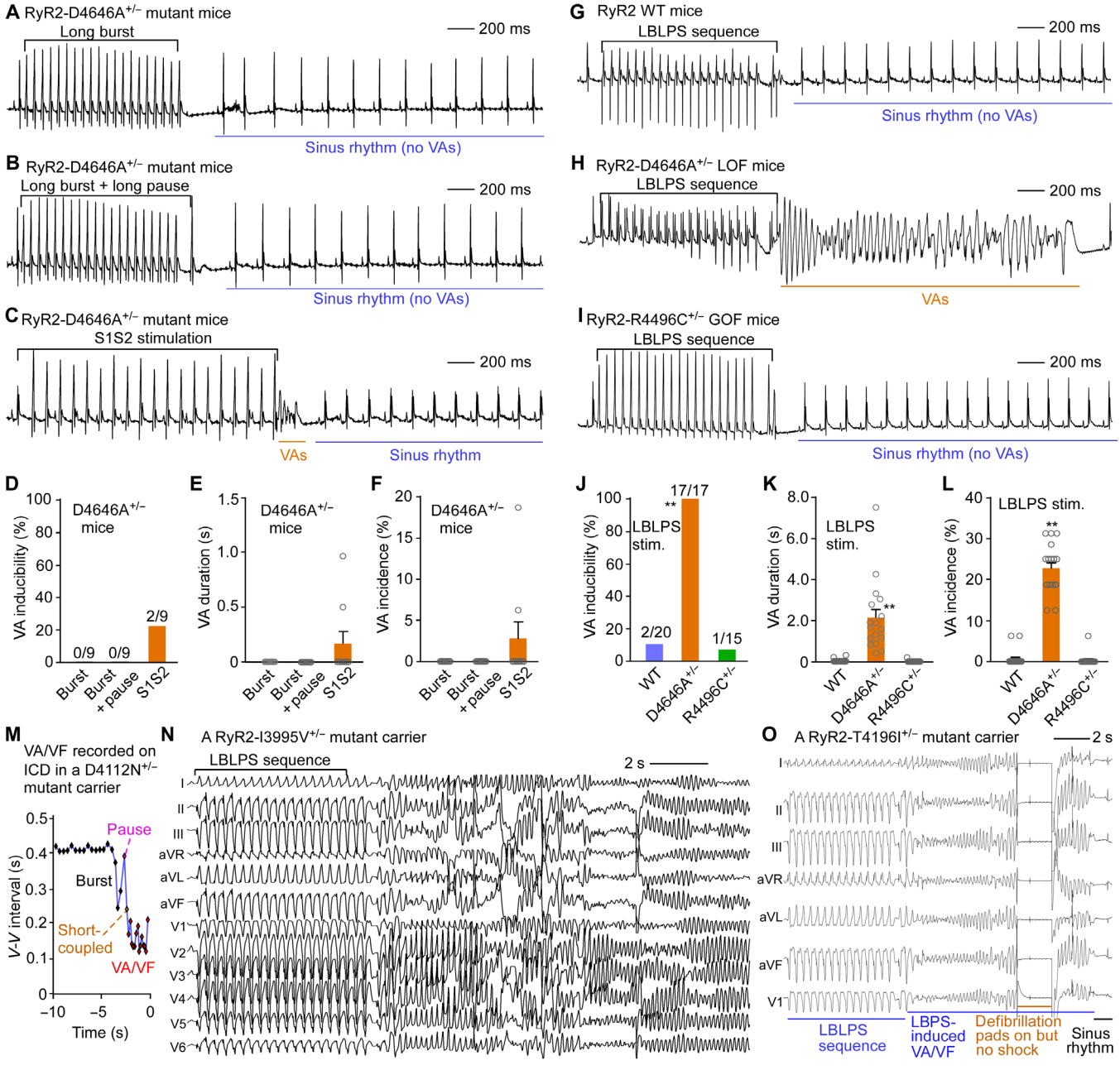

Fig. 5. VA induction in RyR2-WT and mutant mice and in humans with RyR2 LOF mutations by programed electrical stimulation. (**A**) ECG trace after a long burst (20 beats, 60-ms interval). (**B**) ECG trace after a long burst followed by a long pause (122 ms) and a stimulus. (**C**) ECG trace after a basal pacing (S1, 20 beats, 100-ms interval) followed by a short-coupled extra-stimulus (S2). The S1S2 interval was progressively reduced from 78 to 18 ms with 4-ms steps. (**D**) VA inducibility, (**E**) averaged VA duration, and (**F**) VA incidence in RyR2-D4646A$^{+/-}$ mice paced by different stimulation protocols. Data are means ± SEM from D4646A$^{+/-}$ (n = 9 mice). ECG traces recorded in RyR2-WT (**G**), D4646A$^{+/-}$ (**H**), and R4496C$^{+/-}$ (**I**) mice after the long-burst, long-pause, and short-coupled (LBLPS) stimulation protocol. (**J**) VA inducibility, (**K**) averaged VA duration, and (**L**) VA incidence in RyR2-WT, D4646A$^{+/-}$, and R4496C$^{+/-}$ mice after the LBLPS stimulation. Data are means ± SEM from RyR2-WT (n = 20 mice), D4646A$^{+/-}$ (n = 17 mice), and R4496C$^{+/-}$ (n = 15 mice) (chi-square test; Kruskal-Wallis test with Dunn-Bonferroni post hoc test, $^{**}P < 0.01$ versus WT). (**M**) *V-V* intervals recorded on ICD in a RyR2-D4112N$^{+/-}$ mutant carrier before and after the onset of VA/ventricular fibrillation (VF). ECG traces of VAs evoked by the LBLPS stimulation protocol in humans harboring the RyR2-I3995V$^{+/-}$ (**N**) and RyR2-T4196I$^{+/-}$ (**O**) mutations.

quinidine sulfate (40 mg/kg per day for 6 days) or flecainide (20 mg/kg per day for 6 days) markedly reduced the duration and incidence of LBLPS-evoked polymorphic VAs (Fig. 6). This indicates that pharmacological suppression of I_{to}, I_{Na}, and I_{CaL} (combined) may serve as a potentially viable anti-CRDS therapeutic strategy.

Large Ca^{2+} transient amplitude due to enhanced SR Ca^{2+} load triggers LBLPS-evoked VAs in D4646A$^{+/-}$ hearts

We next used the LBLPS protocol to better understand the trigger mechanism of VA in hearts harboring a CRDS RyR2 mutation. To this end, we assessed intracellular Ca^{2+} dynamics in

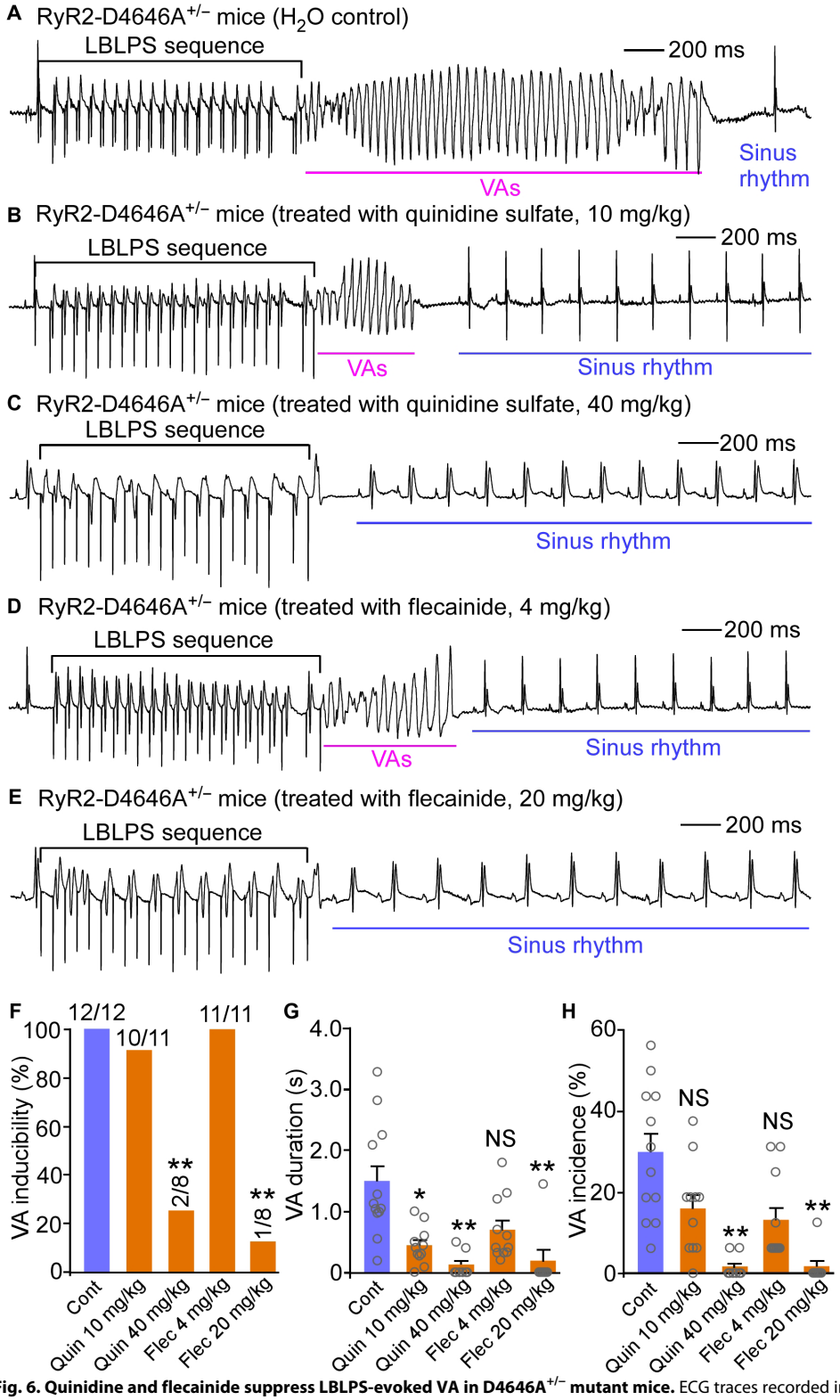

Fig. 6. Quinidine and flecainide suppress LBLPS-evoked VA in D4646A$^{+/-}$ mutant mice. ECG traces recorded in D4646A$^{+/-}$ mice after the LBLPS stimulation after injection of vehicle (H_2O, control) (**A**), quinidine sulfate (10 or 40 mg/kg per day for 6 days, ip) (**B** and **C**) or flecainide (4 or 20 mg/kg per day for 6 days, ip) (**D** and **E**) with VA inducibility (**F**), averaged VA duration (**G**), and VA incidence (**H**) shown. Data are means ± SEM from D4646A$^{+/-}$ mutant mice ($n = 12$ mice for control, $n = 11$ mice for 10 mg/kg per day of quinidine, $n = 8$ mice for 40 mg/kg per day of quinidine, $n = 11$ mice for 4 mg/kg per day of flecainide, and $n = 8$ for 20 mg/kg per day of flecainide) (chi-square test; Kruskal-Wallis test with Dunn-Bonferroni post hoc test, $^*P < 0.05$ and $^{**}P < 0.01$ versus control).

cardiomyocytes in intact hearts from RyR2-WT, RyR2-D4646A$^{+/-}$ (CRDS), or RyR2-R4496C$^{+/-}$ (CPVT) mutant mice using in situ confocal Ca^{2+} imaging. LBLPS induced VA-like irregular Ca^{2+} transients in the CRDS RyR2-D4646A$^{+/-}$ hearts but not in CPVT RyR2-R4496C$^{+/-}$ or WT hearts (Fig. 7, A to F), indicating that the RyR2-CRDS hearts are uniquely prone to LBLPS-induced VA-like Ca^{2+} transient irregularity. During the burst phase of LBLPS stimulation, the amplitude of Ca^{2+} transients (normalized to that at 6 Hz) was reduced in CRDS RyR2-D4646A$^{+/-}$ hearts but not in CPVT RyR2-R4496C$^{+/-}$ hearts (Fig. 7, A to C and G to I). This is likely due to the prolonged SR Ca^{2+} release refractoriness present in the RyR2-D4646A$^{+/-}$ CRDS model heart.

There was no difference in either the amplitude or decay time of the Ca^{2+} transients at 6 Hz in WT, CRDS (D4646A$^{+/-}$), and CPVT (R4496C$^{+/-}$) hearts (Fig. 7, G and H, and fig. S11, A to C). However, the amplitude of Ca^{2+} transients after the long pause (normalized to that at 6 Hz) was increased in CRDS (D4646A$^{+/-}$) hearts but not in CPVT (R4496C$^{+/-}$) hearts (Fig. 7, A to C and J). This increase in Ca^{2+} transient amplitude after the long pause in CRDS (D4646A$^{+/-}$) hearts could reflect an elevation in SR Ca^{2+} load. To directly test this prediction, we measured the SR Ca^{2+} content after the burst and long pause. The SR Ca^{2+} content in CRDS (D4646A$^{+/-}$) ventricular myocytes was elevated compared to WT, whereas the SR Ca^{2+} load in CPVT (R4496C$^{+/-}$) myocytes was reduced (fig. S11, D to G). The elevated SR Ca^{2+} load in the D4646A$^{+/-}$ ventricular myocytes is unlikely to be related to phospholamban (PLB), because phosphorylation of PLB was decreased in the D4646A$^{+/-}$ hearts compared to WT, although the total protein expression of PLB was unchanged (fig. S10).

In light of the enhanced I_{NCX} and increased EAD propensity in CRDS (D4646A$^{+/-}$) hearts, the increased Ca^{2+} transient amplitude after the long pause is highly likely to induce EADs. Thus, the burst-pause–induced increase in the Ca^{2+} transient amplitude may act as a trigger for LBLPS-induced VAs via an EAD-mediated reentrant mechanism. To test this possibility, we performed high-resolution optical mapping to

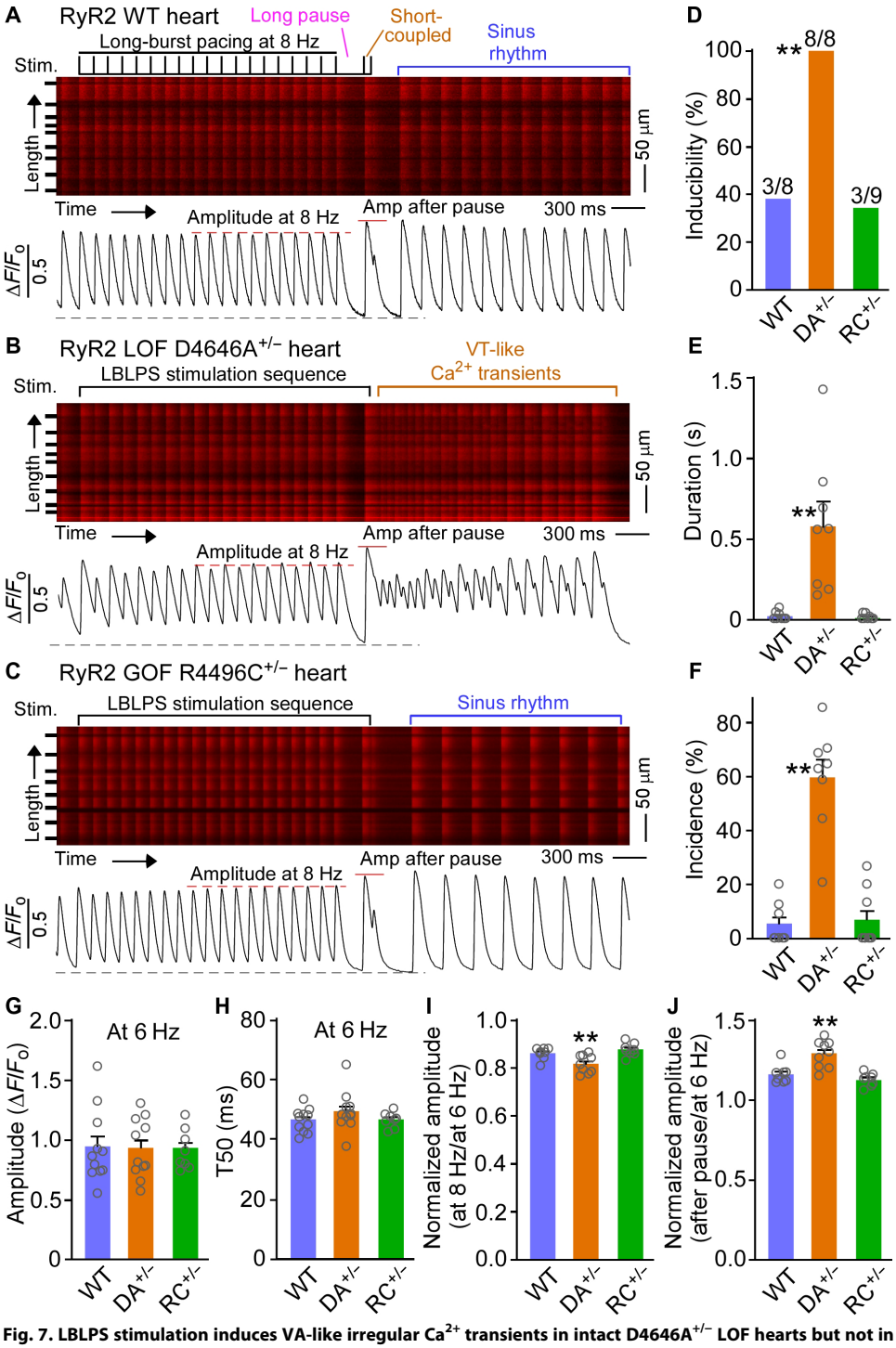

Fig. 7. LBLPS stimulation induces VA-like irregular Ca^{2+} transients in intact D4646A$^{+/-}$ LOF hearts but not in WT or R4496C$^{+/-}$ GOF mouse hearts. Ca^{2+} transients in intact RyR2-WT (**A**), D4646A$^{+/-}$ (**B**), and R4496C$^{+/-}$ (**C**) mutant hearts after the LBLPS stimulation. (**D**) Inducibility, (**E**) average duration, and (**F**) incidence of VA-like irregular Ca^{2+} transients evoked by LBLPS. Data are means ± SEM from RyR2-WT ($n = 8$ hearts), D4646A$^{+/-}$ ($n = 8$ hearts), and R4496C$^{+/-}$ ($n = 9$ hearts) (chi-square test; Kruskal-Wallis test with Dunn-Bonferroni post hoc test, $^{**}P < 0.01$ versus WT). (**G**) Amplitude and (**H**) time to 50% decay of Ca^{2+} transients in intact RyR2-WT, DA$^{+/-}$, and RC$^{+/-}$ hearts paced at 6 Hz. Data are means ± SEM from RyR2-WT ($n = 11$ hearts), DA$^{+/-}$ ($n = 11$ hearts), and RC$^{+/-}$ ($n = 8$ hearts). Amplitudes of Ca^{2+} transients at 8 Hz during the long burst (**I**) and after the long pause (**J**) of the LBLPS protocol, normalized to the transient amplitude at 6 Hz, in RyR2-WT, DA$^{+/-}$, and RC$^{+/-}$ hearts. Data are means ± SEM from RyR2-WT ($n = 8$ hearts), DA$^{+/-}$ ($n = 9$ hearts), and RC$^{+/-}$ ($n = 8$ hearts) (chi-square test; one-way ANOVA with Dunnett's post hoc test, $^{**}P < 0.01$ versus WT).

measure patterns of conduction in isolated Langendorff-perfused RyR2-WT and RyR2-D4646A$^{+/-}$ mutant hearts. As expected, all WT hearts showed activations near the apex of the heart that conducted uniformly through the right and left ventricles with no arrhythmias after LBLPS stimulation. In contrast, all RyR2-D4646A$^{+/-}$ mutant hearts displayed a reentrant pattern of conduction after LBLPS stimulation (fig. S12, A to C). We also observed APD alternans in all RyR2-D4646A$^{+/-}$ mutant hearts but not in WT hearts during the long-burst (9-Hz) component of the LBLPS stimulation sequence (fig. S12D). Given the close link between electrical rotors and reentrant activity, our optical mapping data support the notion that RyR2-CRDS enhances the propensity for reentrant arrhythmias.

DISCUSSION

Multiple RyR2 GOF mutations are known to cause CPVT, which is routinely diagnosed clinically using the EST (*4*, *6*–*8*, *10*, *11*). In the setting of unexplained cardiac arrests, reports have emerged in the literature that have identified patients having RyR2 mutations with negative EST (*12*, *15*–*17*). The pathological significance of these RyR2 mutations is often unclear given that 3% of the general population has a rare RyR2 variant (*18*, *19*). In this context, it may be very difficult to distinguish whether this genetic result is a benign, incidental finding or the underlying culprit responsible for the unexplained cardiac arrests. Recent observations have suggested that pathogenic RyR2 LOF mutations may account for these findings (*12*, *15*–*17*); however, reports to date have been limited to single patients or small families, precluding a definitive link between genotype and phenotype. Unfortunately, this has resulted in patients being left with unclear diagnoses, which has often precluded optimal management of both probands and potentially vulnerable family members. Here, our systematic clinical, genetic, functional, and linkage analyses establish that RyR2 LOF mutations cause a previously unknown disease entity associated with life-threatening VAs, which we refer to as RyR2-CRDS. The clinical importance of establishing RyR2-CRDS as a previously unknown arrhythmia

syndrome extends beyond just providing an explanation to currently unexplained SCD/aSCD cases. Proper diagnosis of RyR2-CRDS not only allows for optimal management of the proband but may also help to save the lives of family members also having life-threatening RyR2 LOF mutations.

RyR2 GOF mutations cause CPVT by promoting abnormal diastolic spontaneous SR Ca^{2+} release (*4*, *21*, *22*, *24*, *30*–*32*), which drives DADs and thus increases the risk of triggered activities and VAs (*4*, *33*–*35*). In stark contrast, we show that CRDS RyR2-D4646A$^{+/-}$ LOF mutation abolished abnormal diastolic spontaneous SR Ca^{2+} release in intact mouse hearts, completely protecting them against DAD-driven VAs. Thus, the arrhythmogenic mechanism associated with RyR2-CRDS is different from that of CPVT. The CRDS RyR2-D4646A$^{+/-}$ mutation causes a substantial electrophysiological remodeling in the heart, increasing I_{to}, I_{CaL}, and I_{NCX}. This alters AP waveform (i.e., shortens APD_{50} and lengthens APD_{90}) and increases the propensity for arrhythmogenic EADs in the CRDS hearts. Thus, RyR2 LOF may cause VAs via an EAD-mediated mechanism, similar to that proposed for the RyR2-A4860G$^{+/-}$ LOF mutation (*14*).

Until now, there have been no diagnostic tests for RyR2-CRDS. However, there is a critical need for developing a diagnostic test capable of unmasking the dangerous RyR2-CRDS phenotype. This would enable classification of a rare RyR2 variant as potentially dangerous or benign without requiring in vitro functional testing. Using our CRDS RyR2-D4646A$^{+/-}$ mouse model, we established a three-component stimulation sequence, termed LBLPS. Although sharing some common features, this LBLPS sequence is slightly different from the previously described "abrupt short-to-long cycle length change" protocol (*36*), in the relatively long-burst pacing period before the long pause. We tested LBLPS on WT, CPVT (RyR2-R4496C$^{+/-}$), and CRDS (RyR2-D4646A$^{+/-}$) mice and demonstrated that LBLPS is an effective and specific test for RyR2-CRDS, because it induced VAs only in CRDS (RyR2-D4646A$^{+/-}$) but not in WT or CPVT (RyR2-R4496C$^{+/-}$) mouse models. An electrocardiogram (ECG) pattern similar to the LBLPS protocol was captured just before VA onset in a patient with RyR2-CRDS, suggesting that LBLPS may be able to trigger VAs in patients with RyR2-CRDS. In two patients with RyR2-CRDS, the LBLPS protocol successfully induced polymorphic VAs. Thus, our LBLPS stimulation protocol represents a promising means to potentially diagnose and assess SCD risk in patients with RyR2-CRDS.

The LBLPS sequence not only provides a potential CRDS diagnostic tool but also provides a means to explore the triggering mechanism underlying RyR2 LOF–associated VAs. Our studies show that LBLPS stimulation results in a substantial increase in SR Ca^{2+} load after a relatively long period of burst pacing and the long pause, likely as a result of increased Ca^{2+} influx (I_{CaL}) and diminished SR Ca^{2+} leak due to RyR2 LOF. Elevated SR Ca^{2+} load has also been observed in the RyR2-A4860G$^{+/-}$ and RyR2-E4872Q$^{+/-}$ LOF mutant mouse models (*14*, *37*). Thus, increased SR Ca^{2+} load may be a common consequence of RyR2 LOF mutations during rapid pacing. The consequence is an aberrantly large Ca^{2+} transient during the post-pause beat in the CRDS (RyR2-D4646A$^{+/-}$) hearts. Given the enhanced I_{NCX} and increased EAD propensity in these hearts, this large Ca^{2+} transient would increase the likelihood that a short-coupled extra-stimulus will induce EADs and EAD-mediated arrhythmias. In other words, the aberrantly large Ca^{2+} transient during the post-pause beat after rapid pacing is likely what triggers VAs in the EAD-prone CRDS RyR2-D4646A$^{+/-}$ heart by the LBLPS sequence. Thus, RyR2 Ca^{2+} release deficiency likely increases the propensity for producing both the trigger and the substrate for EAD-mediated reentrant arrhythmia. In support of this view, we observed reentrant-related electrical rotor activities after LBLPS stimulation in the RyR2-D4646A$^{+/-}$ mutant hearts but not in WT.

Given the broad electrophysiological remodeling occurring in the RyR2 LOF hearts, simply targeting one augmented current (e.g., I_{Na}, I_{to}, I_{CaL}, or I_{NCX}) may not be effective or may even be harmful, as suppressing one of these enhanced currents may perturb the newly adapted balance between depolarization and repolarization in the RyR2 LOF hearts. To minimize potential perturbation to the newly adapted balance, one could simultaneously target both the outward and inward currents. In support of this idea, we found that both quinidine and flecainide (inhibitors of I_{to}, I_{CaL}, and I_{Na}) (*25*, *26*) suppress LBLPS-evoked VAs in CRDS (RyR2-D4646A$^{+/-}$) model hearts, suggesting that these agents may serve as effective anti-CRDS therapeutics.

The pathophysiological ramifications of RyR2 LOF mutations are heterogeneous. The RyR2-A4860G$^{+/-}$ mutation, for example, is associated with idiopathic ventricular fibrillation (*12*). The RyR2-A4860G$^{+/-}$ mutation reduces Ca^{2+} transient amplitude but has no effect on the amplitude of I_{CaL} (*14*). On the other hand, the RyR2-D4646A$^{+/-}$ mutation has no effect on the Ca^{2+} transient amplitude but markedly increases I_{CaL}. The RyR2-I4855M$^{+/-}$ mutation is associated not only with cardiac arrhythmias but also with left ventricular non-compaction (LVNC) (*16*). The RyR2-K4594R$^{+/-}$/I2075T$^{+/-}$ double mutation is associated not only with VAs but also with seizures (*17*). Furthermore, the RyR2-S4938F$^{+/-}$ mutation is associated with short-coupled variant of Torsade de Pointes (scTdP) (*15*). Therefore, not all RyR2 LOF mutations have the same pathogenic ramifications in the heart and affect function of other tissues. The resulting phenotypic heterogeneity is likely due to different degrees of cardiac remodeling and/or various degrees of pathogenic RyR2 dysfunction in other tissues. In this regard, our RyR2-D4646A$^{+/-}$ LOF mutant mouse model is unlikely to recapitulate all of the phenotypes observed with RyR2-CRDS in humans. Thus, CRDS ought to be considered as a multifaceted syndrome.

There are several limitations in the present study. It is unknown how RyR2 LOF results in increased I_{to}, I_{CaL}, and I_{NCX} with unchanged total protein expression. Further detailed and comprehensive investigations are required to assess potential changes in the expression of modulators and posttranslational modifications of these channels/exchangers. It is also unclear why patients with RyR2 LOF mutations have normal QT intervals despite that RyR2 LOF substantially altered the AP waveform in RyR2 LOF model mice. It is possible that the concomitant increases in both the outward K^+ current (I_{to}) and the inward Ca^{2+} current (I_{CaL}) may compensate for each other with respect to the overall APD. As a result, RyR2 LOF may have minimal impact on the QT interval. The low number of patients with RyR2-CRDS that we could recruit for testing is also a limitation. Further electrophysiological studies of more patients with CRDS will be needed to fully establish the CRDS specificity and sensitivity of the LBLPS protocol in humans.

In summary, this study establishes RyR2 LOF as causative for a previously unknown inherited arrhythmia syndrome that we have termed RyR2-CRDS. The RyR2-CRDS phenotype lacks catecholamine-induced ventricular ectopy, distinguishing it from CPVT. Unlike CPVT, ventricular ectopy in RyR2-CRDS arises

secondary to marked electrophysiological remodeling that increases the heart's susceptibility to EAD-triggered VAs. Driven by the observation that RyR2-CRDS is effectively concealed before patients manifesting with potentially lethal events, we developed a ventricular pacing protocol that effectively unmasks the condition and may serve as a CRDS diagnostic test, although additional validation in humans will be required.

MATERIALS AND METHODS

Study design

This study was designed to systematically determine whether RyR2 LOF is linked to a previously unknown disease entity characterized by SCD with negative EST, to understand the molecular mechanism by which RyR2 LOF causes SCD, and to develop diagnostic tools and treatments for patients with RyR2 LOF mutations. To achieve these objectives, we (i) performed clinical and genetic evaluations of families presenting with SCD or aSCD, negative EST, and RyR2 mutations; (ii) functionally characterized the identified RyR2 mutations; (iii) generated a mouse model harboring the RyR2 LOF mutation D4646A and assessed its impact on Ca^{2+} handling, electrophysiological and structural remodeling, and susceptibility to arrhythmias; (iv) developed a programmed stimulation protocol for the diagnosis of RyR2 LOF mutant carriers; and (v) identified potentially efficacious therapies for patients with RyR2 LOF mutations. All animal studies were approved by the Institutional Animal Care and Use Committees at the University of Calgary and were performed in accordance with U.S. National Institutes of Health guidelines. All animal experiments were performed blindly to genotype, and animals were assigned randomly to the experimental groups. Sample sizes for animal studies were calculated on the basis of previous studies and pilot studies. Sample sizes and *P* values can be found in the figure legends. Individual subject-level data are reported in data file S1. The study was performed as part of protocols approved by the research ethics boards of all collaborating institutions that provided human clinical data. All human study participants provided informed consent for their clinical and genetic data to be used for research.

Clinical and genetic evaluations of index cases and families

To systematically establish whether LOF mutations in RyR2 are linked to a previously unknown entity of cardiac arrhythmia distinct from CPVT, we searched for RyR2 mutations that are associated with SCD or aSCD in the setting of negative EST and determined their impact on RyR2 channel function. Individuals who suffered an aborted cardiac arrest requiring resuscitation, SCD, or had documented polymorphic VT and were subsequently identified to have a rare RyR2 mutation [defined as an allele frequency of <0.0001 in the Genome Aggregation Database (gnomAD)] in the setting of EST that did not reveal evidence of prominent VAs during exertion consistent with a diagnosis of CPVT were eligible for inclusion into the study (*18*). All patients were required to have undergone a coronary assessment, either through coronary or computerized tomography coronary angiography, to exclude a myocardial ischemic culprit for their presentation and echocardiography to rule out structural heart disease. Family pedigrees were constructed for each index case. Cascade screening through both clinical phenotyping and genetic testing for the suspected pathogenic RyR2 mutation was performed in all accessible and consenting family members. Electrophysiology studies were performed in eligible affected patients using an LBLPS stimulation protocol. Full details of the electrophysiology studies are provided in the Supplementary Materials. There were no premature ventricular contractions (PVCs) observed during the testing, and QT intervals of our patients under all conditions tested were within the normal limit.

Functional evaluation of RyR2 mutations

The functional ramifications of RyR2 mutations associated with SCD/aSCD were assessed by monitoring spontaneous or caffeine-induced Ca^{2+} release in HEK293 cells (American Type Culture Collection). Free cytosolic Ca^{2+} concentration in HEK293 cells was measured using the fluorescence Ca^{2+} indicator dye Fluo-3-AM or Fura-2/AM (Invitrogen), as previously described (*21*, *22*, *38*).

Generation and characterization of a mouse model of RyR2 Ca^{2+} release deficiency

To understand the molecular and cellular mechanisms of RyR2-CRDS, we generated a mouse model harboring one of the human RyR2 LOF mutations in patients, D4646A, using clustered regularly interspaced short palindromic repeats technology. Briefly, guide RNAs (5′-GGTCATTTCCCAATAACTAC**TGG**-3′) were designed and validated for the efficiency of targeting the *ryr*2 gene in mice. A mixture of active guide RNA transcripts, single-stranded oligodeoxynucleotide donor, and Cas-9 mRNA was injected into the cytoplasm of C57BL/6 embryos. Newborn mice were screened for knock-in of the designed mutation by polymerase chain reaction–based restriction digest using primers 5′-ccaagccacagttcctaaacatt-3′ (forward) and 5′-agagtgtggatttcttggatgct-3′ (reverse) and the Hae III restriction enzyme. Founder mutant mice harboring the RyR2-D4646A mutation were confirmed by DNA sequencing. All mice are maintained in the 129E background. Systolic and diastolic Ca^{2+} dynamics in ventricular myocytes in the Langendorff-perfused hearts were recorded using laser scanning confocal Ca^{2+} imaging as previously described (*39*, *40*). Adult genetically engineered mice RyR2-D4646A (DA) (generated commercially by Applied StemCell) and RyR2-R4496C (RC) (*41*) and WT littermates of both sexes were used. All animal models were housed in the mouse facility of the Cumming School of Medicine, University of Calgary. Only heterozygous RyR2-D4646A$^{+/-}$ mutant mice were produced, suggesting that the homozygous D4646A$^{+/+}$ mutation is embryonic lethal. Functional RyR2s are tetrameric channels formed by four RyR2 monomers. The heterozygous D4646A$^{+/-}$ mutant mice (harboring one WT allele and one D4646A mutant allele) will produce a mixture of homo- and hetero-tetrameric channels that contain the WT, D4646A mutant, or both WT/D4646A mutant monomers. Thus, the RyR2-D4646A mutation can exert its negative impact not only on the function of the D4646A homo-tetramers but also on the function of the WT monomer in the form of the WT/D4646A mutant hetero-tetrameric channels. Note that as in humans, the RyR2-D4646A$^{+/-}$ LOF mutation affects both male and female mice.

Stress-induced VAs in mice

The susceptibility of RyR2-WT and mutant mice to stress-induced VAs was assessed using ECG recordings. Mice were lightly anesthetized with isoflurane vapor (0.5 to 1%) and 95% O_2. Anesthetized mice were placed on a heating pad (37°C), and needle electrodes were inserted subcutaneously into the right upper limb and left lower abdomen for lead II ECG recording (BIOPAC MP System, Goleta, CA). Baseline ECG was recorded for 5 to 10 min. The mice were

subjected to intraperitoneal injection of a mixture of epinephrine (3.0 mg/kg) and caffeine (150 mg/kg). Continuous ECG monitoring was performed for 30 min after the injection (*41*).

Mouse intracardiac ECG recordings

Intracardiac atrial, atrioventricular nodal, and ventricular electrograms were recorded simultaneously in anesthetized RyR2-WT and mutant mice using a 1.1-F octa-polar catheter (EPR-800, Millar Instruments, Houston, TX). To induce VAs, an LBLPS pacing protocol with a long burst (20 beats at a 60-ms cycle length) followed by a long-coupled ventricular extra-stimulus (122 ms) and a subsequent short-coupled extra-stimulus was used. The short-coupled interval was progressively reduced from 78 to 18 ms in 4-ms steps. VA was defined as four or more ventricular ectopic beats after pacing, VA inducibility (%) as the proportion of animals that developed VAs per group, average VA duration as the summed duration of VA/total VA episodes for each group, and VA incidence (%) as the total number of VA episodes/total numbers of pacing trials for each group.

Statistical analysis

All data shown are means ± SEM, unless indicated otherwise. For normally distributed datasets, parametric tests were performed. For non–Gaussian-distributed datasets, nonparametric methods were used. With respect to nonparametric analyses, Mann-Whitney *U* test (two-sided) was used for two groups; Kruskal-Wallis test with Dunn's post hoc test was used for three or more than three groups. With respect to parametric analyses, Student's *t* test (two-sided) was used for two groups; one-way or two-way analysis of variance (ANOVA) followed by either Dunnett's or Bonferroni's post hoc test was used for three or more than three groups. The chi-square test was used to determine significant differences in frequencies between different groups. Sample sizes and *P* values can be found in the figure legends. *P* values smaller than 0.05 were considered statistically significant.

SUPPLEMENTARY MATERIALS

stm.sciencemag.org/cgi/content/full/13/579/eaba7287/DC1
Materials and Methods
Fig. S1. Pedigrees of families with non-CPVT–associated RyR2 mutations.
Fig. S2. Non-CPVT–associated RyR2 mutations suppress caffeine-induced Ca^{2+} release.
Fig. S3. Effects of mutations on the expression and function of RyR2.
Fig. S4. The D4646A mutation suppresses Ca^{2+} activation of single RyR2 channels in lipid bilayers.
Fig. S5. Generation and functional characterization of knock-in mouse model expressing the RyR2 mutation D4646A$^{+/-}$.
Fig. S6. Effects of RyR2-D4646A$^{+/-}$ on caffeine-promoted spontaneous Ca^{2+} release and depolarization-induced Ca^{2+} transients.
Fig. S7. Effects of RyR2-D4646A$^{+/-}$ on Ca^{2+} alternans and Ca^{2+} release refractoriness.
Fig. S8. Effects of RyR2-D4646A$^{+/-}$ on the I_{to} current, cardiac structure and fibrosis, L-type Ca^{2+} channel surface expression, and oxidative stress.
Fig. S9. Effects of RyR2-D4646A$^{+/-}$ on the expression of Ca^{2+} handling proteins, ion channels, and their associated proteins.
Fig. S10. Effects of RyR2-D4646A$^{+/-}$ on the expression of Ca^{2+} handling protein, ion channel, phosphatases, and kinases.
Fig. S11. Effects of RyR2 mutations on Ca^{2+} transients and SR Ca^{2+} contents.
Fig. S12. Electrical conduction in the RyR2-WT and D4646A$^{+/-}$ hearts.
Table S1. LOD scores for each family specified by *RYR2* mutation.
Table S2. Echocardiographic parameters of RyR2-WT and D4646A$^{+/-}$ mutant mice.
Data file S1. Individual subject-level data.
References (*42*–*54*)

View/request a protocol for this paper from *Bio-protocol*.

REFERENCES AND NOTES

1. D. M. Bers, Cardiac excitation–contraction coupling. *Nature* **415**, 198–205 (2002).
2. D. M. Bers, Calcium and cardiac rhythms: Physiological and pathophysiological. *Circ. Res.* **90**, 14–17 (2002).
3. M. Fill, J. A. Copello, Ryanodine receptor calcium release channels. *Physiol. Rev.* **82**, 893–922 (2002).
4. S. G. Priori, S. R. Chen, Inherited dysfunction of sarcoplasmic reticulum Ca^{2+} handling and arrhythmogenesis. *Circ. Res.* **108**, 871–883 (2011).
5. S. G. Priori, C. Napolitano, N. Tiso, M. Memmi, G. Vignati, R. Bloise, V. V. Sorrentino, G. A. Danieli, Mutations in the Cardiac Ryanodine Receptor Gene (*hRyR2*) underlie catecholaminergic polymorphic ventricular tachycardia. *Circulation* **103**, 196–200 (2001).
6. C. Napolitano, S. G. Priori, Diagnosis and treatment of catecholaminergic polymorphic ventricular tachycardia. *Heart Rhythm* **4**, 675–678 (2007).
7. A. Medeiros-Domingo, Z. A. Bhuiyan, D. J. Tester, N. Hofman, H. Bikker, J. P. van Tintelen, M. M. Mannens, A. A. Wilde, M. J. Ackerman, The *RYR2*-encoded ryanodine receptor/calcium release channel in patients diagnosed previously with either catecholaminergic polymorphic ventricular tachycardia or genotype negative, exercise-induced long QT syndrome: A comprehensive open reading frame mutational analysis. *J. Am. Coll. Cardiol.* **54**, 2065–2074 (2009).
8. K. V. Lieve, C. van der Werf, A. A. Wilde, Catecholaminergic polymorphic ventricular tachycardia. *Circ. J.* **80**, 1285–1291 (2016).
9. M. Hayashi, I. Denjoy, F. Extramiana, A. Maltret, N. R. Buisson, J.-M. Lupoglazoff, D. Klug, M. Hayashi, S. Takatsuki, E. Villain, J. Kamblock, A. Messali, P. Guicheney, J. Lunardi, A. Leenhardt, Incidence and risk factors of arrhythmic events in catecholaminergic polymorphic ventricular tachycardia. *Circulation* **119**, 2426–2434 (2009).
10. T. M. Roston, J. M. Vinocur, K. R. Maginot, S. Mohammed, J. C. Salerno, S. P. Etheridge, M. Cohen, R. M. Hamilton, A. Pflaumer, R. J. Kanter, J. E. Potts, M. J. La Page, K. K. Collins, R. A. Gebauer, J. D. Temple, A. S. Batra, C. Erickson, M. Miszczak-Knecht, P. Kubuš, Y. Bar-Cohen, M. Kantoch, V. C. Thomas, G. Hessling, C. Anderson, M.-L. Young, M. C. Ortega, Y. R. Lau, C. L. Johnsrude, A. Fournier, P. J. Kannankeril, S. Sanatani, Catecholaminergic polymorphic ventricular tachycardia in children: Analysis of therapeutic strategies and outcomes from an international multicenter registry. *Circ. Arrhythm. Electrophysiol.* **8**, 633–642 (2015).
11. T. M. Roston, S. Sanatani, S. R. Chen, Suppression-of-function mutations in the cardiac ryanodine receptor: Emerging evidence for a novel arrhythmia syndrome? *Heart Rhythm* **14**, 108–109 (2017).
12. S. G. Priori, C. Napolitano, M. Memmi, B. Colombi, F. Drago, M. Gasparini, L. De Simone, F. Coltorti, R. Bloise, R. Keegan, F. E. S. Cruz Filho, G. Vignati, A. Benatar, A. De Logu, Clinical and molecular characterization of patients with catecholaminergic polymorphic ventricular tachycardia. *Circulation* **106**, 69–74 (2002).
13. D. Jiang, W. Chen, R. Wang, L. Zhang, S. R. W. Chen, Loss of luminal Ca^{2+} activation in the cardiac ryanodine receptor is associated with ventricular fibrillation and sudden death. *Proc. Natl. Acad. Sci. U.S.A.* **104**, 18309–18314 (2007).
14. Y.-T. Zhao, C. R. Valdivia, G. B. Gurrola, P. P. Powers, B. C. Willis, R. L. Moss, J. Jalife, H. H. Valdivia, Arrhythmogenesis in a catecholaminergic polymorphic ventricular tachycardia mutation that depresses ryanodine receptor function. *Proc. Natl. Acad. Sci. U.S.A.* **112**, E1669–E1677 (2015).
15. Y. Fujii, H. Itoh, S. Ohno, T. Murayama, N. Kurebayashi, H. Aoki, M. Blancard, Y. Nakagawa, S. Yamamoto, Y. Matsui, M. Ichikawa, K. Sonoda, T. Ozawa, K. Ohkubo, I. Watanabe, P. Guicheney, M. Horie, A type 2 ryanodine receptor variant associated with reduced Ca^{2+} release and short-coupled torsades de pointes ventricular arrhythmia. *Heart Rhythm* **14**, 98–107 (2017).
16. T. M. Roston, W. Guo, A. D. Krahn, R. Wang, F. Van Petegem, S. Sanatani, S. R. W. Chen, A. Lehman, A novel RYR2 loss-of-function mutation (I4855M) is associated with left ventricular non-compaction and atypical catecholaminergic polymorphic ventricular tachycardia. *J. Electrocardiol.* **50**, 227–233 (2017).
17. C. Paech, R. A. Gebauer, J. Karstedt, C. Marschall, A. Bollmann, D. Husser, Ryanodine receptor mutations presenting as idiopathic ventricular fibrillation: A report on two novel familial compound mutations, c.6224T>C and c.13781A>G, with the clinical presentation of idiopathic ventricular fibrillation. *Pediatr. Cardiol.* **35**, 1437–1441 (2014).
18. M. Lek, K. J. Karczewski, E. V. Minikel, K. E. Samocha, E. Banks, T. Fennell, A. H. O'Donnell-Luria, J. S. Ware, A. J. Hill, B. B. Cummings, T. Tukiainen, D. P. Birnbaum, J. A. Kosmicki, L. E. Duncan, K. Estrada, F. Zhao, J. Zou, E. Pierce-Hoffman, J. Berghout, D. N. Cooper, N. Deflaux, M. De Pristo, R. Do, J. Flannick, M. Fromer, L. Gauthier, J. Goldstein, N. Gupta, D. Howrigan, A. Kiezun, M. I. Kurki, A. L. Moonshine, P. Natarajan, L. Orozco, G. M. Peloso, R. Poplin, M. A. Rivas, V. Ruano-Rubio, S. A. Rose, D. M. Ruderfer, K. Shakir, P. D. Stenson, C. Stevens, B. P. Thomas, G. Tiao, M. T. Tusie-Luna, B. Weisburd, H.-H. Won, D. Yu, D. M. Altshuler, D. Ardissino, M. Boehnke, J. Danesh, S. Donnelly, R. Elosua, J. C. Florez, S. B. Gabriel, G. Getz, S. J. Glatt, C. M. Hultman, S. Kathiresan, M. Laakso, S. M. Carroll, M. I. McCarthy, D. M. Govern, R. M. Pherson, B. M. Neale, A. Palotie, S. M. Purcell, D. Saleheen, J. M. Scharf, P. Sklar, P. F. Sullivan, J. Tuomilehto, M. T. Tsuang, H. C. Watkins, J. G. Wilson, M. J. Daly,

D. G. MacArthur; Exome Aggregation Consortium, Analysis of protein-coding genetic variation in 60,706 humans. *Nature* **536**, 285–291 (2016).
19. J. D. Kapplinger, K. N. Pundi, N. B. Larson, T. E. Callis, D. J. Tester, H. Bikker, A. A. M. Wilde, M. J. Ackerman, Yield of the *RYR2* genetic test in suspected catecholaminergic polymorphic ventricular tachycardia and implications for test interpretation. *Circ. Genom. Precis. Med.* **11**, e001424 (2018).
20. J. Ott, A computer program for linkage analysis of general human pedigrees. *Am. J. Hum. Genet.* **28**, 528–529 (1976).
21. D. Jiang, B. Xiao, D. Yang, R. Wang, P. Choi, L. Zhang, H. Cheng, S. R. W. Chen, RyR2 mutations linked to ventricular tachycardia and sudden death reduce the threshold for store-overload-induced Ca^{2+} release (SOICR). *Proc. Natl. Acad. Sci. U.S.A.* **101**, 13062–13067 (2004).
22. D. Jiang, R. Wang, B. Xiao, H. Kong, D. J. Hunt, P. Choi, L. Zhang, S. R. W. Chen, Enhanced store overload-induced Ca^{2+} release and channel sensitivity to luminal Ca^{2+} activation are common defects of RyR2 mutations linked to ventricular tachycardia and sudden death. *Circ. Res.* **97**, 1173–1181 (2005).
23. M. Cerrone, B. Colombi, M. Santoro, M. R. di Barletta, M. Scelsi, L. Villani, C. Napolitano, S. G. Priori, Bidirectional ventricular tachycardia and fibrillation elicited in a knock-in mouse model carrier of a mutation in the cardiac ryanodine receptor. *Circ. Res.* **96**, e77–e82 (2005).
24. N. Liu, B. Colombi, M. Memmi, S. Zissimopoulos, N. Rizzi, S. Negri, M. Imbriani, C. Napolitano, F. A. Lai, S. G. Priori, Arrhythmogenesis in catecholaminergic polymorphic ventricular tachycardia: Insights from a RyR2 R4496C knock-in mouse model. *Circ. Res.* **99**, 292–298 (2006).
25. Y. Imaizumi, W. R. Giles, Quinidine-induced inhibition of transient outward current in cardiac muscle. *Am. J. Physiol.* **253**, H704–H708 (1987).
26. J. J. Salata, J. A. Wasserstrom, Effects of quinidine on action potentials and ionic currents in isolated canine ventricular myocytes. *Circ. Res.* **62**, 324–337 (1988).
27. F. Scamps, A. Undrovinas, G. Vassort, Inhibition of ICa in single frog cardiac cells by quinidine, flecainide, ethmozin, and ethacizin. *Am. J. Physiol.* **256**, C549–C559 (1989).
28. Z. Wang, B. Fermini, S. Nattel, Effects of flecainide, quinidine, and 4-aminopyridine on transient outward and ultrarapid delayed rectifier currents in human atrial myocytes. *J. Pharmacol. Exp. Ther.* **272**, 184–196 (1995).
29. H. Watanabe, N. Chopra, D. Laver, H. S. Hwang, S. S. Davies, D. E. Roach, H. J. Duff, D. M. Roden, A. A. M. Wilde, B. C. Knollmann, Flecainide prevents catecholaminergic polymorphic ventricular tachycardia in mice and humans. *Nat. Med.* **15**, 380–383 (2009).
30. P. J. Kannankeril, B. M. Mitchell, S. A. Goonasekera, M. G. Chelu, W. Zhang, S. Sood, D. L. Kearney, C. I. Danila, M. De Biasi, X. H. T. Wehrens, R. G. Pautler, D. M. Roden, G. E. Taffet, R. T. Dirksen, M. E. Anderson, S. L. Hamilton, Mice with the R176Q cardiac ryanodine receptor mutation exhibit catecholamine-induced ventricular tachycardia and cardiomyopathy. *Proc. Natl. Acad. Sci. U.S.A.* **103**, 12179–12184 (2006).
31. P. P. Jones, D. Jiang, J. Bolstad, D. J. Hunt, L. Zhang, N. Demaurex, S. R. Chen, Endoplasmic reticulum Ca^{2+} measurements reveal that the cardiac ryanodine receptor mutations linked to cardiac arrhythmia and sudden death alter the threshold for store-overload-induced Ca^{2+} release. *Biochem. J.* **412**, 171–178 (2008).
32. S. Sedej, F. R. Heinzel, S. Walther, N. Dybkova, P. Wakula, J. Groborz, P. Gronau, L. S. Maier, M. A. Vos, F. A. Lai, C. Napolitano, S. G. Priori, J. Kockskämper, B. Pieske, Na^+-dependent SR Ca^{2+} overload induces arrhythmogenic events in mouse cardiomyocytes with a human CPVT mutation. *Cardiovasc. Res.* **87**, 50–59 (2010).
33. E. G. Lakatta, Functional implications of spontaneous sarcoplasmic reticulum Ca^{2+} release in the heart. *Cardiovasc. Res.* **26**, 193–214 (1992).
34. E. Marban, S. W. Robinson, W. G. Wier, Mechanisms of arrhythmogenic delayed and early afterdepolarizations in ferret ventricular muscle. *J. Clin. Invest.* **78**, 1185–1192 (1986).
35. C. H. Orchard, D. A. Eisner, D. G. Allen, Oscillations of intracellular Ca^{2+} in mammalian cardiac muscle. *Nature* **304**, 735–738 (1983).
36. S. Denker, M. Lehmann, R. Mahmud, C. Gilbert, M. Akhtar, Facilitation of ventricular tachycardia induction with abrupt changes in ventricular cycle length. *Am. J. Cardiol.* **53**, 508–515 (1984).
37. W. Chen, R. Wang, B. Chen, X. Zhong, H. Kong, Y. Bai, Q. Zhou, C. Xie, J. Zhang, A. Guo, X. Tian, P. P. Jones, M. L. O'Mara, Y. Liu, T. Mi, L. Zhang, J. Bolstad, L. Semeniuk, H. Cheng, J. Zhang, J. Chen, D. P. Tieleman, A. M. Gillis, H. J. Duff, M. Fill, L.-S. Song, S. R. W. Chen, The ryanodine receptor store-sensing gate controls Ca^{2+} waves and Ca^{2+}–triggered arrhythmias. *Nat. Med.* **20**, 184–192 (2014).
38. P. Li, S. R. Chen, Molecular basis of ca^2+ activation of the mouse cardiac ca^2+ release channel (ryanodine receptor). *J. Gen. Physiol.* **118**, 33–44 (2001).
39. B. Chen, A. Guo, Z. Gao, S. Wei, Y.-P. Xie, S. R. W. Chen, M. E. Anderson, L.-S. Song, In situ confocal imaging in intact heart reveals stress-induced Ca^{2+} release variability in a murine catecholaminergic polymorphic ventricular tachycardia model of type 2 ryanodine receptor$^{R4496C+/-}$ mutation. *Circ. Arrhythm. Electrophysiol.* **5**, 841–849 (2012).
40. Y. Bai, P. P. Jones, J. Guo, X. Zhong, R. B. Clark, Q. Zhou, R. Wang, A. Vallmitjana, R. Benitez, L. Hove-Madsen, L. Semeniuk, A. Guo, L.-S. Song, H. J. Duff, S. R. W. Chen, Phospholamban knockout breaks arrhythmogenic Ca^{2+} waves and suppresses catecholaminergic polymorphic ventricular tachycardia in mice. *Circ. Res.* **113**, 517–526 (2013).
41. Q. Zhou, J. Xiao, D. Jiang, R. Wang, K. Vembaiyan, A. Wang, C. D. Smith, C. Xie, W. Chen, J. Zhang, X. Tian, P. P. Jones, X. Zhong, A. Guo, H. Chen, L. Zhang, W. Zhu, D. Yang, X. Li, J. Chen, A. M. Gillis, H. J. Duff, H. Cheng, A. M. Feldman, L.-S. Song, M. Fill, T. G. Back, S. R. W. Chen, Carvedilol and its new analogs suppress arrhythmogenic store overload–induced Ca^{2+} release. *Nat. Med.* **17**, 1003–1009 (2011).
42. S. N. Ho, H. D. Hunt, R. M. Horton, J. K. Pullen, L. R. Pease, Site-directed mutagenesis by overlap extension using the polymerase chain reaction. *Gene* **77**, 51–59 (1989).
43. M. Zhao, P. Li, X. Li, L. Zhang, R. J. Winkfein, S. R. Chen, Molecular identification of the ryanodine receptor pore–forming segment. *J. Biol. Chem.* **274**, 25971–25974 (1999).
44. U. K. Laemmli, Cleavage of structural proteins during the assembly of the head of bacteriophage T4. *Nature* **227**, 680–685 (1970).
45. H. Towbin, T. Staehelin, J. Gordon, Electrophoretic transfer of proteins from polyacrylamide gels to nitrocellulose sheets: Procedure and some applications. *Proc. Natl. Acad. Sci. U.S.A.* **76**, 4350–4354 (1979).
46. L. Wang, R. C. Myles, N. M. De Jesus, A. K. Ohlendorf, D. M. Bers, C. M. Ripplinger, Optical mapping of sarcoplasmic reticulum Ca^{2+} in the intact heart: Ryanodine receptor refractoriness during alternans and fibrillation. *Circ. Res.* **114**, 1410–1421 (2014).
47. X. Zhong, B. Sun, A. Vallmitjana, T. Mi, W. Guo, M. Ni, R. Wang, A. Guo, H. J. Duff, A. M. Gillis, L.-S. Song, L. Hove-Madsen, R. Benitez, S. R. W. Chen, Suppression of ryanodine receptor function prolongs Ca^{2+} release refractoriness and promotes cardiac alternans in intact hearts. *Biochem. J.* **473**, 3951–3964 (2016).
48. J. Xiao, X. Tian, P. P. Jones, J. Bolstad, H. Kong, R. Wang, L. Zhang, H. J. Duff, A. M. Gillis, S. Fleischer, M. Kotlikoff, J. A. Copello, S. R. W. Chen, Removal of FKBP12.6 does not alter the conductance and activation of the cardiac ryanodine receptor or the susceptibility to stress-induced ventricular arrhythmias. *J. Biol. Chem.* **282**, 34828–34838 (2007).
49. A. E. Palmer, C. Jin, J. C. Reed, R. Y. Tsien, Bcl-2-mediated alterations in endoplasmic reticulum Ca^{2+} analyzed with an improved genetically encoded fluorescent sensor. *Proc. Natl. Acad. Sci. U.S.A.* **101**, 17404–17409 (2004).
50. A. Fabiato, F. Fabiato, Calculator programs for computing the composition of the solutions containing multiple metals and ligands used for experiments in skinned muscle cells. *J. Physiol. Paris* **75**, 463–505 (1979).
51. D. Lang, A. V. Glukhov, High-resolution optical mapping of the mouse sino-atrial node. *J. Vis. Exp.* , e54773 (2016).
52. I. Polina, H. J. Jansen, T. Li, M. Moghtadaei, L. J. Bohne, Y. Liu, P. Krishnaswamy, E. E. Egom, D. D. Belke, S. A. Rafferty, M. Ezeani, A. M. Gillis, R. A. Rose, Loss of insulin signaling may contribute to atrial fibrillation and atrial electrical remodeling in type 1 diabetes. *Proc. Natl. Acad. Sci. U.S.A.* **117**, 7990–8000 (2020).
53. C. O'Shea, A. P. Holmes, T. Y. Yu, J. Winter, S. P. Wells, J. Correia, B. J. Boukens, J. R. De Groot, G. S. Chu, X. Li, G. A. Ng, P. Kirchhof, L. Fabritz, K. Rajpoot, D. Pavlovic, ElectroMap: High-throughput open-source software for analysis and mapping of cardiac electrophysiology. *Sci. Rep.* **9**, 1389 (2019).
54. E. Lander, L. Kruglyak, Genetic dissection of complex traits: Guidelines for interpreting and reporting linkage results. *Nat. Genet.* **11**, 241–247 (1995).

Funding: This work was supported by research grants from the Canadian Institutes of Health Research (PJT-155940) to S.R.W.C. and (PJT 166105 and MOP 142486) to R.A.R.; the National Natural Science Foundation of China (81903611) to B.S.; the Spanish Ministry of Science Innovation and Universities SAF2017-88019-C3-R to L.H.-M. and R.B. and Marato-2015-20-30 to L.H.-M.; the Royal Netherlands Academy of Sciences (CVON 2012-10 PREDICT) to A.A.M.W.; the E-Rare Joint Transnational Call for Proposals 2015 "Improving Diagnosis and Treatment of Catecholaminergic Polymorphic Ventricular Tachycardia: Integrating Clinical and Basic Science" to S.R.W.C., S.S., and A.A.M.W.; the European Research Council Grant "EU-rhythmy" ERC-ADG-2014 (ID: 669387) to S.G.P.; the Novo Nordisk Foundation, Denmark (NNF18OC0031258) to H.K.J.; and the NIH (R01HL057832) to M.F. B.S. and J.Y. are recipients of the Alberta Innovates-Health Solutions (AIHS) Fellowship Award. J.W. is a recipient of the Libin Cardiovascular Institute of Alberta and Cumming School of Medicine Postdoctoral Fellowship Award. X.Z. and W.G. are recipients of the AIHS Studentship Award. S.R.W.C. holds the Heart and Stroke Foundation Chair in Cardiovascular Research. **Author contributions:** B.S., J.Y., M.N., S.S., A.A.M.W., J.D.R., S.G.P., H.K.J., and S.R.W.C. designed

the research. B.S., J.Y., M.N., J.W., X.Z., W.G., L.Z., and R.W. are responsible for molecular, cellular, electrophysiological, and/or whole animal studies; D.B. for echo analysis; Y.-X.C. for histological analysis; and K.V.V.L., A.K.B., T.M.R., I.B., J.A.K., J.C.v.A., and C.N. for clinical studies. B.S., J.Y., M.N., J.W., X.Z., W.G., L.Z., R.W., D.B., Y.-X.C., K.V.V.L., A.K.B., T.M.R., I.B., J.A.K., J.C.v.A., J.L., A.V., L.J.B., R.A.R., R.B., L.H.-M., C.N., R.A.H., S.S., A.A.M.W., J.D.R., S.G.P., H.K.J., and S.R.W.C. analyzed data. B.S., J.Y., M.N., R.W., K.V.V.L., T.M.R., J.L., A.V., L.J.B., R.A.R., R.B., L.H.-M., R.A.H., M.F., S.S., A.A.M.W., J.D.R., S.G.P., H.K.J., and S.R.W.C. wrote the paper. **Competing interests:** The authors declare that they have no competing interests. **Data and materials availability:** All data associated with this study are present in the paper or the Supplementary Materials.

Submitted 30 December 2019
Accepted 7 December 2020
Published 3 February 2021
10.1126/scitranslmed.aba7287

Citation: B. Sun, J. Yao, M. Ni, J. Wei, X. Zhong, W. Guo, L. Zhang, R. Wang, D. Belke, Y.-X. Chen, K. V. Lieve, A. K. Broendberg, T. M. Roston, I. Blankoff, J. A. Kammeraad, J. C. von Alvensleben, J. Lazarte, A. Vallmitjana, L. J. Bohne, R. A. Rose, R. Benitez, L. Hove-Madsen, C. Napolitano, R. A. Hegele, M. Fill, S. Sanatani, A. A. Wilde, J. D. Roberts, S. G. Priori, H. K. Jensen, S. R. W. Chen, Cardiac ryanodine receptor calcium release deficiency syndrome. *Sci. Transl. Med.* **13**, eaba7287 (2021).

Science Translational Medicine

Cardiac ryanodine receptor calcium release deficiency syndrome

Bo Sun, Jinjing Yao, Mingke Ni, Jinhong Wei, Xiaowei Zhong, Wenting Guo, Lin Zhang, Ruiwu Wang, Darrell Belke, Yong-Xiang Chen, Krystien V.V. Lieve, Anders K. Broendberg, Thomas M. Roston, Ivan Blankoff, Janneke A. Kammeraad, Johannes C. von Alvensleben, Julieta Lazarte, Alexander Vallmitjana, Loryn J. Bohne, Robert A. Rose, Raul Benitez, Leif Hove-Madsen, Carlo Napolitano, Robert A. Hegele, Michael Fill, Shubhayan Sanatani, Arthur A.M. Wilde, Jason D. Roberts, Silvia G. Priori, Henrik K. Jensen and S. R. Wayne Chen

Sci Transl Med **13**, eaba7287.
DOI: 10.1126/scitranslmed.aba7287

Calcium and cardiac arrhythmia

Calcium signaling couples cardiac electrical excitation and contraction and is tightly controlled within myocytes via the ryanodine receptor (RyR2). Sun *et al.* investigated loss-of-function mutations in RyR2 identified in families of individuals who experienced sudden cardiac death. RyR2 mutations were linked to cardiac arrhythmias due to prolonged calcium release refractoriness and electrophysiological and structural remodeling. The authors developed a cardiac stimulation protocol that induced ventricular arrhythmias in mice harboring a RyR2 mutation, and similar electrical patterns were seen in patients, which could be used to diagnose the RyR2 calcium release deficiency syndrome. Quinidine and flecainide could suppress arrhythmias in mice, suggesting possible treatments for this disease.

Science Translational Medicine
AAAS

stm.sciencemag.org/cgi/content/full/13/579/eaba7287/DC1

Supplementary Materials for

Cardiac ryanodine receptor calcium release deficiency syndrome

Bo Sun, Jinjing Yao, Mingke Ni, Jinhong Wei, Xiaowei Zhong, Wenting Guo, Lin Zhang, Ruiwu Wang, Darrell Belke, Yong-Xiang Chen, Krystien V.V. Lieve, Anders K. Broendberg, Thomas M. Roston, Ivan Blankoff, Janneke A. Kammeraad, Johannes C. von Alvensleben, Julieta Lazarte, Alexander Vallmitjana, Loryn J. Bohne, Robert A. Rose, Raul Benitez, Leif Hove-Madsen, Carlo Napolitano, Robert A. Hegele, Michael Fill, Shubhayan Sanatani*, Arthur A. M. Wilde*, Jason D. Roberts*, Silvia G. Priori*, Henrik K. Jensen*, S. R. Wayne Chen*

*Corresponding author. Email: swchen@ucalgary.ca (S.R.W.C.); hkjensen@clin.au.dk (H.K.J.); silvia.priori@icsmaugeri.it (S.G.P.); Jason.Roberts@lhsc.on.ca (J.D.R.); a.a.wilde@amsterdamumc.nl (A.A.M.W.); ssanatani@cw.bc.ca (S.S.)

Published 3 February 2021, *Sci. Transl. Med.* **13**, eaba7287 (2021)
DOI: 10.1126/scitranslmed.aba7287

The PDF file includes:

Table S2. Echocardiographic parameters of RyR2-WT and D4646A$^{+/-}$ mutant mice.
References (*42–54*)

Other Supplementary Material for this manuscript includes the following:

(available at stm.sciencemag.org/cgi/content/full/13/579/eaba7287/DC1)

Data file S1 (Microsoft Excel format). Individual subject-level data.

Supplementary Materials:

Materials and Methods

Generation of RyR2 mutations and stable, inducible HEK293 cell lines

All RyR2 mutations were generated in the full-length mouse RyR2 cDNA by using the overlap extension method with PCR (*42, 43*). An AgeI/SalI fragment containing Q3774L, a SalI/MluI fragment containing L3995V or D4112N or a MluI/Bsu36I fragment containing T4196I was separately generated by overlapping PCR. These fragments were then used to replace the corresponding wild-type (WT) fragment in the BsiwI/NotI construct in pBluescript. The BsiwI/NotI construct containing each mutation was then subcloned to the full-length mouse RyR2 in pcDNA5/FRT/TO using BsiWI and NotI. The EcoVI/NotI fragment containing D4646A was generated by overlapping PCR. This fragment containing D4646A was then subcloned into the full-length RyR2 in pcDNA5/FRT/TO using EcoRV and NotI. The NruI/NotI fragment containing Q4879H, A4860G, S4938F, or I4855M was generated using overlapping PCR. This fragment containing each of these mutations was then used to replace the corresponding WT fragment in the full-length mRyR2 in pcDNA5/FRT/TO using NruI and NotI. To make the I2075T and K4594R double mutation, we generated a NruI/EcoRV fragment containing I2075T and a Bsu36I/EcoRV fragment containing K4594R by overlapping PCR. A NruI/EcoRV fragment containing I2075T was then used to replace the corresponding WT fragment in the NheI/BsiwI construct in pBluescript. The Bsu36I/EcoRV fragment containing K4594R was then used to replace the corresponding WT fragment in the BsiwINotI construct in pBluescript. These two constructs were then subcloned together to form the full-length RyR2 cDNA using BsiwI and NotI and then transferred to the pcDNA5/FRT/TO vector. All RyR2 mutations were confirmed by DNA sequencing.

Stable, inducible HEK293 cell lines expressing RyR2-WT and RyR2 LOF mutants were generated using the Flp-In T-REx Core Kit from Invitrogen (*21, 22*). Briefly, the full-length cDNA encoding the RyR2 WT or mutant channel was subcloned into the inducible expression vector, pcDNA5/FRT/TO. Flp-In T-REx-293 cells were then co-transfected with the inducible expression vector, pcDNA5/FRT/TO containing the RyR2-WT or mutant cDNA and the pOG44 vector encoding the Flp recombinase in 1:5 ratios using the Ca^{2+} phosphate precipitation method. Transfected cells were washed with PBS (137 mM NaCl, 8 mM Na2HPO4, 1.5 mM KH2PO4, 2.7 mM KCl) 1 day after transfection and allowed to grow for 1 more day in fresh medium. The cells were then washed again with PBS, harvested, and plated onto new dishes. After the cells had attached (~ 4 hrs), the growth medium was replaced with a selective medium containing 200 μg/ml hygromycin (Invitrogen). The selective medium was changed every 3-4 days until the desired number of cells was grown. The hygromycin-resistant cells were pooled, aliquoted, and stored at -80°C.These positive cells are believed to be isogenic, because the integration of RyR2 cDNA is mediated by the Flp recombinase at a single FRT site.

Caffeine-induced Ca^{2+} release measurements

Free cytosolic Ca^{2+} concentration in transfected HEK293 cells was measured using the fluorescence Ca^{2+} indicator dye fluo-3-AM, as described previously (*38*). HEK293 cells grown on 100-mm tissue culture dishes for 18-20 h after subculture were transfected with 12-16 μg of WT or mutant RyR2 cDNA. Cells grown for 18-20 hr after transfection were washed four times with PBS and incubated in KRH buffer without MgCl2 and CaCl2 (KRH buffer: 125 mM NaCl,

5 mM KCl, 1.2 mM KH2PO4, 6 mM glucose, 1.2 mM MgCl2, 2 mM CaCl2, and 25 mM Hepes, pH 7.4) at room temperature for 40 min and at 37 °C for 40 min. After being detached from culture dishes by pipetting, cells were collected by centrifugation at 1,000 rpm for 2 min. in a Beckman TH-4 rotor. Cell pellets were washed twice with KRH buffer and loaded with 10 μM fluo-3 in KRH buffer plus 0.1 mg/ml BSA and 250 μM sulfinpyrazone at room temperature for 60 min followed by washing with KRH buffer three times and resuspended in 150 μl KRH buffer plus 0.1 mg/ml BSA and 250 μM sulfinpyrazone. The fluo 3 loaded cells were added to 2ml (final volume) KRH buffer in a cuvette. Fluorescence intensity of fluo-3 at 530 nm was measured before and after repeated additions or single additions of various concentrations of caffeine in an SLM-Aminco series 2 luminescence spectrometer with 480 nm excitation at 25 °C (SLM Instruments, Urbana, IL). The peak amplitudes of each caffeine-induced Ca^{2+} release was determined and normalized to the highest amplitude (100%) of caffeine-induced Ca^{2+} release for each experiment. The normalized data were fitted with the Hill equation to calculate the EC_{50} value for each experiment.

Western blotting using HEK293 cell-expressed RyR2-WT and mutants

HEK293 cells grown for 24 h after transfection with RyR2-WT or RyR2 LOF mutant cDNA were washed with PBS plus 2.5 mM EDTA and harvested in the same solution by centrifugation for 8 min at 700 × *g* in an IEC Centra-CL2 centrifuge. The cells were then washed with PBS without EDTA and centrifuged again at 700 × *g* for 8 min. The PBS-washed cells were solubilized in a lysis buffer containing 25 mM Tris, 50 mM Hepes (pH 7.4), 137 mM NaCl, 1% CHAPS, 0.5% soy bean phosphatidylcholine, 2.5 mM DTT, and a protease inhibitor mixture (1 mM benzamidine, 2 μg/ml leupeptin, 2 μg/ml pepstatin A, 2 μg/ml aprotinin, and 0.5 mM PMSF). This mixture was incubated on ice for 1 h. Cell lysate was obtained by centrifuging twice at 16,000 × *g* in a microcentrifuge at 4 °C for 30 min to remove unsolubilized materials. The RyR2 WT and mutant proteins were subjected to SDS-PAGE (5% gel) and transferred onto nitrocellulose membranes at 100 V for 2 h at 4 °C in the presence of 0.01% SDS (*44, 45*). The GAPDH was resolved in 12% SDS page and transferred onto nitrocellulose membranes at 100 V for 1h at 4 °C. The nitrocellulose membranes containing the transferred proteins were blocked for 60 min with 1% casein blocker (Bio-Rad). The blocked membrane was incubated with anti-RyR2 or anti-GAPDH antibodies and then incubated with anti-mouse or anti-rabbit IgG (heavy and light) antibodies conjugated to horseradish peroxidase (1:20,000 dilution). After washing for 10 min three times, the bound antibodies were detected using an enhanced chemiluminescence kit from Pierce. The intensity of each band was determined from its intensity profile obtained by ImageQuant LAS 4000(GE Healthcare/Life Sciences) and, analyzed by ImageJ software, and normalized to that of GAPDH.

Western blotting using mouse heart samples

RyR2-WT and mutant mouse hearts were crushed by a Wollenberger clamp pre-cooled in liquid nitrogen. The crushed heart tissues were stored at −80°C until use. Frozen heart tissues were pulverized in liquid nitrogen and homogenized immediately in 6 volumes of homogenizing buffer containing 30 mM KH_2PO_4 (pH 7.0), 40 mM NaF, 5 mM EDTA, 300 mM sucrose, 4 μM leupeptin, 1 mM benzamidine, 100 μM PMSF, and 0.5 mM DTT, aliquoted, frozen with liquid nitrogen and stored at −80°C until use. Aliquots of homogenates were solubilized in a final 500 μl of solubilizing buffer containing 50 mM Tris-HCl (pH 7.4) plus 3% SDS for 1 h at room temperature and then incubated at 55°C for 10 min. The insoluble materials were removed by

centrifugation at 12,000×g for 10 min. The protein concentration of the supernatant was determined using a BioRad detergent-compatible protein assay kit. Solubilized proteins (15–20 μg) were used for SDS-PAGE. Proteins resolved in 5-10% SDS-PAGE were transferred to nitrocellulose membranes at 100 V for 1-2 h at 4°C depends on the molecular weight in the presence of 0.01% SDS (*44, 45*). The nitrocellulose membranes containing the transferred proteins were blocked for 60 min with phosphate buffered saline (PBS) containing 0.5% Tween-20 and 5% skim milk powder. The blocked membrane was incubated with primary antibodies, and washed with PBS containing 0.5% Tween-20 for three times with shaking, each time for 5 min. The membrane was then incubated with the secondary anti-mouse or anti-rabbit IgG (H&L) antibodies conjugated to horseradish peroxidase (1:20,000) for 60 min. After washing with PBS containing 0.5% Tween-20 for three times, the bound antibodies were detected using an enhanced chemiluminescence kit from Thermo. The intensity of each band was determined from its intensity profile obtained by ImageQuant LAS 4000 (GE Healthcare Life Sciences), analyzed by using the Image-J software, and normalized to that of GAPDH.

Surface biotinylation of Cav1.2

Isolated cardiomyocytes from RyR2-WT or D4646A$^{+/-}$ heart were washed three times with ice-cold PBS and incubated for 30 min with 20 mM EZ-LinkSulfo-NHS-LC-Biotin (Thermo Scientific) to biotinylate cell surface proteins. Cells were then washed three times 5 minutes each with 100 mM glycine to quench the reaction. Cells were collected and lysed with 1% SDS at room temperature for 1 hour. Total protein concentrations were determined and equal amounts of protein were incubated with Streptavidin Agarose Resin (Thermo Scientific) at 4 °C overnight to pull down biotinylated proteins. The beads were washed 5 times and bound surface proteins were eluted by boiling in 4x Laemmli buffer for 10 min. Equal volumes of eluted proteins were loaded on an SDS-PAGE gel. Biotinylated Cav1.2 was detected by Western blotting with anti-Cav1.2 antibody (1:500, Alomone).

Laser scanning confocal Ca^{2+} imaging of intact hearts

WT and mutant mice were sacrificed by cervical dislocation. Their hearts were quickly removed and loaded with 4.4 μM Rhod-2 AM (Biotium, Inc. Hayward, CA) in oxygenated Tyrode's buffer (118 mM NaCl, 5.4 mM KCl, 25 mM $NaHCO_3$, 1 mM $MgCl_2$, 0.42 mM NaH_2PO_4, 11.1 mM glucose, 10 mM taurine, 5 mM creatine, and 1.8 mM $CaCl_2$, pH 7.4) via retrograde Langendorff perfusion system at 25°C for 45 minutes (*39, 40*). The Langendorff-perfused hearts were placed in a recording chamber mounted onto the Nikon A1R microscope for in situ confocal imaging (line-scan) of Ca^{2+} signals from epicardial ventricular myocytes. The temperature of the heart was kept at 35°C throughout the experiment with 5 μM blebbistatin (Toronto Research Chemicals, Toronto, ON) to prevent motion artifact. The pixel size of the resulting line-scan images ranged between 1.8 and 2 ms in the temporal dimension and between 0.1 to 0.4 microns in the spatial dimension. The Rhod-2 loaded hearts were excited using the 561 nm diode laser and the fluorescence emission at 570–620 nm was recorded. The line-scan images were processed and analyzed with the NIS-Elements AR 4.0.

Ca^{2+} alternans in the WT and D4646A hearts was induced by rapid electrical stimulation at increasing frequencies (6-14 Hz, 6 V). Ca^{2+} waves were generated by fast pacing and abrupt cessation of stimulation with increased external Ca^{2+} concentration from 2-10 mM or in the presence of 600 nM epinephrine plus 1.0 mM caffeine. The Rhod-2 AM loaded heart were also subject to an adapted LBLPS stimulation protocol to explore the mechanism of LBLPS induced

VAs. Briefly, the heart was stimulated at 6 Hz for 20 beats to determine the baseline amplitude of the Ca^{2+} transients. The hearts were then stimulated at 8 Hz for 19 beats (S1), followed by a long pause (250 ms) and a short coupled complexed (S2-S3) to induce VAs like transients. The transient amplitude of the S1 and S2 were assessed and normalized to that of basal amplitude to cancel out the variations from dye loading and scan depth.

Determination of refractoriness of SR Ca^{2+} release in intact hearts

The refractoriness of voltage-induced release of Ca^{2+} from the sarcoplasmic reticulum (SR) was determined by using the S1S2 stimulation protocol as described previously (*46, 47*). Briefly, Ca^{2+} transients in Rhod-2 AM loaded intact hearts were first induced at 5 Hz for 6 seconds (S1), followed by a single S2 stimulation at a specific interval. The hearts were repeatedly stimulated by a series of S1S2 protocols with progressively decreased S1S2 intervals (from 200 to 40 ms). Ca^{2+} transients before and after S2 stimulation were continuously recorded by using the Nikon-A1R confocal microscope in the line-scan mode.

Image and signal processing

Signal and image processing methods were developed using MATLAB (The Mathworks, Inc., Boston, MA) as previously described (*40, 47*). Briefly, line-scan fluorescence images were preprocessed using a median filter depending on the noise amount estimated by the median absolute deviation of the image. Segmentation was manually performed by marking cell limits and subsequently the mean temporal fluorescence signal of each cell was obtained. Wavelet filtering was used to further enhance Ca^{2+} release events in each signal from which simple thresholding allowed event detection. For each Ca^{2+} release event, amplitude and duration were measured and the alternans ratio was defined as the relative amplitude difference with the following event. Presence of alternans periods was defined as at least six consecutive peaks with an alternans ratio above 0.05 and a cell's alternans duration was defined as the time ratio of alternans periods over experiment duration.

Single cell Ca^{2+} imaging of isolated mouse ventricular myocyte

Mouse ventricular myocytes were isolated using retrograde aortic perfusion as described previously (*41, 48*). Isolated cells were kept at room temperature in Krebs-Ringers-HEPES (KRH) buffer (125 mM NaCl, 12.5 mM KCl, 25 mM HEPES, 6 mM glucose, and 1.2 mM $MgCl_2$, pH 7.4) containing 20 mM taurine, 20 mM 2,3-butanedione monoxime (BDM), 5 mg/ml albumin, and 1 mM free Ca^{2+} until use. Freshly isolated mouse ventricular myocytes were added to glass coverslips pre-coated with 50 μg/ml laminin, and loaded with 5 μM Rhod-2, AM (Molecular Probes, USA) in KRH buffer containing 1 mM Ca^{2+} for 20 min at room temperature as described previously. The glass coverslip pre-mounted to a recording chamber was then placed onto an inverted microscope (Nikon ECLIPSE Ti) equipped with a Nikon CFI Plan Apo VC 60xWI objective. Then Rhod-2 loaded cells were perfused with KRH buffer containing 2 mM extracellular Ca^{2+} and 5 μM blebbistatin at 35°C. The cells were paced by field stimulation using the S88X electric stimulator (Grass, USA). Confocal line-scanning (512 pixels and 1.9 ms per line) were performed along the longitudinal axis of cells using the Nikon A1R confocal system. SR Ca^{2+} content was determined after steady state stimulation at 8 Hz for 10 seconds by measuring the amplitude of Ca^{2+} release induced by local delivery of 20 mM caffeine.

Ratiometric Ca^{2+} imaging of isolated cardiomyocytes
Freshly isolated ventricular myocytes were loaded with 5 μM Cal Red™ R525/650 AM (AAT Bioquest) at room temperature for 1 hour. The dye loaded cells were then subjected to confocal line-scan imaging along the longitudinal axis of cells using the Nikon A1R confocal system. The Cal Red™ R525/650 fluorescence dye was excited at 488 nm, the emitted fluorescence signal was captured at 525 nm (F525) and 650 nm (F650). Ca^{2+} transients were elicited by field stimulation at 2 Hz with a pair of platinum electrodes. The changes in F525/F650 ratios were determined to monitor intracellular Ca^{2+} dynamics.

Detection of superoxide in live isolated ventricular myocytes
Mitochondrial superoxide was monitored using the fluorescent MitoSOX probe (Thermo Scientific). Freshly isolated mouse ventricular myocytes were added to glass coverslips pre-coated with 50 μg/ml laminin, and incubated with 5 μM MitoSOX for 10 min at 37˚C. After labelling, cells were gently washed 3 times with the KRH buffer. The fluorescent signals of these MitoSOX labelled cells were imaged using the Nikon A1R confocal system. The MitoSOX dye was excited at 514 nm, and emission was captured at 580 nm. Positive controls were performed by treating cells with 50 μM doxorubicin (DOX) for 20 min. Red fluorescence indicates the presence of superoxide.

Single cell cytosolic Ca^{2+} imaging of HEK293 cells
Cytosolic Ca^{2+} concentrations in stable, inducible HEK293 cells expressing RyR2-WT or RyR2 LOF mutations were monitored using single-cell Ca^{2+} imaging and the fluorescent Ca^{2+} indicator dye Fura-2/AM as described previously (*21, 22*). Briefly, cells grown on glass coverslips for 8–18 h after induction (as indicated) by 1 μg/ml tetracycline (Sigma) were loaded with 5 μM Fura-2/AM in KRH buffer (125 mM NaCl, 5 mM KCl, 6 mM glucose, 1.2 mM $MgCl_2$, and 25 mM Hepes (pH 7.4)) plus 0.02% pluronic F-127 and 0.1 mg/ml BSA for 20 min at room temperature (23 °C). The coverslips were then mounted in a perfusion chamber (Warner Instruments) on an inverted microscope (Nikon TE2000-S). The cells were perfused continuously with KRH buffer containing increasing extracellular Ca^{2+} concentrations (0, 0.1, 0.2, 0.3, 0.5, 1.0, and 2.0 mM). Caffeine (10 mM) was applied at the end of each experiment to confirm the expression of active RyR2 channels. Time-lapse images (0.25 frame/s) were captured and analyzed with Compix Simple PCI 6 software. Fluorescence intensities were measured from regions of interest centered on individual cells. Only cells that responded to caffeine were analyzed. The filters used for Fura-2 imaging were λexcitation = 340 ± 26 nm and 387 ± 11 nm and λemission = 510 ± 84 nm with a dichroic mirror (410 nm).

Single cell luminal Ca^{2+} imaging of HEK293 cells
Luminal Ca^{2+} concentrations in HEK293 cells expressing RyR2-WT or the RyR2 LOF mutants were measured using single-cell Ca^{2+} imaging and the fluorescence resonance energy transfer (FRET)-based ER luminal Ca^{2+}-sensitive chameleon protein D1ER as described previously (*31, 49*). The cells were grown to 95% confluence in a 75-cm^2 flask, passaged with PBS, and plated in 100-mm-diameter tissue culture dishes at ~10% confluence 18–20 h before transfection with D1ER cDNA using the Ca^{2+} phosphate precipitation method. After transfection for 24 h, the growth medium was changed to an induction medium containing 1 μg/ml tetracycline. In intact cell studies, after induction for ~22 h, the cells were perfused continuously with KRH buffer containing 5mM caffeine and various concentrations of $CaCl_2$ (0, 1, and 2 mM) for inducing

SOICR, and tetracaine (1 mM) for estimating the store capacity or caffeine (20 mM) for estimating the minimum store amplitude by depleting the ER Ca^{2+} stores at room temperature (23 °C). Images were captured with Compix Simple PCI 6 software every 2 s using an inverted microscope (Nikon TE2000-S) equipped with an S-Fluor ×20/0.75 objective. The filters used for D1ER imaging were λexcitation = 436 ± 20 nm for CFP and λexcitation = 500 ± 20 nm for YFP, and λemission = 465 ± 30 nm for CFP and λemission = 535 ± 30 nm for YFP with a dichroic mirror (500 nm). The amount of FRET was determined from the ratio of the light emission at 535 and 465 nm. We used relative FRET measurements to calculate the activation threshold and termination threshold using the equations shown. F_{SOICR} indicates the FRET amplitude at which SOICR occurs, whereas F_{termi} represents the FRET amplitude at which SOICR terminates. The fractional Ca^{2+}release was calculated by subtracting the termination threshold from the activation threshold. The maximum FRET signal F_{max} is defined as the FRET amplitude after tetracaine treatment. The minimum FRET signal F_{min} is defined as the FRET amplitude after caffeine treatment. The store capacity was calculated by subtracting F_{min} from F_{max}. The activation threshold is calculated using $100\%*(F_{SOICR}-F_{min})/(F_{max}-F_{min})$, and the termination threshold calculated using $100\%*(F_{temi}-F_{min})/(F_{max}-F_{min})$.

Single channel recordings in planar lipid bilayers

Recombinant RyR2-WT and mutant channels were purified from cell lysate prepared from HEK293 cells transfected with the RyR2-WT or mutant cDNA by sucrose density gradient centrifugation as described previously (*22*). Heart phosphatidylethanolamine (50%) and brain phosphatidylserine (50%) (Avanti Polar Lipids), dissolved in chloroform, were combined and dried under nitrogen gas and resuspended in 30 µl of n-decane at a concentration of 12 mg lipid per ml. Bilayers were formed across a 250 µm hole in a Delrin partition separating two chambers. The trans chamber (800 µl) was connected to the head stage input of an Axopatch 200A amplifier (Axon Instruments, Austin, TX). The cis chamber (1.2 ml) was held at virtual ground. A symmetrical solution containing 250 mM KCl and 25 mM HEPES, pH 7.4 was used for all recordings, unless indicated otherwise. A 4-µl aliquot (~1 µg protein) of the sucrose density gradient-purified recombinant RyR2-WT or mutant channels was added to the cis chamber. Spontaneous channel activity was always tested for sensitivity to EGTA and Ca^{2+}. The chamber to which the addition of EGTA inhibited the activity of the incorporated channel presumably corresponds to the cytosolic side of the Ca^{2+} release channel. The direction of single channel currents was always measured from the luminal to the cytosolic side of the channel, unless mentioned otherwise. Recordings were filtered at 2,500 Hz. Data analyses were carried out using the pclamp 8.1 software package (Axon Instruments). Free Ca^{2+} concentrations were calculated using the computer program Fabiato and Fabiato (*50*).

Intra-cardiac ECG recordings

RyR2-D4646A$^{+/-}$ mutant mice and their wild-type littermates were anesthetized with isoflurane (1.5-2%) in 100% oxygen (0.5L/min) and placed onto a temperature-controlled surgical board to maintain body temperature 37 °C ± 1.0 °C and breathing. The right jugular vein was isolated under a high-field microscope (model SMZ1000, Nikon, Japan). A 1.1-F octa-polar catheter (EPR-800, Millar Instruments, Houston, Texas) was inserted via the right jugular vein into the right atrium and right ventricle. Surface ECG and intra-cardiac ECGs including typical atrial, atrioventricular node, and ventricular ECGs were recorded simultaneously. For programmed right ventricle pacing, electrodes on the catheter were connected to a programmed external

Stimulus Isolator (model A365, WPI, USA). Currents with 3-5x ventricular diastolic threshold current were used for right ventricle pacing. To induce ventricular arrhythmias (VAs), several pacing protocols were applied: (1) A long burst (20 bests, 60 ms interval); (2) A long burst + a long pause: bust pacing (20 beats, 60-ms interval) followed by a long pause (122 ms) and an extra-stimulus; (3) S1S2: basal pacing (S1, 20 beats, 100-ms interval) followed by a short-coupled extra stimulus (S2). The S1S2 interval was progressively reduced from 78ms to 18ms in 4ms steps; (4) A long burst + a long pause + a short-coupled sequence (LBLPS): bust pacing (20 bests, 60-ms interval) followed by a long pause (122 ms) and a stimulus, then followed by a short-coupled extra-stimulus. The short-coupled interval was progressively reduced from 78 ms to 18 ms in 4-ms steps. If no VAs were induced after a train of pacing protocol, the pacing protocol was repeated twice. VA was defined as 4 or more ventricular ectopic beats after pacing. VA inducibility (%) was defined as the proportion of animals showed VAs per group. Average VA duration (s) was defined as the summed duration of VA/total VA episodes for each group. VA Incidence (%) was defined as the total VA episodes/total numbers of pacing trials for each group. For testing the acute effect of caffeine, ECGs were recorded in RyR2-D4646A mice following the LBLPS stimulation before and 20-min after injection of caffeine (150 mg/kg, i.p.). For testing the effect of quinidine sulfate, ECGs were recorded in D4646A mice following the LBLPS stimulation after the injection of vehicle (H_2O for 5 days, i.p.) or quinidine sulfate (10 mg/kg/day for 5 days, i.p.). The final dose of drug was administered 30 min before ECG recordings.

Whole cell patch-clamp recording of isolated ventricular myocytes

Mouse ventricular myocytes were isolated from 3-4 month old RyR2-WT and RyR2-D4646A$^{+/-}$ mice and used for whole cell patch clamp recordings. After obtaining whole cell voltage-clamp with a gigaohm seal, whole cell membrane capacitance was calculated as the time integral of the capacitive response to a 10mV hyperpolarizing step. Cells with significant leak current (≥100 pA) were rejected (≈20%). When measuring whole cell currents (depolarized every 10 s), series resistance and membrane capacitance were compensated electronically ≥75%. All recordings were performed at room temperature.

Recording of action potential (AP) and early afterdepolarization (EAD)

APs were measured in a standard external solution containing (in mM) NaCl 148, NaH_2PO_4 0.4, $MgCl_2$ 1, Glucose 5.5, KCl 5.4, $CaCl_2$ 1.0, HEPES 15 (pH adjusted to 7.4 with NaOH). The recording pipettes contained (in mM) KCl 148, $MgCl_2$ 1, EGTA 0.2, HEPES 5, creatine 2, K2-ATP 5, phosphocreatine 5 (pH adjusted to 7.2 with KOH). APs were recorded in current-clamp mode and were elicited by injecting an excitation threshold current pulse of 5 ms in duration. AP duration (APD50 and APD90) was analyzed by the software clampfit. To record EADs, cells were clamped in current-clamp mode, and paced by injecting excitation threshold current pulses at 0.5 Hz, 1 Hz or 2 Hz for 10 seconds.

Recording of the L-type Ca^{2+} current (I_{CaL})

The bath solution for I_{CaL} recordings contained (in mM) NaCl 137, CsCl 5.4, $MgCl_2$ 1, $CaCl_2$ 1.2, HEPES 10, Glucose 10, 4-Aminopyridine (4-AP) 2 with the pH adjusted to 7.4 with NaOH. The intracellular recording pipette solution contained (in mM) CsCl 120, TEA-Cl 20, $MgCl_2$1, MgATP 5, Na_2GTP 0.2, HEPES 10, and EGTA 10, pH adjusted to 7.2 with CsOH. I_{CaL} was elicited by 500-ms steps from -40 to +60 mV in 10-mV steps at 10-s intervals. To inactivate the

Na^+ current, cells were predepolarized to -50 mV by a slow (500-ms) voltage ramp 50 ms before each test depolarization was applied. Current density was calculated by dividing the peak amplitude with the cell membrane capacitance.

Recording of the Na-Ca exchange current (I_{NCX})

The bath solution for I_{NCX} recordings contained (in mM) NaCl 140, KCl 5, $MgCl_2$ 1, $CaCl_2$ 1.8, Glucose 10, HEPES 10, CsCl 10, Ouabain 0.01, Verapamil 0.01 and Niflumic acid 0.1 with the pH adjusted to 7.4 with NaOH. The pipette solution contained (in mM) CsCl 110, TEACl 20, NaCl 10, MgATP 5, HEPES 10, $MgCl_2$ 0.4, $CaCl_2$ 2.5 and EGTA 5, pH adjusted to 7.2 with CsOH. After establishment of the whole-cell mode, the cells were clamped at a holding potential of -80 mV. A descending voltage ramp polarization from +80 mV to -120 mV at 100 mV per s followed by instant return to the holding potential of -80 mV was used. The voltage command was repeated at 10-s intervals. I_{NCX} was measured as the current sensitive to 5 mM Ni^{2+}. Current density was calculated by dividing the peak amplitude with the cell membrane capacitance.

Recording of the transient outward current (I_{to}) currents

Prior to I_{to} current recording the KRH buffer was replaced with a bath solution containing (in mM): NaCl 125, KCl 2.5, HEPES 10, $MgCl_2$ 1, TTX 0.001, TEA 20, glucose 10 (pH adjusted to 7.4 with NaOH). Soft-glass recording pipettes were filled with an internal solution containing (in mM): potassium gluconate 135, KCl 10, HEPES 10, $CaCl_2$ 1, $MgCl_2$ 1, EGTA 10, ATP 1, GTP 0.1 (pH adjusted to 7.3 with KOH). The pipette resistance was 4–6 MΩ after filling with internal solution. I_{to} was elicited by depolarizing pulses to +40 mV from a holding potential of -80 mV in the presence of 20 mM tetraethylammonium (TEA) and 1 μM tetrodotoxin (TTX). In steady-state activation experiments, membrane potential was held at −80 mV, and I_{to} was evoked by a 200-ms depolarizing pulse from a first pulse potential of −50 mV to +80 mV in 10-mV steps at 10-s intervals. Data were analyzed using the equation $G_K = I_K/(V_m - V_{rev})$, where G_K is the membrane K^+ conductance, V_m is the membrane potential, and V_{rev} is the reversal potential for K^+. To study steady-state inactivation of I_{to}, currents were elicited using 1-s conditioning pre-pulses from −110 mV to 0 mV before a 200-ms test pulse of +50 mV. After normalizing each current amplitude to the maximal current, amplitude obtained from the −110 mV pre-pulse was used as a function of the conditioning pre-pulse potential and fitted with the function $I_{to} / I_{to-max} = 1/(1 + \exp((V_{m1/2} - V_m)/k))$, from which, an inactivation curve of I_{to} was obtained, and the V_H value (the voltage at which the current amplitude was half-inactivated) was calculated. Current density was calculated by dividing the peak amplitude with the cell membrane capacitance.

Recording of the Na current (I_{Na})

Ventricular myocytes were bath in a recording solution contained (in mM) NaCl 7, CsCl 133, HEPES 5, $CaCl_2$ 1.8, $MgCl_2$ 1.2, Glucose 11 and nifedipine 0.005, pH adjusted to 7.4 with CsOH. Pipettes were filled with an internal solution contained (in mM) NaCl 3, CsCl 133, TEACl 2, HEPES 5, $MgCl_2$ 2, EGTA 10, and Na_2ATP 2, pH adjusted to 7.3 with CsOH. I_{Na} was elicited by 200-ms steps from -120 to +50 mV in 10-mV steps at 10-s intervals with a holding potential at -120 mV. Data were analyzed using the equation $G_{Na} = I_{Na}/(V_m - V_{rev})$, where G_{Na} is the membrane Na^+ conductance, V_m is the membrane potential, and V_{rev} is the reversal potential for Na^+. To study steady-state inactivation of I_{Na}, currents were elicited using 500-ms conditioning pre-pulses from −160 mV to 0 mV before a 50-ms test pulse of +50 mV. After

normalizing each current amplitude to the maximal current, amplitude obtained from the −160 mV pre-pulse was used as a function of the conditioning pre-pulse potential and fitted with the function $I_{Na} / I_{Na-max} = 1/(1 + \exp((V_{m1/2} - V_m)/k))$, from which, an inactivation curve of I_{Na} was obtained, and the V_H value (the voltage at which the current amplitude was half-inactivated) was calculated. Current density was calculated by dividing the peak amplitude with the cell membrane capacitance.

Optical mapping

High-resolution optical voltage mapping of Langendorff-perfused mouse hearts was performed as described previously (*51*). Hearts were rapidly excised and perfused in a Langendorff apparatus with oxygenated (95% O_2 / 5% CO_2) at 37°C in a modified Tyrode's solution (128.2 mM NaCl, 4.7 mM KCl, 1.19mM NaH_2PO_4, 1.05mM $MgCl_2$, 1.3mM $CaCl_2$, 20.0mM $NaHCO_3$, and 11.1mM glucose (pH 7.35). Perfusion flow rate (3.5 mL/min) was adjusted to maintain a perfusion pressure of 60–80 mmHg. ECG signal was monitored using a 2-lead electrocardiogram in the perfusion bath. Voltage-sensitive dye RH237 (20 μL, 2.5 mg/mL in DMSO; Biotium) was dissolved in 1ml Tyrode's solution and slowly injected into the heart through coronary perfusion over a period of 7 min using a 3-way injection port. After dye loading, blebbistatin (10 μM) was added to the perfusate to minimize motion artifacts during the entire optical mapping experiment. The heart preparation was illuminated with light from the X-Cite Xylis Broad Spectrum LED Illumination System (Excelitas Technologies) and filtered with a 520/35 nm excitation filter (Semrock). Emitted fluorescence was separated by a dichroic mirror (560 nm cut-off; Semrock) and filtered by a 715 nm long-pass emissions filter (Andover Corp.). Recordings were captured using a high-speed CMOS camera (MiCAM03-N256, SciMedia). Data were captured from an optical field of view of 11 x 11 mm at a frame rate of 1000 frames/s using BrainVision software (BrainVision Inc.). The spatial resolution was 42.5 x 42.5 μM for each pixel. Magnification was constant in all experiments and no pixel binning was used. For generating activation maps and phase map videos, all optical data were analyzed using a custom software written in Matlab (t the software is available upon reasonable request and an MTA would be required). Pseudo color electrical activation maps were generated from measurements of activation time at individual pixels as defined by assessment of dF/dt max. In all cases background fluorescence was subtracted and no pixel binning was used (*52*). The open-source software, ElectroMap (*53*), was used to generate the average action potential (AP) traces using optical imaging data from the whole heart. The optical data were processed using a Gaussian spatial filter (sigma = 1.5) and 5th order Savitzky-Golay temporal filter.

Human studies

The human aspects of the study were performed as part of protocols approved by the research ethics boards of the participating institutions. All living human study participants provided informed consent.

RyR2 LOF index cases and families

Individuals that had suffered an aborted cardiac arrest requiring resuscitation, sudden cardiac death, or had documented polymorphic ventricular tachycardia and were subsequently identified to possess a rare *RyR2* mutation (defined as allele frequency < 0.001 in the Genome Aggregation Database [gnomAD]) in the setting of EST that did not reveal evidence of prominent ventricular arrhythmias during exertion consistent with a diagnosis of CPVT were eligible for inclusion into

the study (*18*). All patients were required to have undergone a coronary assessment, either through coronary angiography or CT coronary angiography, in order to exclude an ischemic culprit for their presentation. Family pedigrees were constructed for each index case and cascade screening through both clinical phenotyping and genetic testing for the suspected pathogenic *RYR2* mutation was performed in all accessible and consenting family members.

The following variables were collected for all probands and family members when available: age at presentation and last clinical follow-up, sex, familial status, history of a cardiac event (including activity at time of event, specific arrhythmia identified, and intervention performed to terminate arrhythmia [if any]), results of cardiac investigations (ECG, treadmill test, Holter monitor, echocardiogram, and cardiac magnetic resonance imaging (MRI), when available), and details regarding medical and device therapy. Genetic details of the *RyR2* mutation, including the nucleotide and amino acid change, were obtained for each case.

Electrophysiology studies in humans

Electrophysiology studies were performed in a patient with the RyR2-I3995V mutation and a patient with the RyR2-T4196I mutation following informed consent. All were performed in the post-absorptive state and anti-arrhythmic drugs had been stopped for a minimum of 5 half-lives prior to the procedure. In the case of the RyR2-I3995V patient, femoral venous access was obtained and quadripolar and decapolar catheters were positioned in the right ventricular apex and coronary sinus, respectively. A programed electrical stimulation protocol consisting of Long-Burst, Long-Pause, Short-coupled (LBLPS) ventricular extra-stimuli were performed following drive train cycle lengths of 500 ms, 430 ms, 370 ms, and 300 ms. Following the drive train, a long cycle of 800 ms or 50 ms shorter than the sinus cycle length preceded delivery of the first extra-stimulus (S2). The second extra-stimulus began at 400 ms (S3) and was decremented by 20 ms intervals down to refractoriness or 180 ms, whichever occurred first. In the case of the RyR2-T4196I patient, the electrophysiology study was performed using her ICD in the presence of conscious sedation with midazolam. The LBLPS protocol was administered through the right ventricular ICD lead. An initial drive train of 15 beats at a cycle length of 500 ms was delivered, followed by a long interval of 600 ms (S2), and a short interval that began at 400 ms (S3) and was decremented by 20 ms intervals down to refractoriness or 200 ms, whichever occurred first. This protocol was subsequently repeated using a drive train of 400 ms.

Genetic analyses and clinical evaluation of RyR2 mutant carriers presenting with life-threatening ventricular arrhythmias distinct from CPVT

In this study, we identified 6 RyR2 mutations (Q3774L, I3995V, D4112N, T4196I, D4646A, and Q4879H) in 6 families (Table 1). Clinical and genetic evaluation of the RyR2-T4196I family members (Fig. 1A) revealed that all 3 of the T4196I mutant carriers have suffered from SCD or aSCD, whereas all T4196I-negative members are asymptomatic. The RyR2-D4112N pedigree (Fig.1B) reveals that 5 of the 7 D4112N carriers/obligate-carriers experienced SCD or aSCD, while no mutation-negative family members had cardiac events. The RyR2-D4646A pedigree (Fig. 1C) indicates that 5 mutant carriers/obligate-carriers had SCD or aSCD, but again no mutation-negative family members experienced such adverse cardiac events. The RyR2-I3995V pedigree shows that 5 of the 8 mutant carriers/obligate carriers had aSCD/SCD, but none of the 16 mutation-negative family members had cardiac events (fig. S1A). For the Q3774L pedigree, the mutation-positive proband had aSCD, while 3 other mutant carriers and 1 non-mutant carrier

are currently asymptomatic (fig. S1B). Q4879H is a de novo aSCD-associated RyR2 mutation found in the proband. Neither parent was clinically or genetically affected.

Family Q3774L

The proband of this family (II:1) presented with an aborted sudden cardiac death (aSCD) as a result of ventricular fibrillation (VF) at the age of 12 during an intensive argument with a sibling. The family history was negative for cardiac diseases including unexplained syncope and sudden death. The ECG showed an abnormal repolarization pattern with negative T-waves throughout the precordial and inferior leads in the setting of a normal QTc, which sustained during follow up. Further extensive cardiac evaluation including echo, cardiac MRI and CT-coronary angiography, was within normal limits. Notably, exercise stress testing did not reveal any PVCs and an adrenaline challenge (0.5 μg/kg/min) was within normal limits. Subsequent genotyping was performed on an arrhythmia panel with 52 genes and identified a variant in *RYR2* (c.11321A>T, Q3774L). A subcutaneous ICD was implanted as secondary prevention for sudden death and the patient started medical treatment with slow-release propranolol (1.5 mg/kg/day). The patient was asymptomatic for 2.5 years until she had an appropriate ICD shock for VF while biking to school. This episode occurred despite medical treatment with propranolol. After this event, the dose of propranolol was increased to 2.7 mg/kg/day and slow-release flecainide (1.7 mg/kg/day) was added to her therapeutic regime. Three of the proband's siblings also tested positive for the RyR2-Q3774L mutation and all have had normal cardiac evaluations, including normal exercise stress tests. To date, all mutant positive siblings have been asymptomatic and are currently treated with propranolol. Both parents also had a normal cardiac evaluation, including implantable loop recording in one of them. The pedigree has been anonymized. For privacy reasons the genotypes of the parents are not indicated.

Family I3995V

The proband is a 60-year old female (III-6). Ten years ago, familial cascade screening identified her as a carrier of a RyR2-I3995V (c.11983A>C) missense mutation. The variant was initially identified during molecular autopsy in two cousins (III-11 and III-12), who both suffered autopsy negative sudden cardiac death at the age of 28 and 32 years, respectively. The father of the two cousins died suddenly at the age of 57 years; autopsy was not performed. The father (II-3) of the proband was an asymptomatic carrier of the I3995V mutation until he suffered a sudden unexplained death at the age of 84; no autopsy was performed. The proband experienced syncope at the age of 52 while watching television. Previous clinical work-up showed that ECG-12, echocardiography, Holter monitoring and coronary angiography were normal. No arrhythmias were elicited upon maximally tolerated exercise stress test. An ICD was implanted and the patient was discharged on metoprolol (50mg/day). During follow-up, the proband experienced episodes of pre-syncope where ICD recordings showed non-sustained polymorphic ventricular tachycardia/ventricular fibrillation. Her brother (III-7) and two children (IV-1 and IV-2) are all asymptomatic carriers of the I3995V mutation. All mutation carriers clearly lacked the typical CPVT phenotype of adrenergic-dependent and reproducible arrhythmias, but the proband and two cousins presented with non-sustained idiopathic polymorphic ventricular tachycardia/ventricular fibrillation and SCD, respectively.

Family D4112N

The proband (III-3) of this family presented with aSCD as a result of ventricular fibrillation at the age of 15 while playing soccer. The patient had a positive family history of sudden death, including a SCD of an older sibling (III-2) at the age of 15 and a cousin with an aSCD at the age of 15 (IV-1). Extensive cardiologic evaluation was performed, including cardiac echo, MRI, coronary angiography and exercise stress testing, and all were within normal limits. An implantable cardioverter-defibrillator (ICD) was implanted for secondary prevention of sudden cardiac death. During follow up the patient had three appropriate ICD discharges, all for VA or VF elicited by adrenergic activity. After the third event, nadolol was initiated (40 mg/d) and the patient has been event-free ever since. Multiple exercise tests were performed during follow up, but none of them revealed any PVCs. Two years after the initial event in the proband, a sibling (III-4) presented with aSCD during mildly adrenergic settings at the age of 12. Cardiac evaluation (including an EST and an adrenaline challenge off medication) did not reveal any abnormalities, and an ICD was implanted. Over the past six years, the patient had two ICD shocks for VF in a three-month period. On both occasions, the ICD shock occurred under mild adrenergic activity. The patient admitted to not taking his prescribed nadolol regularly. After these events, the patient started taking nadolol 40 mg/day on a regular basis and has received no subsequent ICD therapies.

Family T4196I

The proband (II-1) was a previously healthy 17-year old female that presented with recurrent episodes of syncope with exertion in 1993. Clinical evaluation revealed a normal ECG, 24-hour Holter-monitor, and echocardiogram. Exercise stress testing revealed normal QT behavior and no ventricular arrhythmias (peak heart rate 185 bpm). As no clear diagnosis was identified, medical therapy was not initiated. Two years later, the proband died suddenly while running after her dog. Autopsy revealed a structurally normal heart and no cause of death was identified. Family screening of her 4 siblings, including ECGs, exercise stress tests, Holter monitors, and echocardiograms was within normal limits. Twelve years later, the 33-year old sister (II-2) of the proband collapsed while running on a treadmill. She had been previously well and was receiving no medications. On arrival approximately 20 minutes later, paramedics found her to be in ventricular fibrillation and she was successfully defibrillated to sinus rhythm. Following intubation and arrival to hospital, a systemic hypothermia protocol was initiated for neuroprotection and she subsequently made a complete neurological recovery. ECG was normal and echocardiography initially revealed global moderate left ventricular systolic dysfunction, which subsequently normalized and was presumed secondary to cardiac stunning. Coronary angiogram and cardiac MRI were both within normal limits and signal average ECG revealed no evidence of late potentials. A procainamide challenge revealed no evidence of a type 1 Brugada ECG. No ventricular arrhythmia was observed on exercise stress testing (peak heart rate 178 bpm). QT behavior during exercise stress testing was considered at the upper limit of normal (maximum QTc value was 455) and the patient was given a possible diagnosis of concealed long QT syndrome (LQTS). Cascade screening of her 3 living siblings was repeated and ECGs and echocardiograms were again normal and exercise stress testing again revealed no ventricular arrhythmias. Two siblings (II-4 and II-6) were felt to have QTc values at the upper limit of normal on exercise stress testing (maximum value was 450 ms), were given possible diagnoses of concealed LQTS, and were initiated on intermediate dose of beta-blocker. Genetic testing for LQTS (*KCNQ1, KCNH2, SCN5A, KCNE1,* and *KCNE2*) and select exons within *RyR2* was

performed and no pathogenic mutations were identified. Eleven years later, broad panel arrhythmia genetic testing was performed on patient II-2 and a *RyR2* c.12587 C>T (T4196I) mutation was identified that was classified as a variant of unknown significance. Two months later, her brother that had been considered to have a normal phenotype (II-5) died suddenly while rounding third base during a baseball game. Autopsy revealed a structurally normal heart and no cause of death, while molecular autopsy identified the presence of the RyR2-T4196I mutation. Subsequent cascade screening revealed that the mutation was present in the proband and absent from the remaining living family members.

Family D4646A

The proband is a 51-year-old female that experienced syncope and aborted sudden cardiac death (aSCD) with ventricular fibrillation being observed on the ambulance monitor at the age of 39. The patient was successfully resuscitated and brought to the ICU where an episode of fast polymorphic ventricular tachycardia was observed and treated with DC shock. After a few days, the initial neurological impairment resolved. ECG, Holter monitoring, echocardiography, and coronary angiography were within the normal limits. No arrhythmias were elicited upon maximally tolerated exercise stress test (EST). On the basis of these findings, the case was labelled as idiopathic ventricular fibrillation (IVF). An ICD was inserted and the patient was discharged on metoprolol (100 mg/day). In 2002, the patient experienced a syncopal episode during acute emotional stress with appropriate ICD intervention. No subsequent syncopal episodes or arrhythmias were recorded on EST, Holter, or ICD during follow-up (end of 2013). Assessment of the family history revealed 5 cases of SCD in the maternal branch of the family, occurring between 16 and 43 years of age, and triggered by acute emotional stress. Molecular screening of the RyR2 gene identified a single nucleotide variation in exon 96 (n.13937A>C), leading to the RyR2-D4646A amino acid substitution. The mutation was also found in the 17-year old proband's son and an asymptomatic 20-year old nephew. Both carriers showed normal cardiac phenotypes, including exercise stress test. Thus, D4646A mutant carriers clearly lacked the typical CPVT phenotype of adrenergic-dependent and reproducible arrhythmias, but presented with a personal and/or familial history of IVF and SCD.

Family Q4879H

The proband is a previously healthy young male who survived an aSCD. At 11 years of age, he was involved in a minor altercation at school when he was pushed into a desk and collapsed to the ground. He was found to be in cardiac arrest, and bystander cardiopulmonary resuscitation was promptly initiated. He received a single successful shock from an automated external defibrillator for ventricular fibrillation (VF). In hospital, his resting ECG and telemetry monitoring were normal. An echocardiogram showed mild global ventricular dysfunction, but there were no wall motion abnormalities to suggest cardiac contusion. An exercise stress test did not provoke any arrhythmias, or QT interval prolongation. His VF cardiac arrest was felt to be idiopathic, and he received a secondary prevention subcutaneous implantable cardioverter defibrillator prior to discharge from hospital. He made a full neurological recovery and returned to school. No subsequent cardiac events have occurred over 1.5 years of follow-up, and no anti-arrhythmic medications were initiated. Commercial genetic testing of 120 genes linked to cardiomyopathy and cardiac channelopathy revealed a variant of unknown significance in RyR2 (Q4879H), and a benign variant MYPN (M1045V). There is no known family history of sudden

cardiac arrest, arrhythmic syncope or inherited cardiac disease. Neither parent carries the RyR2-Q4879H variant, making it de novo in the proband.

Family A4860G

The proband is a female (8 years old) who was referred to medical attention after an aborted sudden cardiac death (aSCD) and documented ventricular fibrillation (VF). No specific trigger for the event was identified. The young girl was previously asymptomatic with no history of cardiac disease and/or arrhythmias. A few hours after the aSCD, ECG, echocardiogram, and blood tests were within the normal limits. A review of family history identified two additional cases of sudden unexplained death: her mother (38 years old) and her maternal uncle (22 years old). The proband's sister (17 years old) was asymptomatic and one brother died immediately postpartum for unknown causes. An exercise stress test performed one week after the event was unremarkable with no arrhythmias elicited (maximal heart rate 155 bpm). QTc was normal during exercise and recovery (QTc 420 ms). Programmed electrical stimulation with up to 3 extra-stimuli (including short-long-short sequences) did not induce any arrhythmia. Further, no arrhythmias were induced during isoproterenol administration in a subsequent invasive electrophysiological study. An intravenous flecainide test did not elicit Brugada-like ECG pattern. Beta-blocking therapy was started (nadolol, 40 mg) and a single-chamber ICD was inserted. The patient remained completely asymptomatic for the following 10 years until she experienced one syncopal episode. ICD interrogation showed VF correctly treated by the device. In the following 4 years, there were two additional arrhythmic events correctly treated by the device with no recurrence after increasing the dose of nadolol to 100 mg. The patient was referred to us for genetic testing. Based on the evidence of borderline QT interval and responsiveness to beta blockers, we sequenced the open reading frame (ORF) of major LQTS and RYR2 genes. A mutation, A4860G, was identified in the RyR2 gene. The same mutation (A4860G) was also found in the asymptomatic proband's sister. Complete clinical evaluation of proband's sister, including ECG, echocardiogram, exercise stress test (up to 152 bpm), and flecainide test, was negative. These clinical studies reveal that, unlike the typical CPVT patients, IVF/SCD patients carrying the RyR2 A4860G mutation exhibit no arrhythmias during exercise stress test.

Families S4938F and I4855M have been reported previously (*15, 16*).

Linkage analysis in *RYR2* mutation families

To provide additional statistical support for a causal relationship between the specific *RYR2* mutations and affected status in these families, we employed two-point linkage analysis using LIPED (*20*). The hypothesis of positive linkage of cardiac phenotypes to each candidate *RYR2* mutation was tested assuming a dominant model of inheritance. Logarithm of odds (LOD) scores were obtained considering all affected subjects defined as either sudden cardiac death, aborted sudden cardiac death, left ventricular non-compaction cardiomyopathy, or idiopathic ventricular fibrillation. We were interested in whether the particular *RYR2* mutation in each family was linked with the respective arrhythmia phenotype, hence we focused on the lowest recombination fraction within the model ($\theta = 0.0001$) to rule out the null hypothesis of no linkage between phenotype and genotype. In total, we included information from 146 individuals from 9 families. We did not adjust penetrance within the model, but instead did not specify a binary phenotype (i.e. neither "affected" nor "unaffected") in the six youngest asymptomatic carriers

from the most recent generations in four families (i.e. family A4860G, individual II-2; family I3995V, individual IV-1 and IV-2; family D4646A, individuals III-1 and III-3; and family R4594K/I2075T, individual IV-9). By conventional a priori criteria, the hypothesis of linkage was accepted or rejected when combined LOD score was >3.0 or <−2.0, respectively (*54*).

Individual LOD scores in families identified by mutation are shown below. In five families (D4112N, T4196I, D4646A, I4855M and R4594K/I2075T) the LOD scores were maximal at θ=0.0001; the combined LOD score from these families was 7.751, equivalent to odds of 177,400,000:1 in favor of complete linkage between phenotype and genotype. The LOD score in a sixth family (I3995V) was -0.191, but increased to 3.728 when a single individual (III-7) was reclassified from "unaffected" to "undetermined". By including these results, the combined LOD score was 11.479, equivalent to odds of 301,300,000,000:1 in favor of complete linkage between phenotype and genotype in six families. Linkage could not be calculated because of recombination between phenotype and genotype in the earliest informative meiosis in two families (Q3774L and S4938F). In one family (A4860G), there were too few informative meioses to calculate linkage (table S1).

Supplementary Figures:

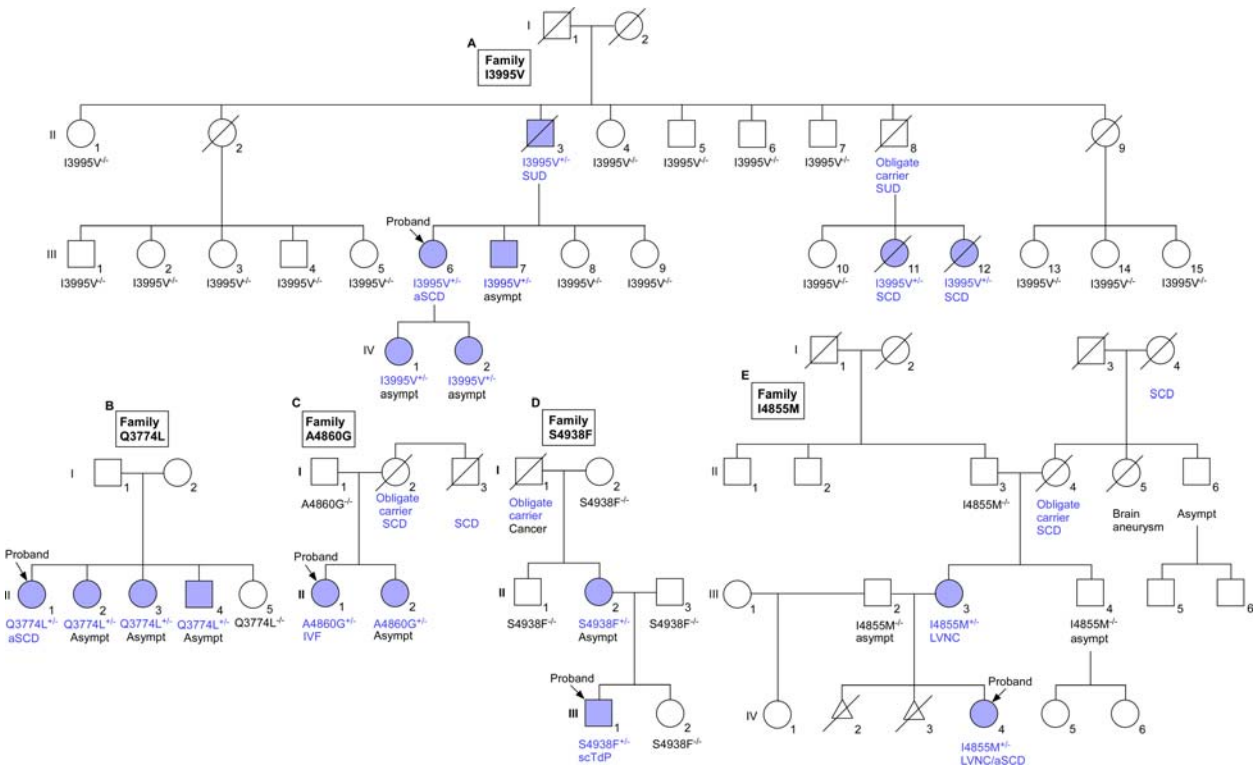

Fig. S1. Pedigrees of families with non-CPVT–associated RyR2 mutations. Pedigrees and major clinical phenotypes of families with non-CPVT-associated RyR2 mutations I3995V$^{+/-}$ (**A**), Q3774L$^{+/-}$ (**B**), A4860G$^{+/-}$ (**C**). S4938F$^{+/-}$ (**D**), and I4855M$^{+/-}$ (**E**). Squares and circles indicate males and females, respectively; blue symbols represent mutation carriers/obligate carriers; open symbols represent mutation negative/unaffected persons; symbols with a slash represent deceased persons. Triangles indicate 1st trimester fetal loss. Probands are indicated by an arrow. SUD: sudden unexplained death; SCD: sudden cardiac death; aSCD: aborted SCD; LVNC: left ventricular noncompaction; scTdP: short-coupled variant of Torsade de Pointes; asympt: asymptomatic.

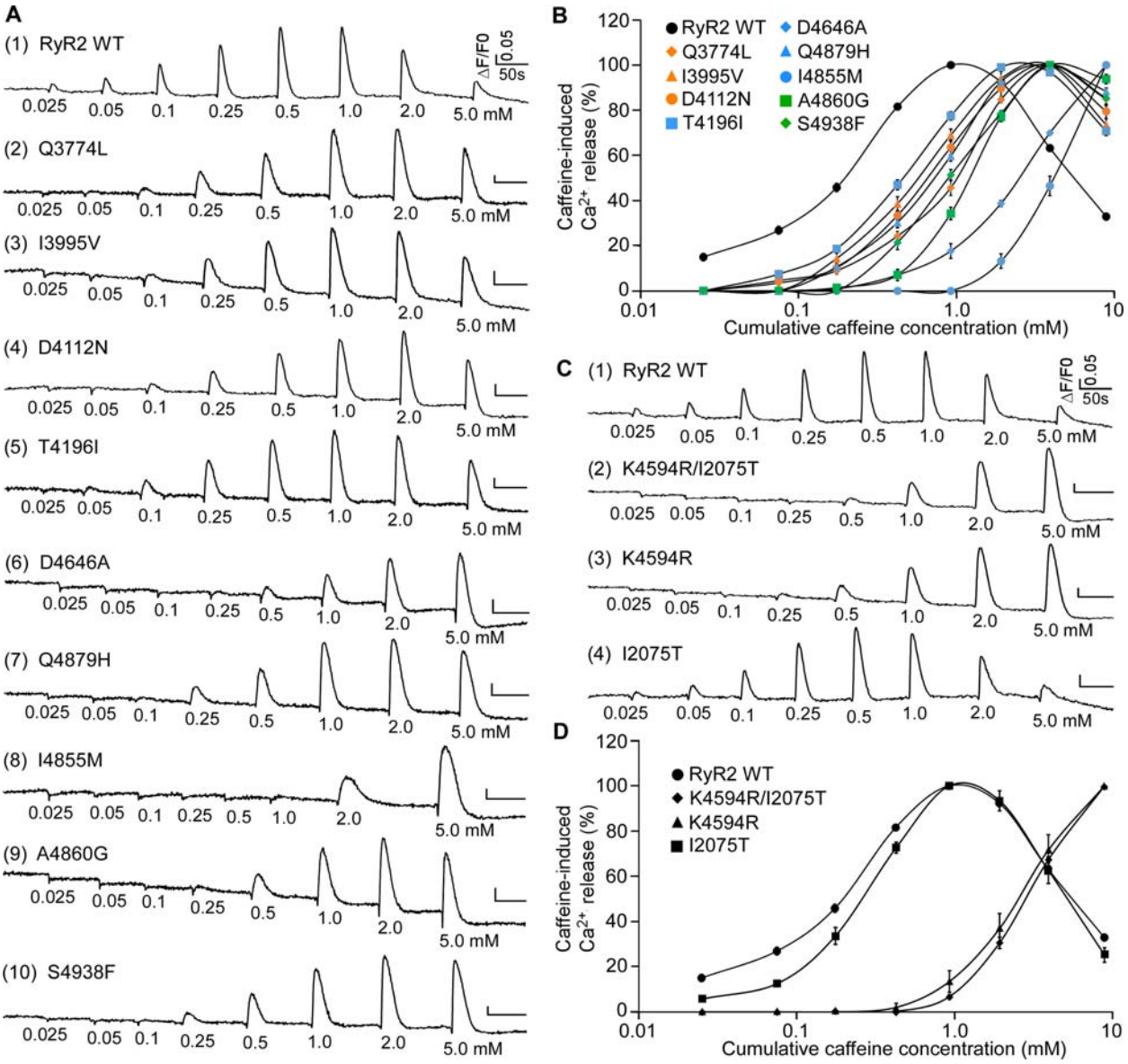

Fig. S2. Non-CPVT–associated RyR2 mutations suppress caffeine-induced Ca^{2+} release. HEK293 cells were transfected with RyR2-WT or mutants. The fluorescence intensity of the fluo-3-loaded transfected cells was monitored continuously before and after each caffeine addition **(A)**. The amplitude of each caffeine peak was normalized to that of the maximum peak for each experiment. (**B**) The relationships between Ca^{2+} release and cumulative caffeine concentrations in HEK293 cells transfected with RyR2-WT or mutants. Data are mean ± s.e.m. from RyR2 WT **(**n=18), Q3774L (n=3), I3995V (n=3), D4112N (n=3), T4196I (n=6), D4646A (n=3), Q4879H (n=4), I4855M (n=3), A4860G (n=5), and S4938F (n=3). (**C**) The fluorescence intensity of the fluo-3-loaded transfected cells before and after each caffeine addition, and (**D**) the relationships between Ca^{2+} release and cumulative caffeine concentrations in HEK293 cells transfected with RyR2-WT or the K4594R/I2075T double, K4594R or I2075T single mutations. Data are mean ± s.e.m. from RyR2-WT (n=18), K4594R/I2075T (n=3), K4594R (n=3), and I2075T (n=3).

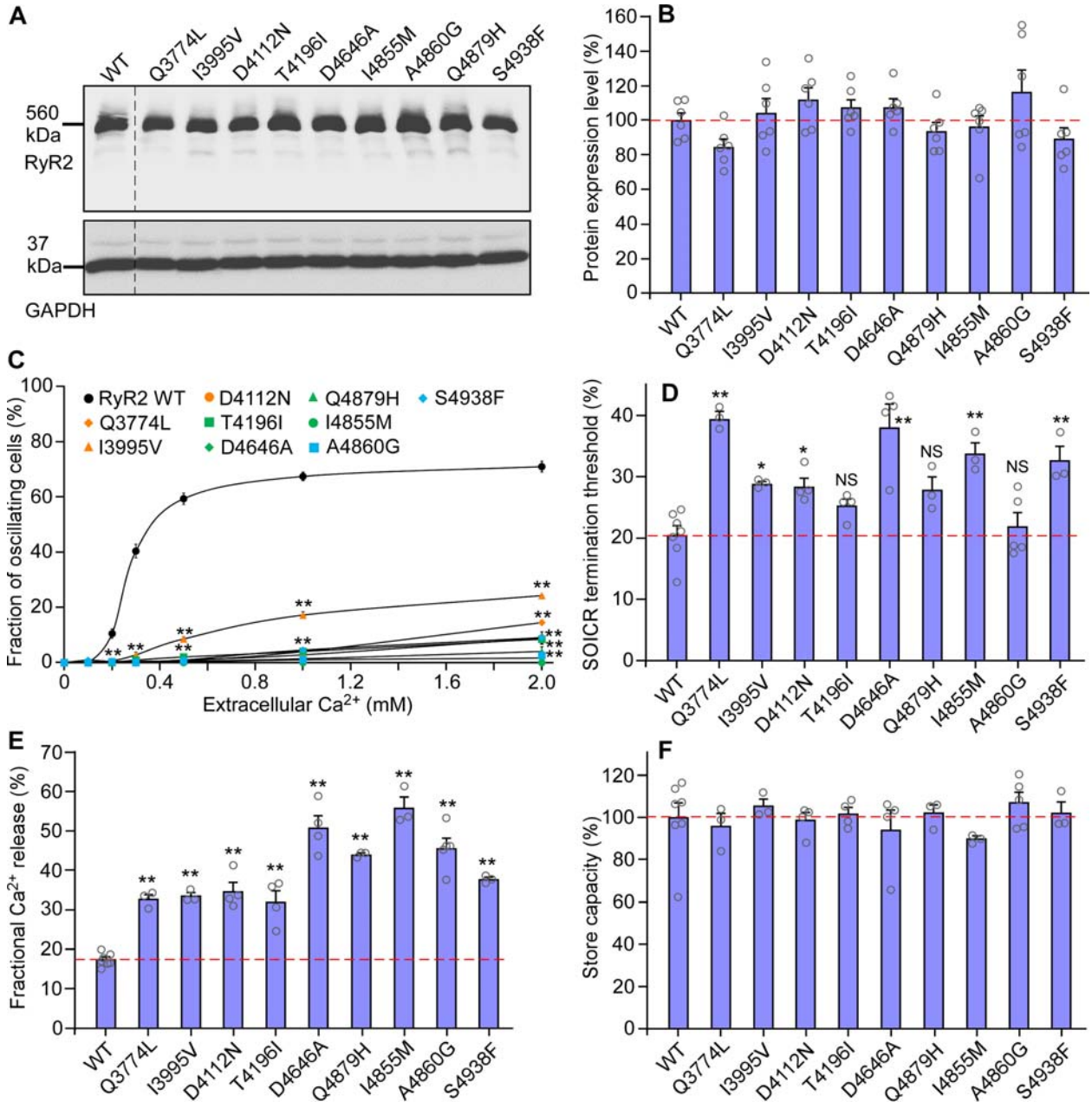

Fig. S3. Effects of mutations on the expression and function of RyR2. The same amount of cell lysate protein from HEK293 cells transfected with RyR2-WT or mutants was used for Western blotting using the anti-RyR2 antibody and anti-GAPDH antibody **(A)**. Normalized expression of RyR2-WT and mutants **(B)**. Data are mean ± s.e.m. from RyR2-WT and mutants (n=6 for each condition, one-Way ANOVA with a Dunnett's post hoc test). Ca^{2+} oscillations in stable, inducible, Fura-2/AM-loaded HEK293 cells expressing RyR2-WT or mutants were monitored using epifluorescence single-cell Ca^{2+} imaging. (**C**) The fraction of cells displaying Ca^{2+} oscillations at various extracellular Ca^{2+} concentrations (0-2mM). Data are mean ± s.e.m. from RyR2-WT (n=7), Q3776L (n=3), I3995V (n=3), D4112N (n=3), T4196I (n=3), D4646A (n=3), Q4879H (n=3), I4855M (n=3), A4860G (n=3), and S4938F (n=3) (Two-Way ANOVA

repeated measurement with a Bonferroni post hoc test, **p<0.01 versus WT). Stable, inducible HEK293 cells expressing RyR2-WT or mutants were transfected with the FRET-based ER luminal Ca^{2+}-sensing protein D1ER to investigate the effect of RyR2 mutations on the store-overload-induced-Ca^{2+}-release (SOICR) termination threshold **(D)**, fractional Ca^{2+} release **(E)**, and store capacity **(F)**. Data are mean ± s.e.m. from RyR2-WT (n=7), Q3774L (n=3), I3995V (n=3), D4112N (n=4), T4196I (n=4), D4646A (n=4), Q4879H (n=3), I4855M (n=3), A4860G (n=5), and S4938F (n=3) (One-Way ANOVA with a Dunnett's post hoc test, *p<0.05, **p<0.01 versus WT).

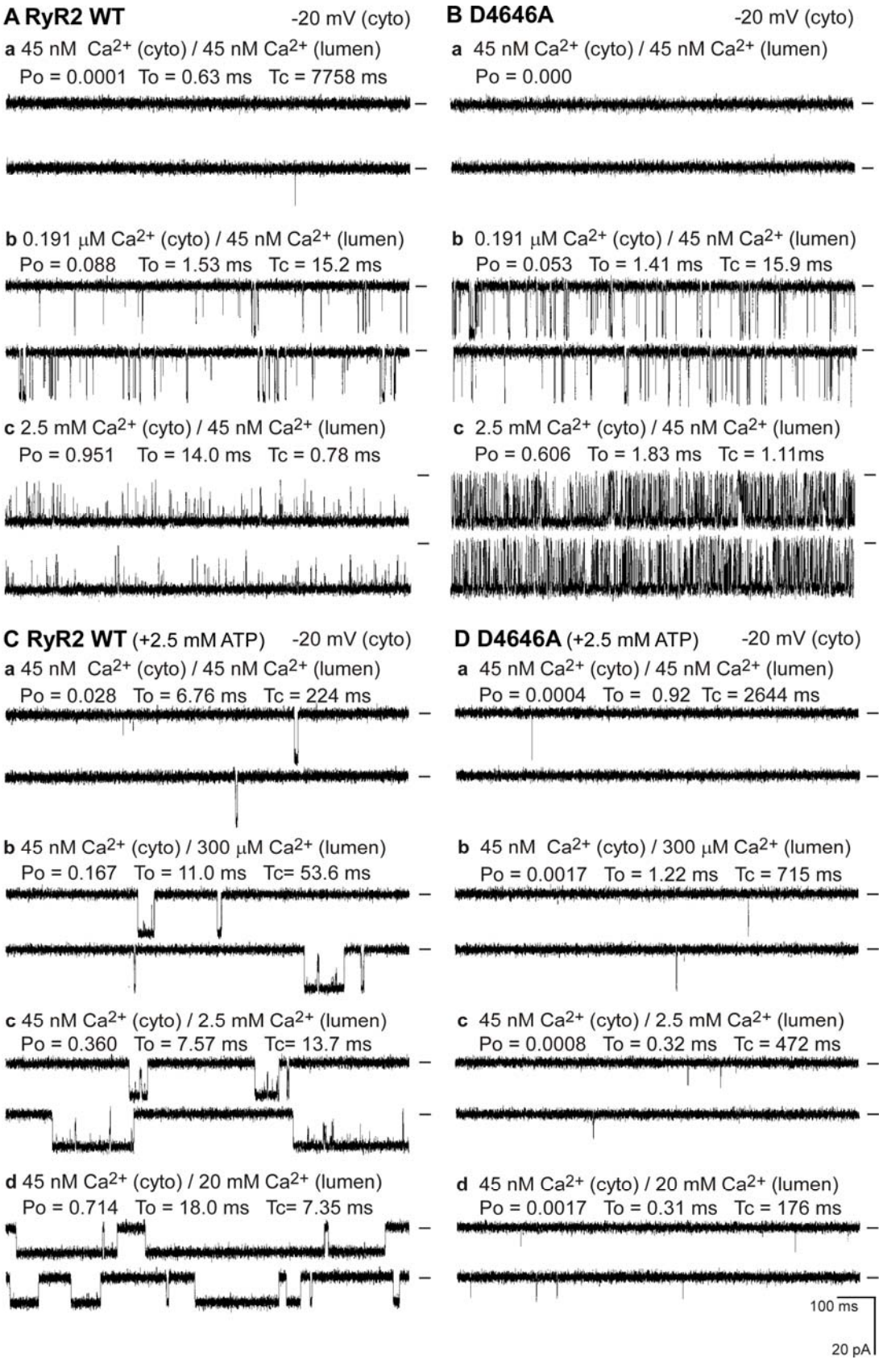
A RyR2 WT
-20 mV (cyto)
a 45 nM Ca2+ (cyto) / 45 nM Ca2+ (lumen)
Po = 0.0001 To = 0.63 ms Tc = 7758 ms
b 0.191 μM Ca2+ (cyto) / 45 nM Ca2+ (lumen)
Po = 0.088 To = 1.53 ms Tc = 15.2 ms
c 2.5 mM Ca2+ (cyto) / 45 nM Ca2+ (lumen)
Po = 0.951 To = 14.0 ms Tc = 0.78 ms
B D4646A
-20 mV (cyto)
a 45 nM Ca2+ (cyto) / 45 nM Ca2+ (lumen)
Po = 0.000
b 0.191 μM Ca2+ (cyto) / 45 nM Ca2+ (lumen)
Po = 0.053 To = 1.41 ms Tc = 15.9 ms
c 2.5 mM Ca2+ (cyto) / 45 nM Ca2+ (lumen)
Po = 0.606 To = 1.83 ms Tc = 1.11ms
C RyR2 WT (+2.5 mM ATP)
-20 mV (cyto)
a 45 nM Ca2+ (cyto) / 45 nM Ca2+ (lumen)
Po = 0.028 To = 6.76 ms Tc = 224 ms
b 45 nM Ca2+ (cyto) / 300 μM Ca2+ (lumen)
Po = 0.167 To = 11.0 ms Tc= 53.6 ms
c 45 nM Ca2+ (cyto) / 2.5 mM Ca2+ (lumen)
Po = 0.360 To = 7.57 ms Tc= 13.7 ms
d 45 nM Ca2+ (cyto) / 20 mM Ca2+ (lumen)
Po = 0.714 To = 18.0 ms Tc= 7.35 ms
D D4646A (+2.5 mM ATP)
-20 mV (cyto)
a 45 nM Ca2+ (cyto) / 45 nM Ca2+ (lumen)
Po = 0.0004 To = 0.92 Tc = 2644 ms
b 45 nM Ca2+ (cyto) / 300 μM Ca2+ (lumen)
Po = 0.0017 To = 1.22 ms Tc = 715 ms
c 45 nM Ca2+ (cyto) / 2.5 mM Ca2+ (lumen)
Po = 0.0008 To = 0.32 ms Tc = 472 ms
d 45 nM Ca2+ (cyto) / 20 mM Ca2+ (lumen)
Po = 0.0017 To = 0.31 ms Tc = 176 ms
100 ms
20 pA

Fig. S4. The D4646A mutation suppresses Ca^{2+} activation of single RyR2 channels in lipid bilayers. Single channel activities were recorded in a symmetrical recording solution containing 250 mM KCl and 25 mM HEPES, pH 7.4. Representative current traces of single RyR2-WT (n=6) (**A**) and D4646A (n=6) (**B**) channels in the presence of various cytosolic Ca^{2+} concentrations and 45 nM luminal Ca^{2+}. Representative current traces of single RyR2-WT (n=8) (**C**) and D4646A (n=5) (**D**) channel in the presence of 45 nM cytosolic Ca^{2+} and various luminal Ca^{2+} concentrations.

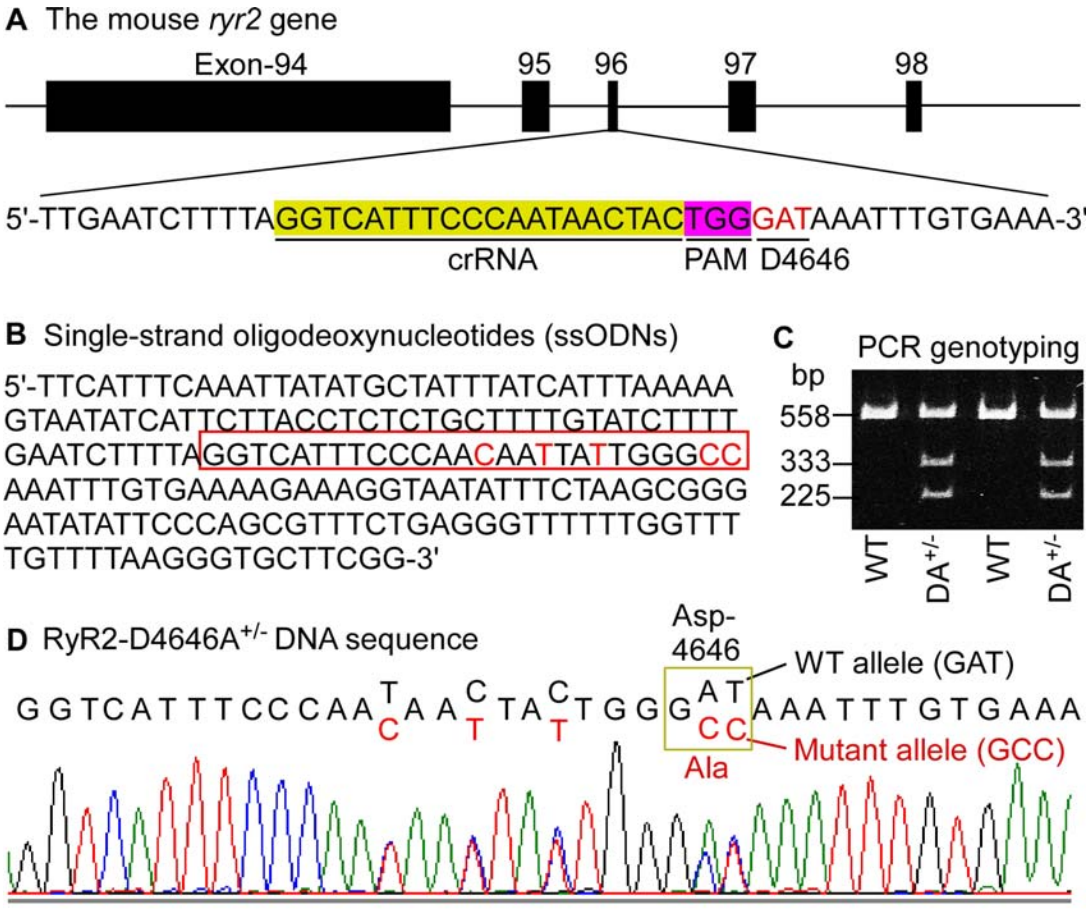

Fig. S5. Generation and functional characterization of knock-in mouse model expressing the RyR2 mutation D4646A$^{+/-}$. (A) Location of residue RyR2-D4646 in exon 96 of the mouse *ryr2* gene and the clusters of regularly interspaced short palindromic repeats RNA (crRNA) and the protospacer adjacent motif (PAM) sequence used for CRISPR-mediated mutagenesis of RyR2-D4646A. (**B**) Sequence of the single-strand oligodeoxynucleotides (ssODNs) used for homologous DNA repair. (**C**) PCR-based genotyping of RyR2-WT and D4646A$^{+/-}$ (DA$^{+/-}$) heterozygous mice. (**D**) Confirmation of the D4646A mutation in heterozygous mouse samples by DNA sequencing.

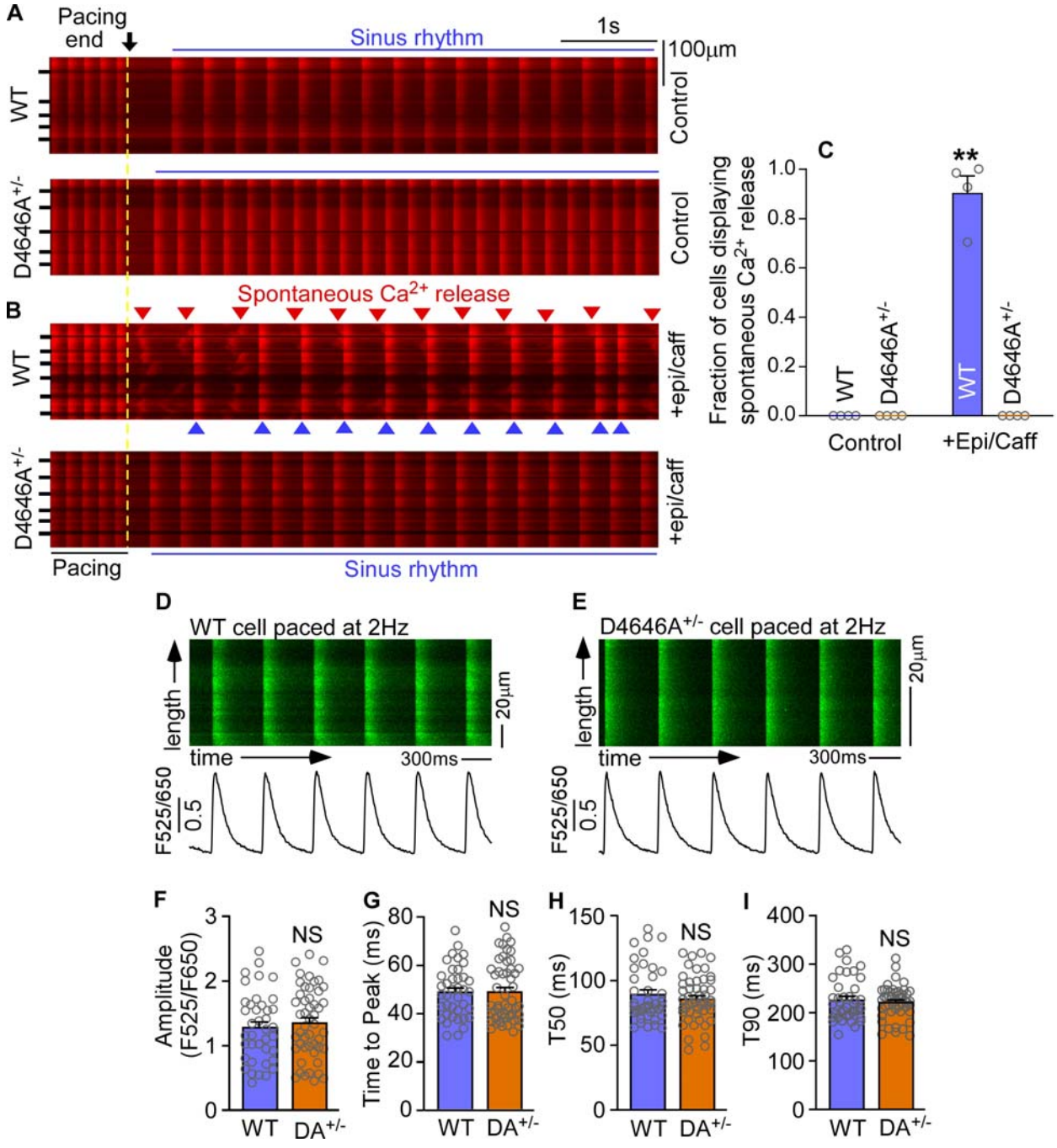

Fig. S6. Effects of RyR2-D4646A$^{+/-}$ on caffeine-promoted spontaneous Ca^{2+} release and depolarization-induced Ca^{2+} transients. In situ confocal line-scanning imaging of Ca^{2+} transients in Rhod2-AM loaded intact RyR2-WT and D4646A$^{+/-}$ mutant mouse hearts perfused without **(A)** or with (**B**) epinephrine (600 nM) and caffeine (1 mM) and paced at 6 Hz followed by an abrupt cessation. Red arrowheads indicate spontaneous Ca^{2+} release events, and blue arrowheads/lines indicate sinus rhythm. **(C)** Fraction of cells in intact WT (n=4) or D4646A$^{+/-}$ (n=4) hearts that were exposed to epinephrine and caffeine and displayed spontaneous Ca^{2+} waves (Mann Whitney *U* test, **p<0.01 versus WT). Representative confocal images of Ca^{2+}

transients in RyR2-WT **(D)** or D4646A$^{+/-}$ **(E)** cells. Isolated cardiomyocytes were loaded with Cal Red R525/650-AM and paced at 2 Hz. The traces of the F525/F650 ratio depict the average ratiometric fluorescence signal of the scan area. (**F**) Amplitude, (**G**) time to peak, **(H)** time to 50% decay of Ca^{2+} transients, and **(I)** time to 90% decay of Ca^{2+} transients at 2 Hz. Data shown are mean ± s.e.m. from RyR2-WT (n=39 cells, 3 hearts) and D4646A$^{+/-}$ (n=49 cells, 3 hearts) (Mann Whitney *U* test for Time to peak or Student's *t* test for amplitude, T50, and T90), NS, no significant versus WT).

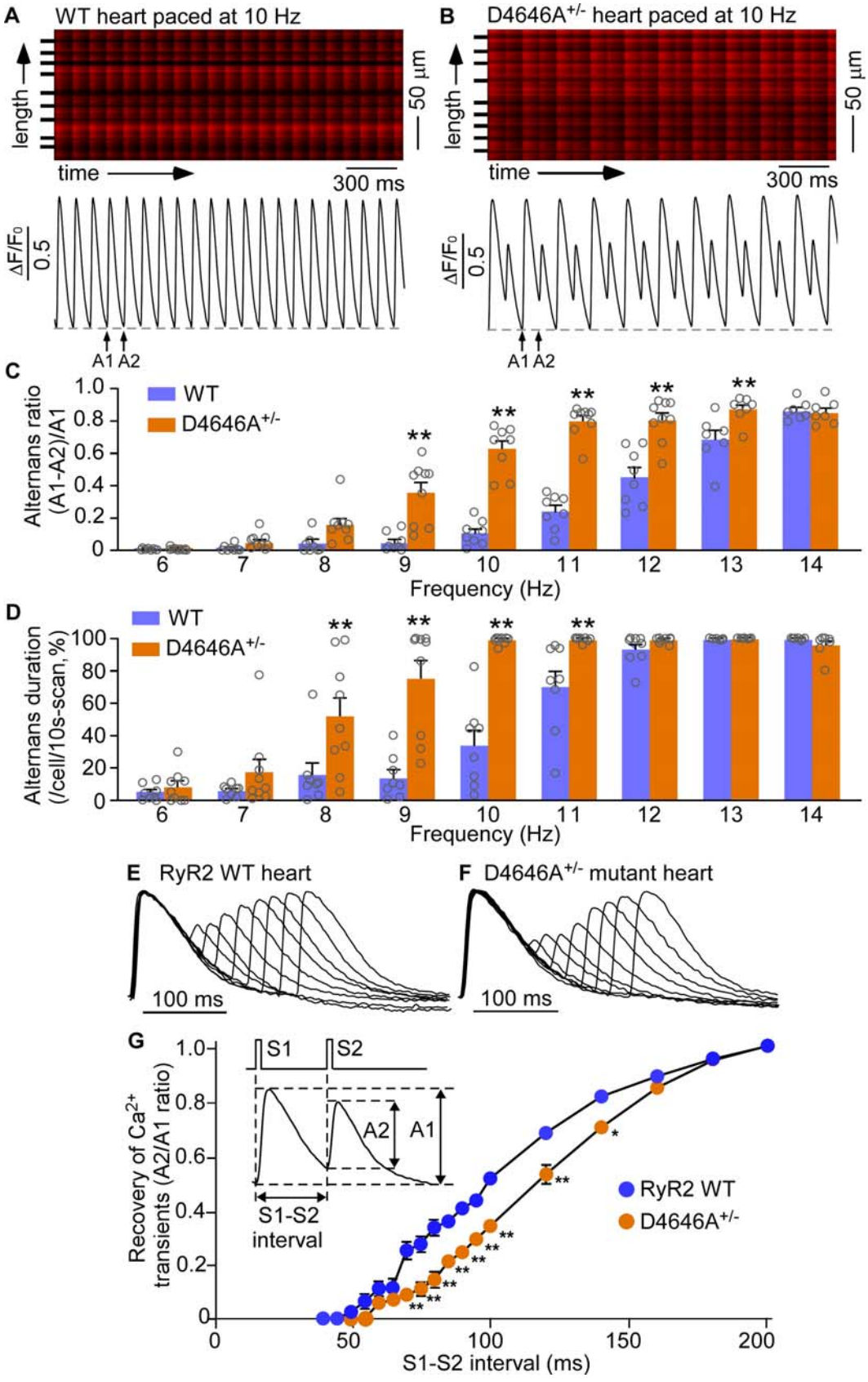
A
WT heart paced at 10 Hz
length
50 μm
time
300 ms
ΔF/F0
0.5
A1 A2
B
D4646A+/- heart paced at 10 Hz
length
50 μm
time
300 ms
ΔF/F0
0.5
A1 A2
C
Alternans ratio (A1-A2)/A1
WT
D4646A+/-
1.0
0.8
0.6
0.4
0.2
0
**
6 7 8 9 10 11 12 13 14
Frequency (Hz)
D
Alternans duration (/cell/10s-scan, %)
WT
D4646A+/-
100
80
60
40
20
0
**
6 7 8 9 10 11 12 13 14
Frequency (Hz)
E RyR2 WT heart
100 ms
F D4646A+/- mutant heart
100 ms
G
Recovery of Ca2+ transients (A2/A1 ratio)
1.0
0.8
0.6
0.4
0.2
0
S1
S2
A2
A1
S1-S2 interval
RyR2 WT
D4646A+/-
*
**
0 50 100 150 200
S1-S2 interval (ms)

Fig. S7. Effects of RyR2-D4646A$^{+/-}$ on Ca^{2+} alternans and Ca^{2+} release refractoriness. Representative line-scan images of Ca^{2+} transients in RyR2-WT **(A)** and D4646A$^{+/-}$ **(B)** hearts paced at 10 Hz**.** The average alternans ratio **(C)** and average alternans duration (**D**) from RyR2-WT and D4646A$^{+/-}$ hearts at various stimulation frequencies (6-14 Hz). Data shown are mean ± s.e.m. from RyR2-WT (n=8 hearts for 6-12 Hz and n=7 for 13-14 Hz) and D4646A$^{+/-}$ (n=9 hearts for 6-9 Hz, n=8 for 10 Hz, n=9 for 11-12 Hz, and n=7 for 13-14 Hz) (Two-way ANOVA repeated measurement with a Bonferroni's post hoc test, **p < 0.01versus WT). Langendorff perfused, Rhod-2 AM loaded intact RyR2 WT **(E)** and D4646A$^{+/-}$ mutant **(F)** hearts were first stimulated at 5 Hz for 30 beats (S1) followed by a single S2 stimulation. A series of S1S2 stimulations were repeatedly applied with progressively reduced S1S2 intervals from 200 ms to 40 ms. Ca^{2+} transients were recorded using confocal line-scanning imaging. (**G**) The relationship between the A2/A1 ratio of the Ca^{2+} transient amplitude and S1S2 interval. Data shown are mean ± s.e.m. from RyR2-WT (n=8 hearts) and D4646A$^{+/-}$ (n=7 hearts) (Two-way ANOVA repeated measurement with a Bonferroni's post hoc test, **p < 0.01, *P<0.05 versus WT).

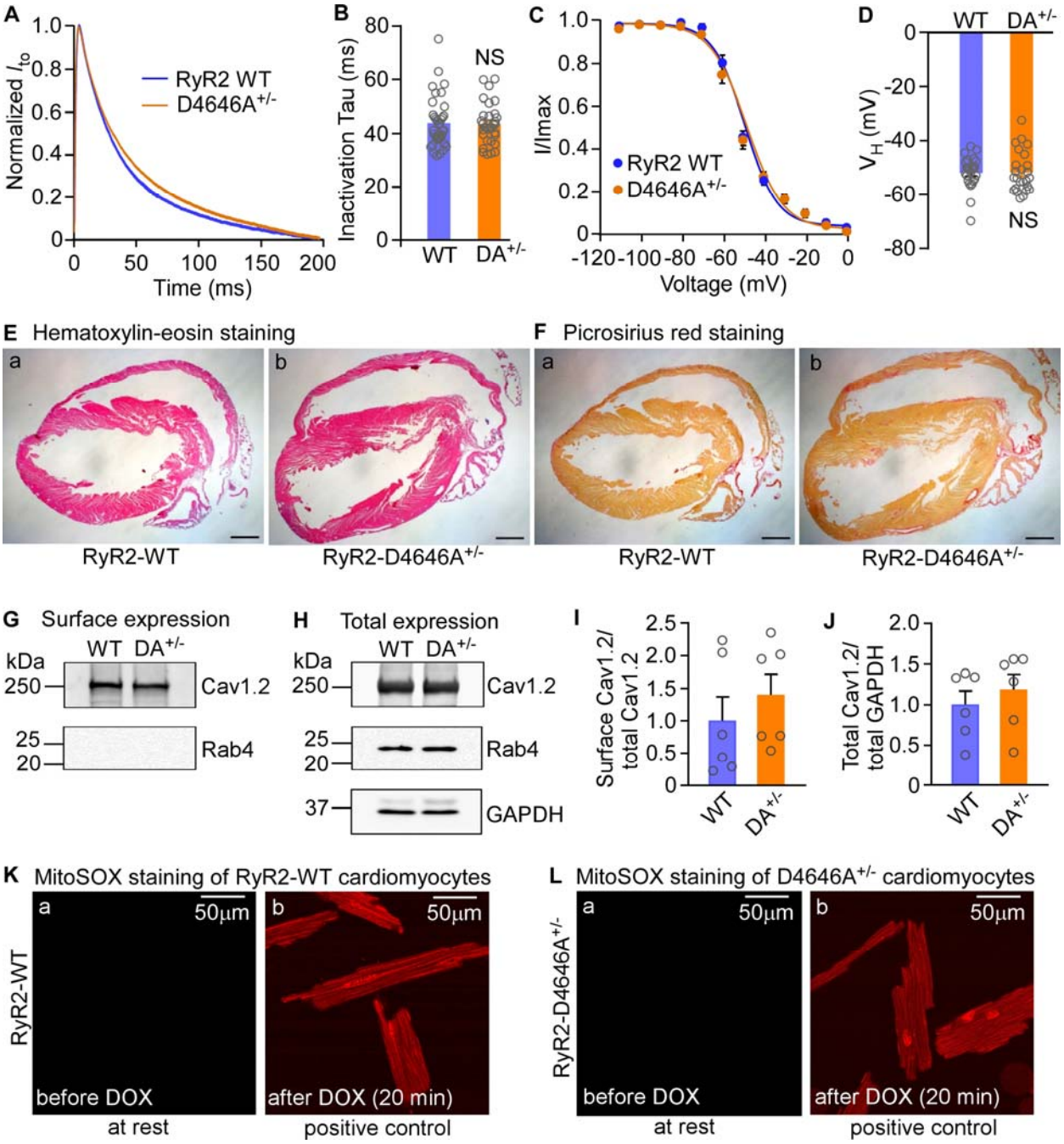

Fig. S8. Effects of RyR2-D4646A$^{+/-}$ on the I_{to} current, cardiac structure and fibrosis, L-type Ca^{2+} channel surface expression, and oxidative stress. (A) Normalized I_{to} traces showing the decay of I_{to} in RyR2-WT and D4646A$^{+/-}$ mouse ventricular myocytes. (**B**) The inactivation Tau of I_{to}. Data are mean ± s.e.m. from RyR2-WT (n=38 cells, 4 mice) and D4646A$^{+/-}$ (DA) (n=33 cells, 5 mice). (**C**) Voltage dependence of steady-state inactivation of I_{to}. (**D**) Half-inactivated voltage (V_H) of I_{to}. Data are mean ± s.e.m. from RyR2-WT (n=25 cells, 4 mice) and D4646A$^{+/-}$ (DA$^{+/-}$) (n=25 cells, 5 mice) (Mann Whitney *U* test and Student's *t* test; NS, not significant). Representative images of hematoxylin/eosin (H&E) staining **(E)** and Picrosirius red (PSR)

staining **(F)** of the RyR2-WT and D4646A$^{+/-}$ hearts (scale bar 1 mm). **(G)** Surface expression as revealed by biotinylation/labelling of Cav1.2 and Rab4 proteins in cardiomyocytes isolated from RyR2-WT (WT) and RyR2-D4646A$^{+/-}$ (DA$^{+/-}$) hearts. **(H)** Total expression Cav1.2, Rab4 and GAPDH detected by Western immunoblotting. **(I, J)** Quantification of surface (**I**) and total **(J)** expression of Cav1.2 in RyR2-WT (WT) and RyR2-D4646A$^{+/-}$ (DA$^{+/-}$) cardiomyocytes. Data shown are mean ± s.e.m. from 6 independent experiments (Student's *t* test; NS, not significant). Detection of mitochondrial superoxide in RyR2-WT and D4646A$^{+/-}$ cardiomyocytes. Live cardiomyocytes isolated from WT or D4646A$^{+/-}$ hearts were loaded with MitoSOX to assess oxidative stress. Representative confocal images of WT cardiomyocytes from 6 hearts **(K)** and D4646A$^{+/-}$ cardiomyocytes from 6 hearts **(L)** before (at rest) and after treatment with 50 μM doxorubicin (DOX) for 20 min (positive control). Red fluorescence indicates the presence of superoxide.

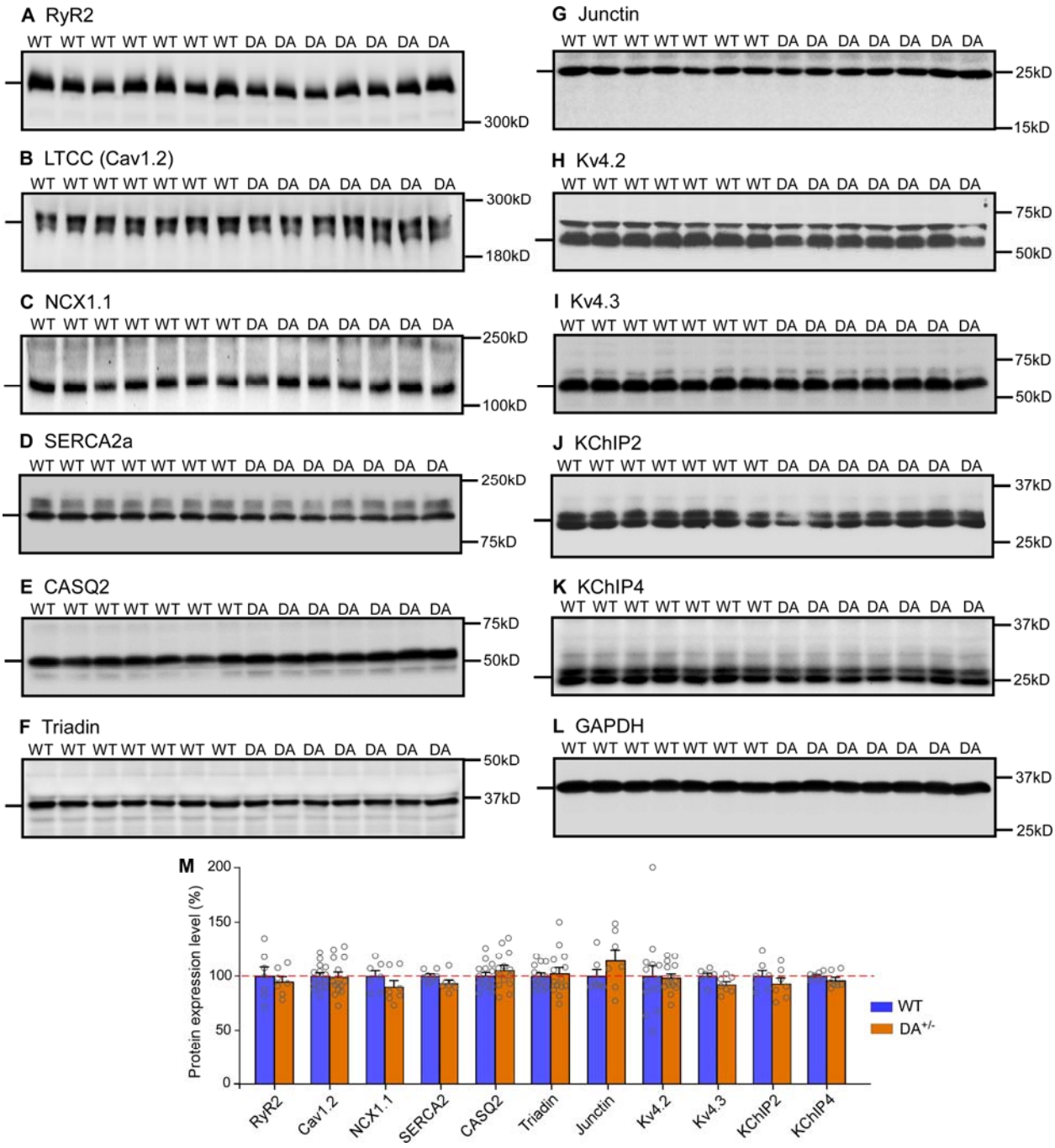

Fig. S9. Effects of RyR2-D4646A$^{+/-}$ on the expression of Ca^{2+} handling proteins, ion channels, and their associated proteins. Whole heart homogenates from RyR2-WT and D4646A$^{+/-}$ heterozygous mutant mice were used for immunoblotting analyses using antibodies against RyR2 **(A)**, L-type Ca^{2+} channel (Cav1.2) **(B)**, Na/Ca exchanger (NCX1.1) **(C)**, SERCA2a **(D)**, CASQ2 **(E)**, triadin **(F)**, junctin **(G),** Kv4.2 **(H)**, Kv4.3 **(I),** KChIP2 **(J)**, KChIP4 **(K)**, or GAPDH **(L)**. (**M**) Normalized expression of the above proteins in RyR2-WT and D4646A$^{+/-}$ (DA) hearts. Data are mean ± s.e.m. from RyR2-WT and D4646A$^{+/-}$ (n=7-14 hearts for each

group, Mann Whitney *U* test for Kv4.2 or Student's *t* test for the rest of proteins, NS, no significant versus WT).

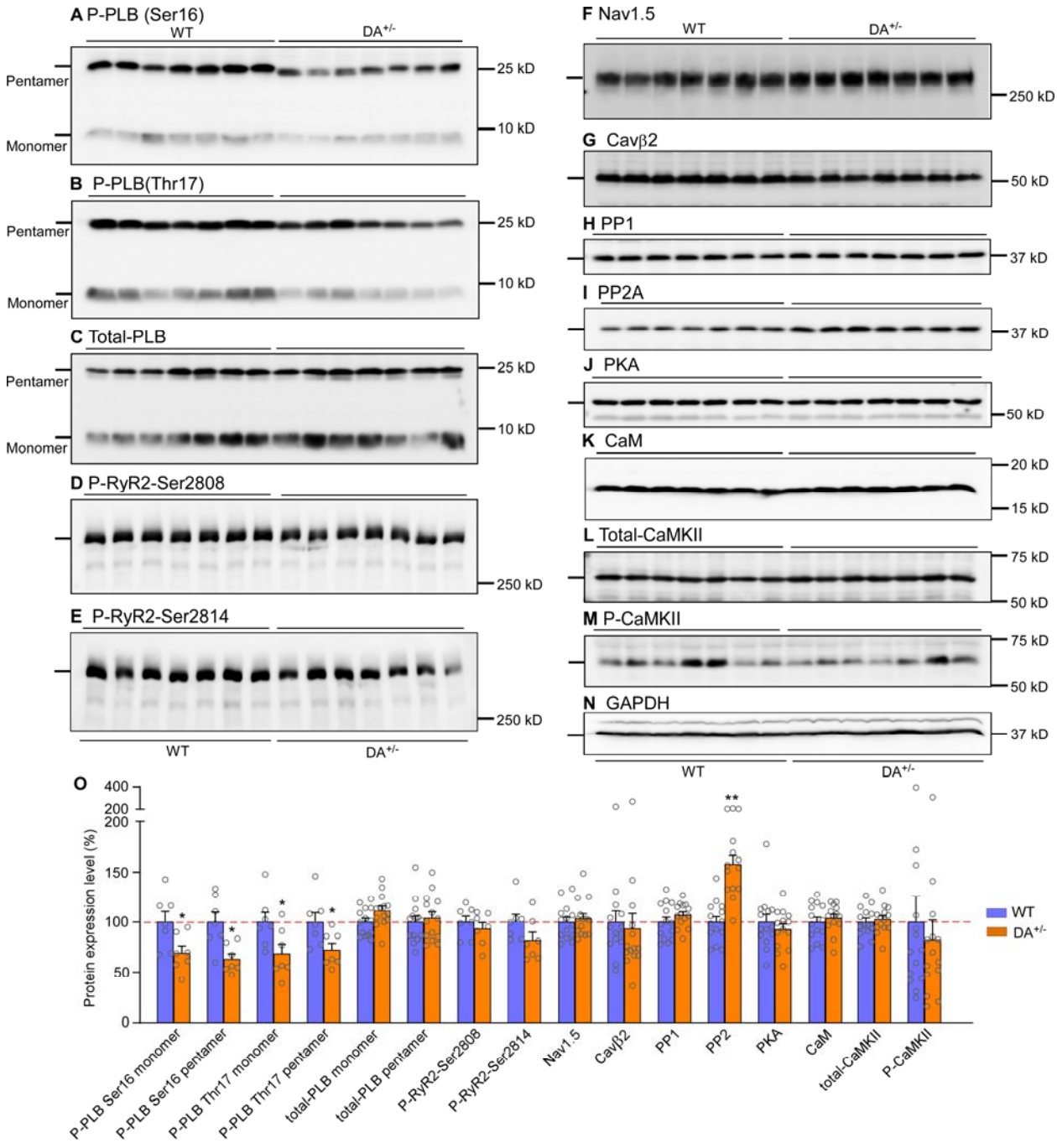

Fig. S10. Effects of RyR2-D4646A$^{+/-}$ on the expression of Ca^{2+} handling protein, ion channel, phosphatases, and kinases. Whole heart homogenates from RyR2-WT and D4646A$^{+/-}$ mice were used for immunoblotting analyses using antibodies against phosphorylated phospholamban (P-PLB, Ser16) **(A)**, phosphorylated phospholamban (P-PLBThr17) **(B)**, total phospholamban **(C)**, phosphorylated RyR2 (P-RyR2-Ser2808) **(D)**, phosphorylated RyR2 (P-

RyR2-Ser2814) **(E)**, Nav1.5 **(F)**, the β2 subunit of the L-type voltage-gated Ca^{2+} channel **(G),** protein phosphatase-1 (PP1) **(H)**, protein phosphatase-2 (PP2) **(I),** protein kinase A (PKA) **(J)**, calmodulin (CaM) **(K)**, total Ca^{2+}/CaM dependent protein kinase II (Total-CaMK□) **(L)**, phosphorylated CaMKII (P-CaMKII) **(M)**, and GAPDH **(N)**. (**O**) Normalized expression of the above proteins in RyR2-WT and D4646A$^{+/-}$ (DA$^{+/-}$) hearts. Data shown are mean ± s.e.m. from RyR2-WT and D4646A$^{+/-}$ (n=7 hearts for P-PLB (Ser16), P-PLB (Thr17), P-RyR2-Ser2808, P-RyR2-Ser2814; n=14 hearts for Total-PLB, Nav1.5, Cavβ2, PP1, PP2, PKA, CaM, P-CaMK□ and total-CaMK□) (Mann Whitney *U* test for P-CaMK□ and Cavβ2 or Student's *t* test for the rest of proteins; *p<0.05, **p<0.01 versus WT).

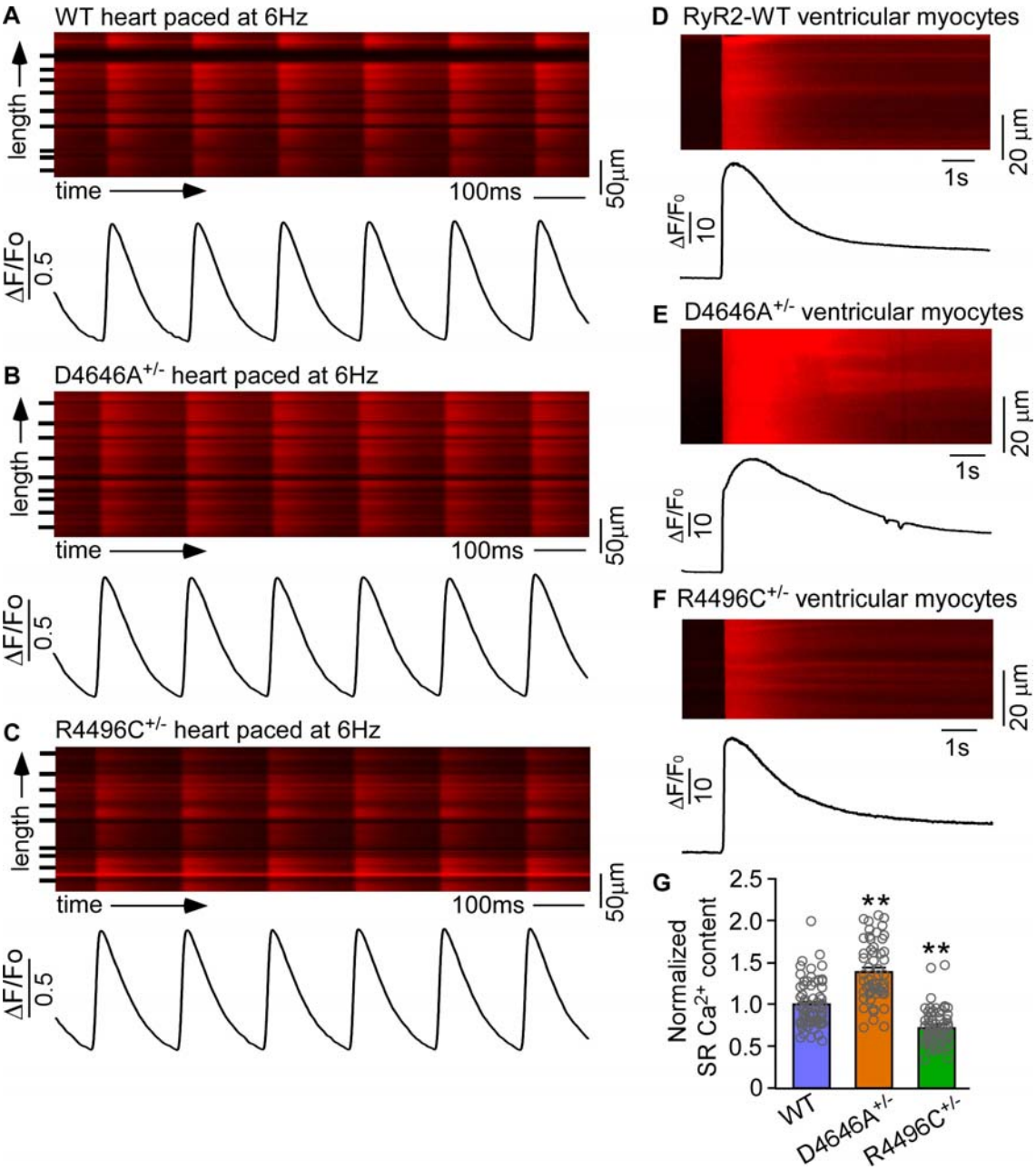

Fig. S11. Effects of RyR2 mutations on Ca^{2+} transients and SR Ca^{2+} contents. Ca^{2+} transients in Langendorff-perfused, Rhod-2 AM-loaded intact RyR2-WT **(A)**, D4646A$^{+/-}$ **(B),** and R4496C$^{+/-}$ **(C)** hearts paced at 6 Hz were recorded using confocal line-scanning imaging. Cell boundaries were indicated by short bars to the left. The $\Delta F/F_0$ traces depict the average fluorescence signal of the scan area. Sarcoplasmic reticulum (SR) Ca^{2+} contents in Rhod-2 AM loaded RyR2-WT **(D)**, D4646A$^{+/-}$ **(E)**, R4496C$^{+/-}$ **(F)**, mouse ventricular myocytes were determined by measuring the amplitude of caffeine (20 mM)-induced Ca^{2+} release (**G**). Data are mean ± s.e.m. from RyR2-WT (n=66 cells, 4 mice), D4646A$^{+/-}$ (n=53 cells, 3 mice), and R4496C$^{+/-}$ (n=61 cells, 3 mice) (Kruskal-Wallis test with Dunn-Bonferroni post hoc test, **p<0.01 versus WT).

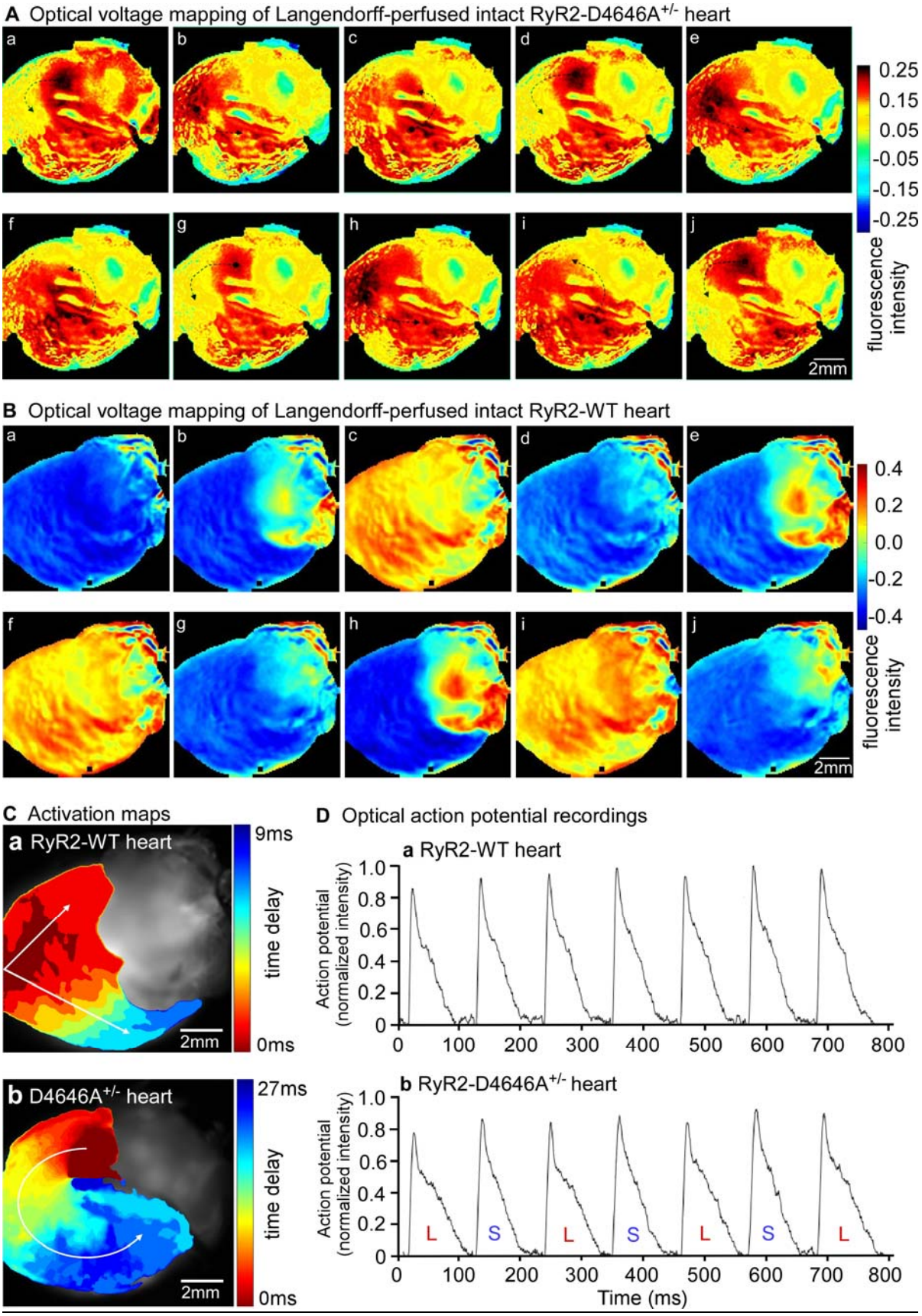
A Optical voltage mapping of Langendorff-perfused intact RyR2-D4646A+/- heart
a
b
c
d
e
f
g
h
i
j
0.25
0.15
0.05
-0.05
-0.15
-0.25
fluorescence intensity
2mm
B Optical voltage mapping of Langendorff-perfused intact RyR2-WT heart
0.4
0.2
0.0
-0.2
-0.4
fluorescence intensity
2mm
C Activation maps
a RyR2-WT heart
9ms
time delay
0ms
2mm
b D4646A+/- heart
27ms
time delay
0ms
2mm
D Optical action potential recordings
a RyR2-WT heart
Action potential (normalized intensity)
1.0
0.8
0.6
0.4
0.2
0
0
100
200
300
400
500
600
700
800
b RyR2-D4646A+/- heart
Action potential (normalized intensity)
L
S
L
S
L
S
L
Time (ms)

Fig. S12. Electrical conduction in the RyR2-WT and D4646A$^{+/-}$ hearts. (A) A series of representative images (**a-j**) from phase map videos of fluorescence recordings of the RH237 voltage dye-loaded, Langendorff perfused RyR2-D4646A$^{+/-}$ (**A**) and RyR2-WT (**B**) hearts, showing a re-entrant conduction pattern in the RyR2-D4646A$^{+/-}$ mutant heart but not in WT. Pseudo colors depict the fluorescence intensity of the voltage-sensitive dye RH237. Black arrows (in **A**) indicate the direction of rotor movements in the D4646A$^{+/-}$ heart. **(C)** Activation maps of the RyR2-WT (**a**) and D4646A$^{+/-}$ (**b**) hearts. **(D)** Optical action potential (AP) traces of the RyR2-WT (**a**) and D4646A$^{+/-}$ (**b**) hearts, showing AP duration (APD) alternans ("L" for long and "S" for short) in the D4646A$^{+/-}$ but not in WT hearts during electrical pacing at 9 Hz (corresponding to the long-burst component of the LBLPS stimulation sequence). The AP traces were generated by averaging the AP signal from the whole heart. Similar results were obtained from 3 RyR2-WT and 3 D4646A$^{+/-}$ mutant hearts.

Table S1. LOD scores for each family specified by *RYR2* mutation.

RyR2 mutation	Total individuals included	LOD at θ = 0.0001
Q3774L	5	ND
I3995V	28	3.728*
D4112N	14	1.660
T4196I	11	1.775
D4646A	17	1.843
I4855M	18	0.602
A4860G	5	0.0
S4938F	7	ND
R4594K/I2075T	41	1.871

*Post hoc reclassification of a single individual (III-7) from "unaffected" to "undetermined" increased the LOD score from -0.191 to 3.728, maximal at θ=0.0001. The calculation of the LOD score for the double mutation R4594K/I2075T family is based on the family's pedigree reported previously (*17*).

Table S2. Echocardiographic parameters of RyR2-WT and D4646A$^{+/-}$ mutant mice. E velocity, peak velocity of early filling of mitral inflow; A velocity, peak velocity of late filling of mitral inflow; LVEDs, left ventricular end-systolic diameter (systolic); LVEDd, left ventricular end-diastolic diameter (diastolic); LVAWs, left ventricular anterior wall (systolic); LVAWd, left ventricular anterior wall (diastolic); LVPWs, left ventricular posterior wall (systolic); LVPWs, left ventricular posterior wall (diastolic); EF, ejection fraction; FS, fractional shortening; LAA, left atrium area; CO, cardiac output. Data shown are mean ± s.e.m. (*P<0.05 vs WT; **P<0.01 vs WT) (Mann Whitney *U* test and Student's *t* test; *P<0.05, **P<0.01 versus WT).

Parameters	WT (n=17)	DA$^{+/-}$ (n=15)
E velocity (mm/s)	376.49 ± 22.95	363.26 ± 20.36
A velocity (mm/s)	170.83 ± 13.69	174.30 ± 18.01
E/A ratio	2.39 ± 0.20	2.38 ± 0.25
Heart Rate (BPM)	359.48 ± 8.67	326.76 ± 11.65*
LVEDs (mm)	3.03 ± 0.09	2.98 ± 0.11
LVEDd (mm)	4.20 ± 0.08	4.24 ± 0.10
LVAWs (mm)	1.30 ± 0.05	1.53 ± 0.07*
LVAWd (mm)	0.82 ± 0.03	1.00 ± 0.05**
LVPWs (mm)	1.03 ± 0.03	1.22 ± 0.07*
LVPWd (mm)	0.78 ± 0.04	0.93 ± 0.06*
EF (%)	53.90 ± 2.04	57.11 ± 2.10
FS (%)	27.84 ± 1.35	29.95 ± 1.37
Max LAA (mm^2)	5.75 ± 0.30	6.26 ± 0.34
Min LAA (mm^2)	4.01 ± 0.29	4.22 ± 0.38
Systolic volume (µL)	29.89 ± 1.59	29.56 ± 3.08
Diastolic volume (µL)	56.60 ± 2.13	59.13 ± 3.92
Stroke Volume (µL)	26.71 ± 1.52	29.57 ± 2.79
CO (mL/min)	8.95 ± 0.44	9.03 ± 0.82